ENDANGERED PLANT SPECIES FOR POTENTIAL DRUG LEADS AND ANTICANCER PROTOTYPES FOR TREATMENT OF BREAST AND PANCREATIC CANCERS

A Dissertation
presented in partial fulfillment of requirements
for the degree of Doctor of Philosophy
in Pharmaceutical Sciences with Emphasis in Pharmacognosy
The University of Mississippi

by

JOONSEOK OH

December 2015

ABSTRACT

This research features the isolation, structural elucidation, and synthesis of natural products from rare and endangered plant species and marine sponges.

Part I elaborates the identification of bioactive phytochemicals from several rare or endangered plant species including *Lindera melissifolia*, *Rhododendron brachycarpum,* and *Diplostephium rhododendroides*. Worldwide at least 13% of known flora are endangered or threatened and the United States Department of Agriculture (USDA) reported that there are over 780 endangered or threatened plant species in the US and its territories. The essential oil and solvent extracts from *L. melissifolia* (pondberry) drupes were gathered, purified, and analyzed by various spectrometric techniques. The essential oil exhibited a significant dose dependent repellent activity against ticks reported to be vectors of significant pathogenic human diseases such Lyme disease. A Korean endangered plant *R. brachycarpum* was also rigorously investigated for bioactive molecules. *R. brachycarpum* is a broad-leaved shrub native to northern parts of Korea and Japan. The high mobility group box 1 protein (HMGB1) could be a specific target for the discovery of effective agents to alleviate severe sepsis. The first bicyclic megastigmane glucoside rhododendroside A was isolated from the leaves of *R. brachycarpum*. Gauge-invariant atomic orbital (GIAO) NMR chemical shift calculations were implemented for elucidation of stereochemical details of rhododendroside A with accuracy improved by application of DP4 analysis. One of the rare South American plant species *D. rhododendroides* Hieron. afforded diplostephiosides A and B. These secondary metabolites exerted inhibitory activity of protein tyrosine phosphatase 1B (PTP1B) that has captured widespread attention in development of agents

for the treatment of metabolic disorders. Comprehensive induced-fit docking simulations were implemented with diplostephiosides A and B and they demonstrated excellent docking scores with the allosteric binding sites.

Part II delineates not only the characterization of the stereostructure of BRCA1-IRIS (IRIS) inhibitory peptide exhibiting potent in vivo cytotoxic activity on triple-negative breast cancer (TNBC) but also the partial synthesis of a sponge-derived cytotoxic drug prototype for treatment of pancreatic cancer. Breast cancer is the second most diagnosed cancer in American women. Based on a recent study corroborating that the oncogenicity of IRIS resides with the intron 11 peptide domain, an IRIS-inhibitory peptide (IRIS-IP), composed of the oncogenic intron sequence attached to a nuclear penetrating signal, was designed and its 3D structure was elucidated utilizing high-field NMR spectroscopic and computational tools. Pancreatic cancer has also been recognized as a major cause of death in the West. In 2015, an estimated 48,960 people in the US will be diagnosed with pancreatic cancer and about 20,710 will die from the serious disease. Discorhabdin X, isolated from *Latrunculia* species collected in the deep waters off the Aleutian Islands, possesses intriguing ring systems and exhibited selective cytotoxic activity on pancreatic cancer. A partial structural moiety of this antineoplastic molecule is being synthesized to further evaluate in vivo cytotoxic activity for the development of a practical drug prototype targeting the treatment of pancreatic cancer and its related fatalities.

DEDICATION

This work is dedicated to my loving family.

ACKNOWLEDGMENTS

I would like to extend my deepest gratitude to my advisor Dr. Mark T. Hamann for his continuous support towards earning my doctoral degree. None of my work could have been accomplished without his extensive collaboration, patience, tenacity, guidance, and motivation. I would also like to thank my committee members Dr. Daneel Ferreira, Dr. Jordan Zjawiony, and Dr. Seongbong Jo for their strong support, patience, and motivation in conducting my research. I would especially express my gratitude to Dr. Ferreira, Dr. Robert Doerksen, Dr. Marc Tius, and Dr. Jo for not only broadening my academic horizon in stereochemistry, computational studies, and targeted synthesis but also sharpening my concise scientific writing and speaking skills. I would recognize Dr. Zjawiony for providing me with practical and useful instructions for preparing my on-site interview for my postdoc position. I also thank Dr. Mitchell Avery, Dr. Marc Slattery, Dr. Dale G. Nagle, Dr. Yu-Dong Zhou, Casey Stauber, Candace Lowstuter, Sherrie Gussow, Taylor Stephens, Amber Hayes, Randy Allen, and Danielle Noonan for all of their practical teaching, administrative help, and inspiration throughout my entire time at The University of Mississippi. I also recognize Dr. Stephen Cutler, Dr. John Rimoldi, Dr. Nurhayat Tabanca, and Dr. Tracy Brooks for their encouragement, helpful discussions, and financial support in implementing my studies.

I would like to thank Dr. MinKyun Na and the late Dr. Seungho Lee for their financial and emotional help, timely advice and guidance, and inspiration in initiating and completing my doctoral degree program. I also appreciate Dr. Takashi Tomioka, Dr. Amar Chittiboyina, and Dr. Yusuke Takahashi for sharing their expertise and practices in synthesis-oriented projects described

in my dissertation. I would also like to express special acknowledgement Dr. Amanda Waters, Dr. John J. Bowling, Dr. Bin Wang, Dr. James W. Sims, Dr. Charlotte Gény, Dr. Sridevi Ankisetty, Dr. Yann Fromentin, Dr. Pradeep Lasonkar, Dr. Gang Fu, Dr. Haining Liu, Sam Abbas, Frank Wiggers, Olivia Dale, Eric Bow, Dr. Rama Gadepalli, Dr. Melissa Jacob, Mohamed Albadry, Dr. Cristina Avonto, Dr. Marco Mottinelli, Dr. Mohamed Ibrahim, Munia Sowaileh, and Yike Zou for their continuous help and support, encouragement, guidance, and kindness in conducting my primary research projects. I also thank all of our former and current lab members. I would especially like to thank Dr. Jungeun Bae, Abhijeet Maurya, Hyung Kyung Lee, Dr. Jun-Bom Park, Dr. Ji-Yeoung Bae, and Dr. Min Hye Yang for their constructive discussions and advice for my research, and emotional support. I also recognize Samuel H. Abbas, Kimberly Auker, Dr. Christina Coleman, Dr. Sarah Scarry, Dr. Rob Smith, Dr. J. Brian Morgan, Dr. Rohit Bhat, and Dr. Kevin Lewelly for their assistance and friendship. I would also thank the members of Korean Student Association and Oxford Korean Church for their emotional support, kindness, and generosity.

I would like to thank the National Cancer Institute for the NCI 60 cancer cell line data of monanchocidin A, Mississippi Center for Supercomputing Research for providing supercomputer access and technical supports (Dr. Brian Hopkins), and the University of Alabama at Birmingham for acquiring high-field NMR data. I sincerely appreciate Kraft Food Global Inc., Biosortia, Department of BioMolecular Sciences, and Dr. Larry Walker for financial support. I would like to also recognize Dr. Jonathan M Goodman, Dr. Michael Lodewyk, and Mike Brown for their technical supports in accomplishing computational work and unusual NMR experiments.

Lastly, I would like to thank my family (Grandmother, Father, Mother, Hyunseok, Buyoung, Suhyun, Uncle, Aunt, Rua, Rubin, Yujoon) for all of the love and support they have given me over the years. Without them, I would not be where I am today.

TABLE OF CONTENTS

LIST OF TABLES

LIST OF FIGURES

PART I: INVESTIGATION OF GLOBAL ENDANGERED SPECIES FOR NEW CHEMISTRY AND DRUG PROTOTYPES

CHAPTER 1

INVESTIGATION OF TICK REPELLENT ACTIVITY OF VOLATILES FROM THE SOUTHEASTERN US ENDANGERED PLANT *LINDERA MELISSIFOLIA*

CHAPTER 2

CONFIGURATIONAL ASSIGNMENT OF CONFORMATIONALLY RESTRICTED MEROTERPENOIDS FROM *L. MELISSIFOLIA*

CHAPTER 3

DISCOVERY OF DRUG LEADS FOR TREATMENT OF SEPSIS FROM THE KOREAN ENDANGERED SPECIES *RHODODENDRON BRACHYCARPUM*

CHAPTER 4

SCRUTINY OF THE SOUTH AMERICAN ENDANGERED SPECIES *DIPLOSTEPHIUM RHODODENDROIDES* FOR ANTIDIABETIC DRUG LEADS CAPABLE OF INHIBITING PROTEIN TYROSINE PHOSPHATASE 1B

CHAPTER 1: INVESTIGATION OF TICK REPELLENT ACTIVITY OF VOLATILES FROM THE SOUTHEASTERN US ENDANGERED PLANT *LINDERA MELISSIFOLIA*

(The contents of this Chapter were reprinted or modified from the original article published in *Phytochemistry* with permission from the publisher via Rightslink® service, Copyright 2012 Elsevier B.V., Confirmation No. 11305540)

INTRODUCTION

A recent report on the decline of global biodiversity suggests that the rate has not decreased and several factors have worsened the decline.[1] The pressure on biodiversity has been recognized for several years, yet progress toward limiting exacerbating factors worldwide appears sluggish. Globally at least 13% of known flora are endangered or threatened[2] and the United States Department of Agriculture (USDA)[3] claimed that there are currently at least 780 endangered or threatened species of plants in the United States (US) and its territories. Although environmental factors such as habitat destruction, fragmentation, and climate change[4] are the most widespread causes of plant species endangerment worldwide,[4] biological threats such as competition with non-native species and invasion of fungi,[5] viruses,[6] and exotic arthropods[7] are also significant factors driving those species to extinction.

The Lauraceae are comprised of about 55 genera and over 2000 species are found in the family.[8] The members are generally known for their high content of essential oils used in the perfume and spice industries.[8] Several studies on essential oils found in this family reveal associated chemistry and a variety of bioactivities.[9-13] *Lindera melissifolia* (Walt.) Blume (Lauraceae), commonly known as pondberry, is a member of the Lauraceae family but has not been investigated for its potential bioactive constituents. It is an aromatic, rhizomatous, dioecious shrub that grows in seasonally flooded wetlands and on the edges of sinks and ponds in the Southeastern US.[14,15] The US Fish and Wildlife Service (USFWS) listed pondberry as an endangered species in 1986[16] because of habitat loss.[15]

During the past approximately 30 years, Lyme disease has become a major human health problem in the US with many cases reported annually.[17,18] In New England, the Mid-Atlantic, and the Great Lake areas the causative spirochete *Borrelia burgdorferi* is transmitted by the bite of the

blacklegged tick *Ixodes scapularis* whereas the Pacific blacklegged tick *Ixodes pacificus* is the vector of the pathogenic spirochete on the West Coast.[19,20] The lone star tick *Amblyomma americanum* is another tick species of medical and veterinary importance[21] and this arthropod has spread from South Central and Southeastern states northward and somewhat westward into the Mid-Atlantic US states.[22]

With proper application, insect repellents reduce disease transmission caused by arthropod vectors.[23] *N, N*-diethyl-3-methylbenzamide (DEET) is a broad-spectrum synthetic repellent that has been effective against several species of mosquitoes, chiggers, ticks, and biting flies.[24-28] However, repeated use of synthetic repellents disrupts natural biological systems and promotes resistance.[23,29] Additionally, DEET has been reported to exert toxic reactions in humans under certain circumstances and age groups,[30,31] which motivates exploration and development of natural product-based repellents.

Plants are considered to be a source of safe repellents since they may have less harmful side effects from regular use.[32] A number of essential oils from plants exhibit insect repellent properties.[32] Natural repellents are commonly regarded to be effective for short durations but some botanically based repellents such as *p*-menthane-3,8-diol from the lemon-scented gum tree *Corymbia citriodora* have recently shown sustained potency for protection against mosquitoes.[33,34] Consequently, more interest has been focused on plant extracts or essential oils as potential alternative repellent agents.[35]

As part of a conscious effort to conserve plant resources that still exist in the US but are threatened with extinction, *L. melissifolia* is investigated herein for the chemical constituents and

potential biomedical herein. The crude essential oil of fresh pondberry drupes was collected and the oil and a hexanes extract were evaluated for tick-repellent activity.

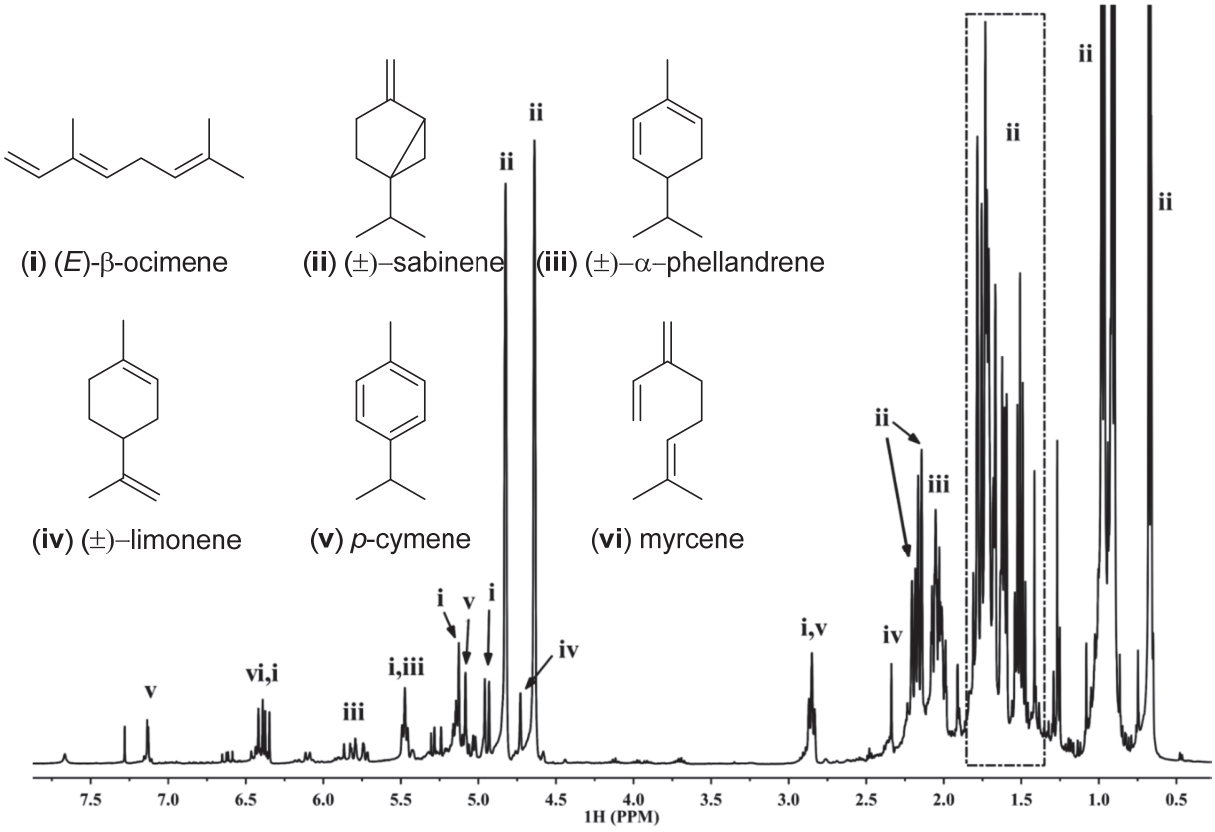

Figure 1. ^{1}H NMR spectrum of pondberry essential oil and the identified major components ($CDCl_3$, 400 MHz) (i) (*E*)-β-ocimene, (ii) (±)-sabinene, (iii) (±)-α-phellandrene, (iv) (±)-limonene, (v) *p*-cymene, (vi) myrcene

RESULTS AND DISCUSSION

Crude Essential Oil Analysis/ Preliminary Tick Repellent Assay

Gas chromatography (GC) and GC-MS analyses were used to investigate the components of the essential oil and hexanes extract from *L. melissifolia* drupes (**Table 1**). The major components of the essential oil were (±)-sabinene (66.2%), (*E*)-β-ocimene (12.9%), (±)-α-phellandrene (4.1%), β-caryophyllene (2.6%), (±)-limonene (2.3%), myrcene (2.1%), and *p*-cymene (0.5%), the structures of which were confirmed by 1D NMR analysis. In the ^{1}H NMR spectrum (**Figure 1**), the characteristic and strong resonances for exo-olefinic (4.65–4.84 ppm)

and cyclopropyl functional groups (0.66–0.68 ppm) were observed in component (**ii**), indicating the presence of (±)-sabinene which was proven to be the most abundant component in the essential oil by GC and GC-MS analyses (**Table 1**). The presence of a noticeable resonance for component (**i**) at 6.39 ppm displaying typical *cis* and *trans* vicinal couplings (dd, *J*=17.6, 10.7 Hz) implied the presence of a monosubstituted vinyl group. Comparison of the ^{13}C NMR chemical shift values and their relative intensities with literature data[36] revealed that component (**i**) is (*E*)-β-ocimene. An aromatic signal resonated at 7.13 ppm (d, *J*=2.3 Hz) for component (**v**) suggested the presence of a phenyl group. Further NMR analysis characterized the component as *p*-cymene. Additionally, normal phase preparative high-performance liquid chromatography (HPLC) provided a minor

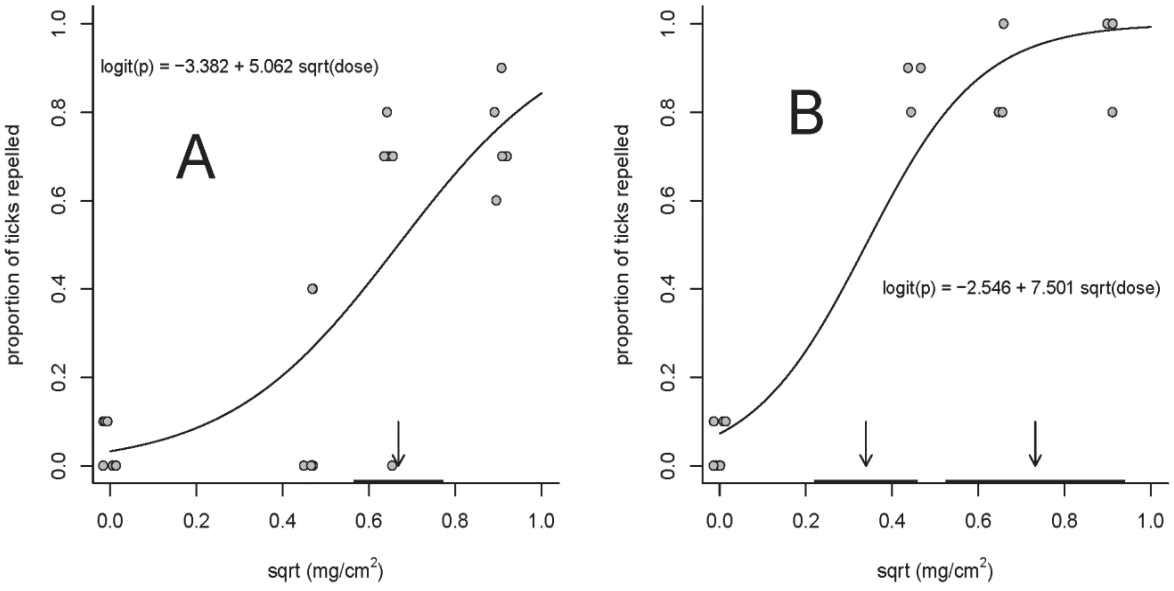

Figure 2. Responses of *A. americanum* nymphs to pondberry extract (A), DEET (B), and acetone (concentration of zero) in vertical filter paper bioassays. Estimated EC_{50} (A and B) and EC_{95} (B only) indicated by arrows.

component, *trans*-sabinene hydrate.[36]

The vertical filter paper bioassay was employed to assess repellent potential of the pondberry extract against the blacklegged tick *I. scapularis* and lone star tick *A. americanum*. The essential oil at 0.827 mg extract/cm^2 filter paper repelled 74% of the *A. americanum* nymphs (7.40 ± 0.51 of 10 ticks per replicate) and was significantly more repellent than the acetone

Table 1. GC and GC-MS analyses of pondberry crude essential oil (A) and hexanes extract (B) from *L. melissifolia* drupes

RRI [a]	Components	A% [b]	B% [b]	RRI [a]	Components	A% [b]	B% [b]	RRI [a]	Components	A% [b]	B% [b]
1000	Decane		0.2	1290	terpinolene	0.5	0.3	1740	α-muurolene		tr
1032	α-pinene	1.0	0.1	1474	*trans*-sabinene hydrate	0.2	0.5	1765	geranyl acetate	0.2	2.2
1035	α-thujene	0.5	0.1	1487	citronellal	0.6	1.1	1772	citronellol	0.5	4.3
1058	3-hexanone		0.4	1497	α-copaene		0.4	1773	δ-cadinene		0.7
1072	α-fenchene	0.1		1544	α-gurjunene		0.3	1807	α-cadinene		0.3
1076	camphene	0.1		1549	β-cubebene		0.2	1808	nerol	tr	tr
1118	β-pinene	1.2	0.3	1542	*cis*-sabinene hydrate acetate	tr	0.1	1857	geraniol	tr	0.3
1132	sabinene	66.2	17.7	1553	linalool	tr	0.2	2008	caryophyllene oxide		0.4
1159	δ-3-carene	0.2		1572	pregeijerene B	0.2	0.4	2069	germacrene D-4β-ol		3.9
1174	myrcene	2.1	0.4	1589	β-ylangene		1.1	2096	elemol		6.6
1176	α-phellandrene	4.1	1.1	1591	bornyl acetate	0.2	0.4	2187	*t*-cadinol		0.2
1188	α-terpinene	0.2	tr	1600	β-elemene		1.5	2226	methyl palmitate		0.3
1203	limonene	2.3	0.3	1612	β-caryophyllene	2.6	15.5	2255	α-cadinol		0.2
1213	1,8-cineole	1.1	tr	1659	γ-gurjunene		0.6	2257	β-eudesmol		0.2
1218	β-phellandrene	0.5	tr	1668	citronellyl acetate	0.3	1.7	2260	citronellic acid		0.4
1246	(*Z*)-β-ocimene	0.2	tr	1687	α-humulene	0.1	1.5	2369	(2*E*,6*E*)-farnesol		tr
1255	γ-terpinene	0.3	tr	1704	γ-muurolene		0.2	2431	methyl stearate		0.7
1266	(*E*)-β-ocimene	12.9	3.0	1706	α-terpineol	0.1	0.4	2456	methyl oleate		2.3
1280	*p*-cymene	0.5	0.2	1726	germacrene D	0.8	13.4	2492	ethyl oleate		0.2
1286	2-methylbutyl 2-methyl butyrate	0.2	tr	1733	neryl acetate	tr	0.4	2509	methyl linoleate		1.5
								2931	hexadecanoic acid		2.7

[a] RRI: relative retention indices calculated against *n*-alkanes; [b] Calculated from GC-flame ionization detector (FID) data; tr: trace (< 0.1%); Some components could exist as racemic mixtures

control ($P = 0.001$). DEET repellence was 93% (9.33 ± 0.67 of 10 ticks per replicate). The fit of the data for determining half maximal effective concentration (EC_{50}) and 95% maximal effective concentration (EC_{95}) values, the slopes and intercepts of the regression equations, and dispersion parameters for the pondberry essential oil and DEET are shown in **Figure 2** and **Table 2**.

Table 2. Concentrations of *L. melissifolia* essential oil and DEET estimated to repel 50 and 95% of *A. americanum* nymphs

Sample	Concentration [a] (±SE)	Intercept (±SE)	Slope (±SE)	Dispersion Parameter
Essential Oil	EC_{50} 0.668 (sqrt) (±0.050) EC_{95} 1.250 (sqrt) (±1.250)	-3.3820 (±0.695)	5.062 (±1.051)	2.050
DEET	EC_{50} 0.339 (sqrt) (±0.058) EC_{95} 0.731 (sqrt) (±1.022)	-2.546 (±0.719)	7.501 (±1.640)	2.663

[a] Concentrations as mg extract or DEET/cm^2 filter paper; sqrt: square root; SE: standard error

There was no EC_{95} determined for repellency of the pondberry essential oil against ticks because the necessary proportion of ticks was not repelled. The slope of the regression equation for DEET was significantly higher ($P = 0.001$) than that of the tested essential oil. At 0.413 mg/cm^2 filter paper, the examined essential oil repelled significantly more *I. scapularis* adults per replicate ($P < 0.0001$) with an average of 9.75 ± 0.25 (97.5%) ticks repelled compared to the acetone controls with 1.67 ± 0.33 (16.1%) adults repelled. This contrasts with *A. americanum* which required an estimated 0.668 ± 0.05 mg extract/cm^2 filter paper to repel half the ticks (**Table 2**).

The most abundant component (±)-sabinene was ineffectual ($P = 0.3168$) against *A. americanum* nymphs at 2000 nmole/cm^2 filter paper repelling an average of 1.33 ± 0.88 (13.3%) ticks per replicate. However, the same concentration of *trans*-sabinene hydrate repelled an average of 5.0 ± 1.0 (50%) *A. americanum* nymphs per replicate ($P = 0.0398$). Pondberry extract is clearly repellent to *A. americanum* and *I. scapularis* and apparently more so to *I. scapularis*. Other

repellents (e.g. DEET, SS220) tested in the vertical filter paper bioassay required higher concentrations to repel *A. americanum* nymphs than to repel *I. scapularis* nymphs.[37] A minor constituent, *trans*-sabinene hydrate (0.2% of the pondberry essential oil), showed some moderate repellent activity against *A. americanum* and may act in conjunction with other minor components.

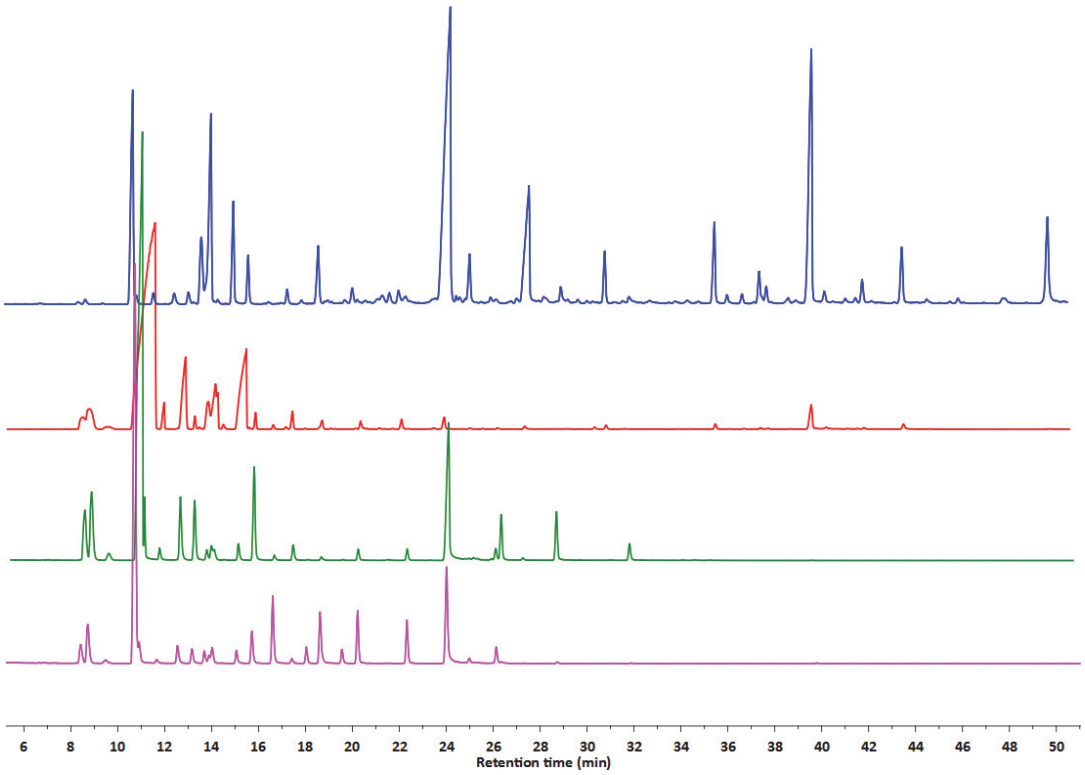

Figure 3. Stacked GC chromatograms of fractions generated by fractional freezing at -20, -42, -61, and -200 °C (from top to bottom)

Enrichment of Active Components in Pondberry Essential Oil

After the crude pondberry oil was shown to be an effective repellent against ticks, a solvent-efficient method was devised to enrich the active components. Fractional freezing, which has been traditionally utilized for purifying solvents using their different freezing points,[38,39] was employed to separate groups of volatile components from the pondberry drupes in this study (**Figure 3** and **Table 3**). The stacked GC-MS chromatograms of fractions generated by the

fractional freezing technique are shown in **Figure 3** and components in each fraction were identified using the aforementioned method (**Table 3**). The most abundant monoterpene in the crude oil was (±)-sabinene (retention time: 10-11 min, **Figure 3**) and likewise it dominated all but the -20 °C fraction (**Table 3**). Fractions collected at -20 °C and -42 °C repelled the *A. americanum* ticks to a similar extent as the crude oil (**Figure 4**), indicating that fractional freezing was effective in accumulating tick repellent components from the essential oil. Comparative analysis of each fraction (**Figure 5** and **Table 3**) identified previously reported tick repellents [geraniol (S), citronellol (AF), geranyl acetate (AD), citronellal (Q), terpinen-4-ol (U), and citronellyl acetate (AB)][40] and suggested that additional components [myrcene (F), bornyl acetate (T), β-caryophyllene (W), α-humulene (X), germacrene D (Y), and β-elemene (AE)] also possess repellent activity.

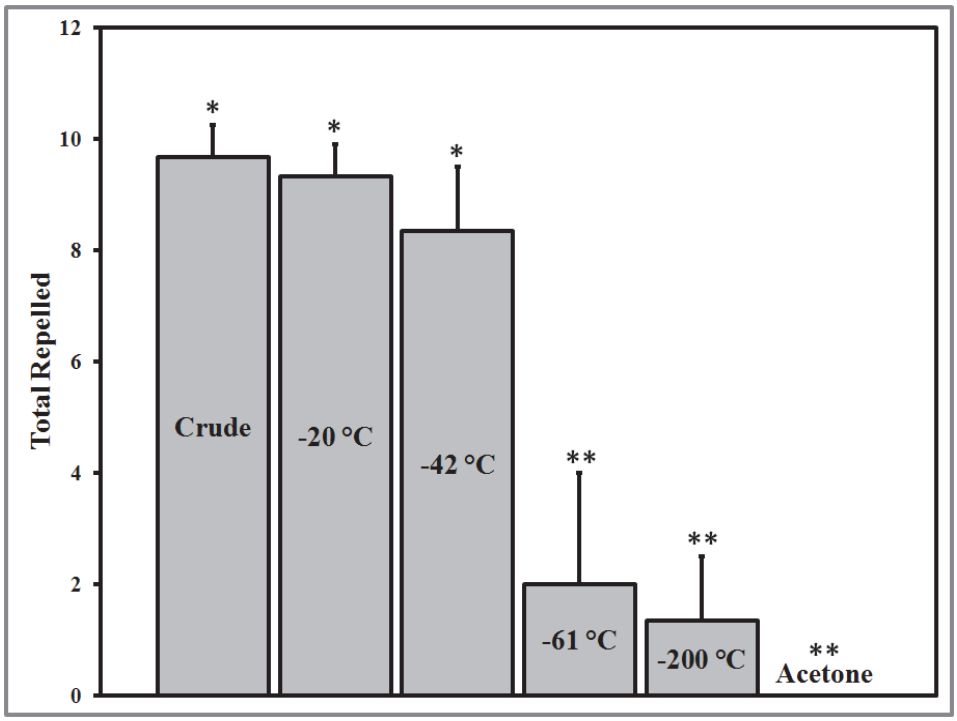

Figure 4. Mean numbers of *A. americanum* ticks repelled by pondberry crude oil, fractions (-20, -42, -61, and -200 °C), and acetone in vertical filter paper bioassay. Columns with the same number of asterisks do not differ significantly ($P > 0.05$) according to analysis of variance.

Table 3. Components (%) identified in the essential oil fractions generated by fractional freezing technique. *tr=trace

Components	Code	Fractions by Fractional Freezing			
		-20 °C	-42 °C	-61 °C	-200 °C
α-pinene	A		3.20	7.27	7.13
α-thujene	B		1.52	5.46	3.47
camphene	C		0.45		
β-pinene	D	0.28	0.32	2.67	2.87
sabinene	E	9.23	61.42	62.89	70.93
myrcene	F	0.43	1.30		
α-phellandrene	G	0.53	6.66	4.91	2.70
α-terpinene	H	0.47	0.50	4.56	2.16
limonene	I		3.87	1.10	*tr
1,8-cineole	J	8.78	1.39	0.85	2.50
(*E*)-β-ocimene	K	3.53		1.21	1.76
γ-terpinene	L	1.64	11.04	7.14	4.71
p-cymene	M	3.30	2.47	0.76	1.77
2-methylbutyl 2-methyl butyrate	N		0.48		
alloocimene	O		0.42		
terpinolene	P	0.52	0.87	1.18	
citronellal	Q	0.54	0.50		
linalool	R	2.39			
geraniol	S	0.55			
bornyl acetate	T	1.90	0.22		
terpinen-4-ol	U	28.90	0.65		
α-terpinyl acetate	V	1.87			
β-caryophyllene	W	13.80	1.69		
α-humulene	X	0.90	0.08		
germacrene D	Y	2.30	0.33		
pregeijerene B	Z		0.12		
sabina ketone	AA	0.30			
citronellyl acetate	AB	3.10	0.29		
α-copanene	AC	0.37			
geranyl acetate	AD	1.22			
β-elemene	AE	0.61	0.05		
citronellol	AF	8.34	0.17		
caryophyllene oxide	AG	4.21			

% Calculated from areas of each peaks corresponding to each components on GC chromatogram; tr : trace (< 0.1%); Some components may exist as racemic mixtures

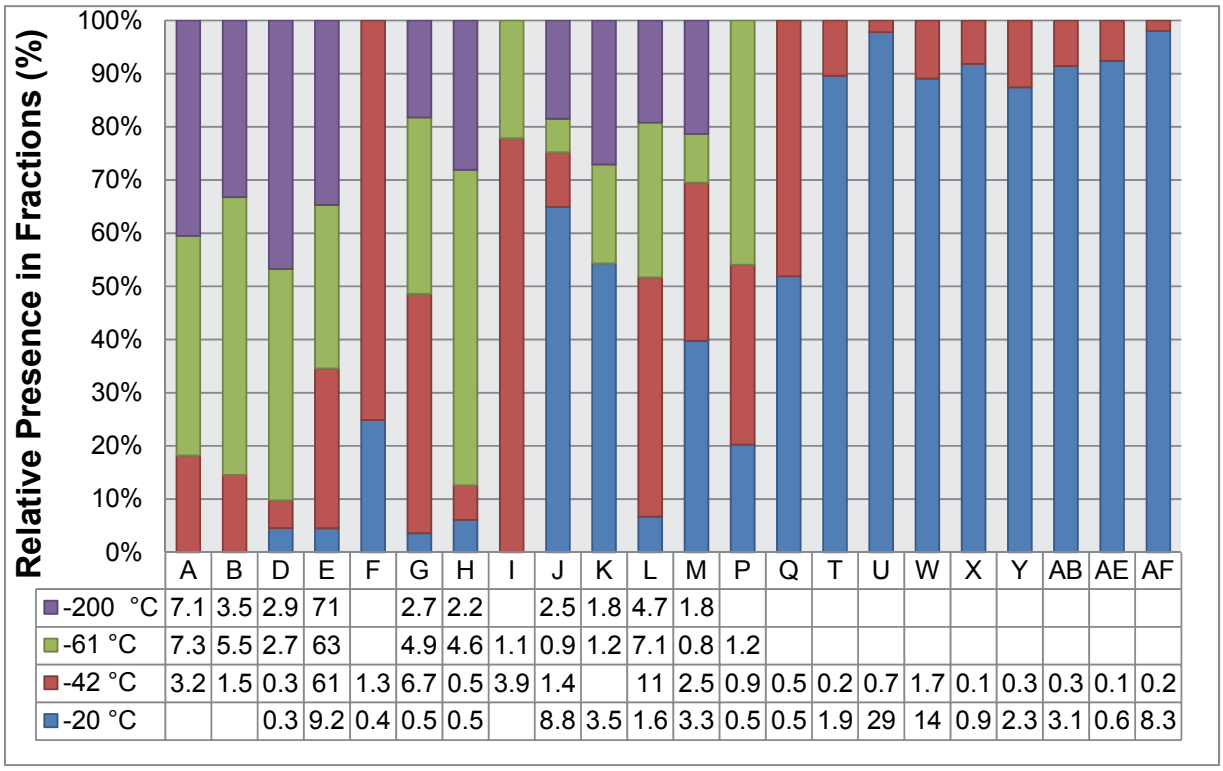

	A	B	D	E	F	G	H	I	J	K	L	M	P	Q	T	U	W	X	Y	AB	AE	AF
-200 °C	7.1	3.5	2.9	71		2.7	2.2		2.5	1.8	4.7	1.8										
-61 °C	7.3	5.5	2.7	63		4.9	4.6	1.1	0.9	1.2	7.1	0.8	1.2									
-42 °C	3.2	1.5	0.3	61	1.3	6.7	0.5	3.9	1.4		11	2.5	0.9	0.5	0.2	0.7	1.7	0.1	0.3	0.3	0.1	0.2
-20 °C			0.3	9.2	0.4	0.5	0.5		8.8	3.5	1.6	3.3	0.5	0.5	1.9	29	14	0.9	2.3	3.1	0.6	8.3

Figure 5. Scaled distribution of potential tick repellent components in the fractions generated by fractional freezing. The components detected in only one fraction were excluded for more relevant analysis. The entire list of components is shown in **Table 3**.

CONCLUSION

GC and GC–MS analyses of the essential oil from *L. melissifolia* drupes identified various mono- and sesqui-terpenoids (**Table 1**). The major constituent of the pondberry essential oil and its hexanes extract was (±)-sabinene. The NMR fingerprinting process coupled with GC and GC-MS verified that (*E*)-β-ocimene, (±)-sabinene, (±)-α-phellandrene, (±)-limonene, *p*-cymene, and myrcene were characteristic markers of the essential oil from pondberry (**Figure 1**). The essential oil repelled both the lone star and blacklegged ticks, which indicates it could be developed into a nature-derived broad spectrum repellent. Fractional freezing was verified to be an effective and solvent-efficient method to accumulate the tick repellent components in the pondberry essential oil. Although extraction with hexanes may provide a similar product (**Table 1**) it is not clear from

our tests if the hexanes extract would be active as a tick repellent. Based on our analysis of the fractions generated by fractional freezing, β-caryophyllene (W), α-humulene (X), germacrene D (Y), and β-elemene (AE) warrant further investigation as tick repellents (**Figure 5**). Although the reported compounds may be readily obtained from other plant sources or synthetic routes, agricultural techniques involving strain selection based on the metabolome of the plant may also satisfy supply requirements. Additionally, the endangered plant metabolome would provide a valuable tool for strain selection for disease and insect resistance. Thus utilization of products obtained from endangered or threatened plant species can potentially support their conservation and commercial development.

EXPERIMENTAL SECTION

General Experiments

NMR spectra were obtained using a Bruker Avance 400 MHz spectrometer referenced by residual dichloromethane and chloroform resonances. Precoated silica gel 60 F254 plates from Merck were used for thin-layer chromatography (TLC). Pentane and dichloromethane (4:1) was used to develop TLC. A vanillin-sulfuric acid stain and iodine were utilized for visualizing TLC. The application of HPLC was carried out with a Phenomenex silica column (10 × 250 mm, 5 μm) for semi-preparative injections with a Waters dual pump model 510 (flow rate 8 mL/min) and a UV absorbance detector model 486. Each fraction was collected employing a Foxy 200 fraction collector with one minute increment and identified by TLC. DEET and *trans*-sabinene hydrate used for the tick assay were purchased from Sigma-Aldrich. The major compound (±)-sabinene was isolated from the pondberry essential oil with standard chromatography techniques. In addition to the purchased *trans*-sabinene hydrate, the monoterpenoid was purified from the pondberry crude oil utilizing an HPLC method elaborated above.

Plant Material

The drupes of *L. melissifolia* (5 kg) were collected in September 2009 at the Flooding Research Facility (FRF)[41] on USFWS land in Sharkey Co., MS, jointly maintained by the USFWS and US Forest Service. The species was authenticated by Danny Skojac and Tracy Hawkins (US Forest Service). The drupe sample was combined from plants of nine female clones previously collected from the Delta National Forest, Sharkey Co., MS and USFWS property in Bolivar Co., MS. These clones were reproduced from tissue culture[42] and planted into the FRF for a large-scale physiology experiment. A voucher specimen (# 01157) has been deposited at the Herbarium of the US Forest Service Southern Hardwoods Laboratory, Washington Co., MS.

Essential Oil Extraction

Pondberry drupes (5 kg) were coarsely ground in a blender and placed in the chamber of a Speed Vac® (SC210A, Thermo Scientific, Waltham, MA) evaporator. The essential oil was collected in the glass chamber of a refrigerated vapor trap (ca. 100 °C) (RVT 4104, Thermo Scientific, Waltham, MA) under high vacuum. The essential oil contents of the trap were defrosted and collected using a separation funnel or extracted with dichloromethane. Removal of the residual solvent was completed by carefully blowing with nitrogen gas. The amount of the collected crude oil was approximately 30 g (0.6% wet weight) and the oil was stored at -20 °C. The remaining material was extracted three times by ultrasound in hexanes, which yielded 300 g of the hexanes extract.

GC, GC-MS, and NMR Analysis of Crude Essential Oil

The GC-MS analysis was carried out with an Agilent 5975 GC-mass selective detector system. A fused silica capillary column (60 m × 0.25 mm, 0.25 μm film thickness, Innowax, HP) was used with helium as carrier gas (0.8 mL/min). The GC oven temperature was kept at 60 °C

for 10 min and increased to 220 °C at a rate of 4 °C/min. This temperature was maintained for 10 min and increased to 240 °C at a rate of 1 °C/min. The injector temperature was set at 250 °C. Mass spectra were recorded at 70 eV with a mass range from *m/z* 35 to 450. The GC was carried out using an Agilent 6890N GC system. The temperature of the flame ionization detector (FID) was 300 °C. To obtain the identical elution order with GC-MS, simultaneous auto-injection was performed on a duplicate of the same column applying the consistent operational conditions described above. Relative percentage amounts of the separated components were calculated from FID chromatograms. Identification of the essential oil components was carried out by comparison of their relative retention times (t_R) with those of authentic samples or by comparison of their relative retention index (RRI) to a series of *n*-alkanes. Component identification was implemented by computer matching against commercial databases (Wiley GC/MS Library, Adams Library, MassFinder 3 Library),[43,44] and the in-house "Başer Library of Essential Oil Constituents" established based on genuine compounds of known essential oils and literature data.[45,46] Major components of pondberry essential oil, i.e. (*E*)-β-ocimene, (±)-sabinene, (±)-α-phellandrene, (±)-limonene, *p*-cymene, myrcene, and β-caryophyllene were also characterized by comparison of ^{1}H and ^{13}C NMR chemical shift data with literature data.[36,47]

Tick Repellent Assay

The tick repellent assay was implemented with reference to previous studies.[25,37,48] The *A. americanum* nymphs were obtained from a colony at Oklahoma State University, Stillwater, OK and held at 23–24 °C, ≈97% relative humidity (RH) and a photoperiod of 16 : 8 h [Light phase (L) : Dark phase (D)]. Test solutions of pondberry extracts were prepared in acetone, (±)-sabinene and *trans*-sabinene hydrate were prepared in ethyl acetate. The repellent activity of the test solutions was evaluated based on the tendency of host-seeking ticks to climb described in detail in

previous studies.[37] Ticks were tested in replicates of 10 ticks per combination of concentration of pondberry extracts or DEET. The extracts and DEET were tested against five replicates of *A. americanum* at 0.827, 0.413, 0.206, 0.103 and 0 (acetone control) mg/cm^2 filter paper. Four replicates of 10 adult *I. scapularis* ticks each were tested against 0.413 mg pondberry crude extract /cm^2 and two replicates of 10 ticks and one replicate of 11 ticks against the acetone control. Three replicates of 10 *A. americanum* nymphs each were tested against 2000 and 0 (ethyl acetate control) nmole (±)-sabinene and *trans*-sabinene hydrate/cm^2. Tests for repellency differences between components were conducted using the generalized linear models function of the R software.[49] This permitted modeling of the counts as samples from binomial distributions using the logit link function. The estimated dose to repel 50% and 95% percent of ticks and approximate 95% fiducial (inverse regression) confidence limits was estimated using the dose.p function in the package MASS.[50]

Fractional Freezing

Four different cold temperature baths (-20, -42, -61, and -200 °C) were generated and high vacuum (700 mTorr) was applied to fractionate the collected crude essential oil. The four temperatures were produced by a recirculating chiller (-20 °C), acetonitrile (-42 °C) and chloroform (-61 °C) cooled by adding dry ice and liquid nitrogen (-200 °C). The temperatures were maintained by adding coolants every 10 min. Extraction of each collected oil fraction was completed as described in the **Essential Oil Extraction** section. GC-MS analysis of the fractions generated by the fractional freezing was carried out with an HP 6890 series equipped with a split/splitless capillary injector, an HP 6890 Series injector autosampler, and a DB-5ms column (30 m × 0.25 mm × 0.25 μm, Agilent). The GC was interfaced to an HP 5973 quadrupole mass selective detector through a transfer line set at 240 °C. The injector temperature was 220 °C and 1

μL injections were performed in the split (1 : 10) mode. The column flow was set at a constant pressure of 10 psi, providing a nominal initial flow of 1.2 mL/min with helium as carrier gas. The oven temperature was raised from 60 to 300 °C at a rate of 3 °C/min for a total run time of 80 min. The filament was operated at 70 eV with an emission current of 35 μA. The multiplier voltage was automatically set to 2094 V. The ion source and quadrupole temperatures were set with 230 and 120 °C, respectively. The acquisition range was *m/z* 35–800 at 1.95 scans per second, starting 2.5 min after injection. Components of the four fractions were identified by the identical fashion delineated in the **GC, GC-MS and NMR Analysis of Crude Essential Oil** section.

CHAPTER 2: CONFIGURATIONAL ASSIGNMENTS OF CONFORMATIONALLY RESTRICTED MEROTERPENOIDS FROM *L. MELISSIFOLIA*

INTRODUCTION

Endangered plant species are an underutilized source for new chemistry. These discoveries ironically hold the potential for development into a commercial application that would justify the conservation of those plant species in jeopardy. This is evidenced by a recent phylogenic analysis which shows drug producing plant families are concentrated around families which contain endangered species.[51] However, the challenge associated with such limited resources often prohibits the full elucidation of new structures utilizing conventional techniques such as X-ray crystallography or spectrometric techniques. The discovery of new meroterpenoid-based hydroquinones from a US endangered plant provides a unique opportunity in this regard. Owing to the conformationally restricted assemblies, investigation of these hydroquinones permits the demonstration of how quantum mechanical (QM) calculations combined with NMR and electronic circular dichroism (ECD) studies can assign three dimensional structures in cases where investigation of such stereochemical detail might not otherwise be feasible due to mass limitations.

The endangered status of *L. melissifolia* found in the Southeastern US prompted our study of the plant as an example of how endangered US plants can yield novel chemistry that could potentially be lost due to extinction. The drupes of *L. melissifolia* commonly called pondberry exhibits a dose-dependent tick repellency as discussed in **Chapter 1**.[52] The ethyl acetate extract of pondberry drupes exerting anti-infective activities was investigated to identify two new hydroquinone-based meroterpenoid hydroquinones named melissifolianes A (**1**) and B (**2**) (**Figure 6**). The structures of the melissifolianes combine a common 2-(hydroquinone) acetic acid ester moiety flanked uniquely by two monoterpenoid units in contrast to a single monoterpenoid moiety as reported in *Magnolia denudata*.[53] The limited amounts of the melissifolianes neither enabled

assignment of their stereostructure by chemical methods nor facilitated investigation of appropriate conditions for crystallization. However, the conformationally restricted state, associated with the acetic ester moiety that bridged hydroquinone and terpenoids moieties, provided the opportunity to employ computational methods to establish stereochemical details of those meroterpenoids. Herein, we report the use of NMR and ECD analysis coupled with QM calculations for the full structural assignment of natural products like the melissifolianes possessing conformationally restricted moieties.

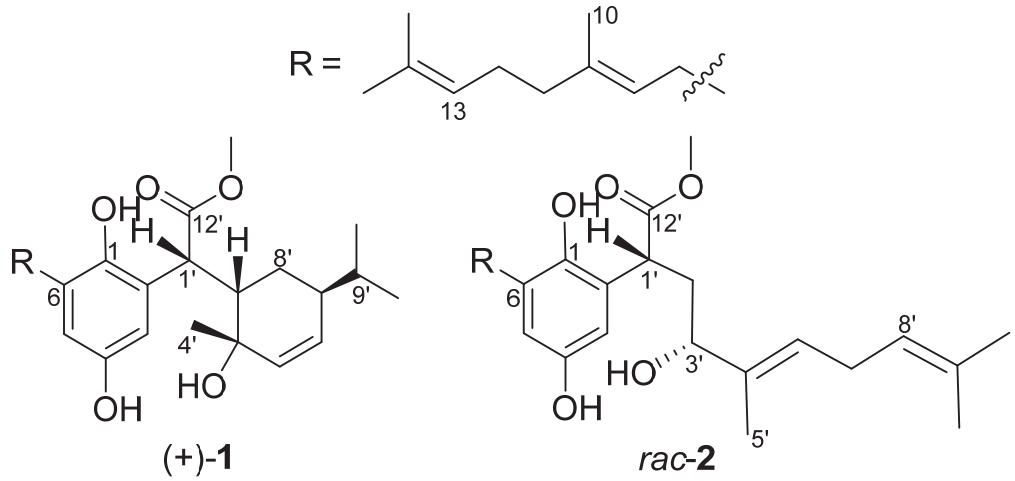

Figure 6. Structure of melissifolianes A (**1**) and B (**2**)

RESULTS AND DISCUSSION

The ^{1}H NMR data of melissifolane A (**1**) (**Table 4**) showed resonances for isopropyl-type methyl protons (δ_H 0.98, 0.93), two *m*-coupled aromatic protons (δ_H 6.58, 6.56), and three allylic methyls and one methyl group attached to an oxygenated carbon (δ_H 1.70, 1.33, 1.63, 1.69). Deshielded methyl protons were observed at δ_H 3.83, suggesting a methyl ester functional group which was confirmed by a heteronuclear multiple-bond correlation spectroscopy (HMBC) correlation between the protons and ester carbonyl at δ_C 173.4. The ^{13}C NMR resonances deduced

from the heteronuclear single-quantum correlation spectroscopy (HSQC) spectrum indicated a benzene ring bearing two oxygenated carbons (δ_C 148.4, 144.2, 131.2, 117.0, 115.8, 113.3).

Table 4. ^{1}H and ^{13}C NMR data of melissifolianes A and B (**1** and **2**). The numberings shown in this Table are corresponding to those in **Figure 6**.

	1		**2**	
	^{1}H (multi, *J* in Hz)	^{13}C	^{1}H (multi, *J* in Hz)	^{13}C
1		144.2		146.9
2		117.0		118.8
3	6.56 (1H, br d, 2.6)	113.3	6.47 (1H, br d, 2.9)	111.3
4		148.4		148.5
5	6.58 (1H, br d, 2.4)	115.8	6.57 (1H, br d, 2.7)	115.8
6		131.2		131.3
7	3.31, 3.18 (2H, dd, 14.9, 7.5)	28.3	3.27 (2H, d, 7.5)	28.1
8	5.28 (1H, t, 7.03)	122.2	5.30 (1H, t, 7.5)	121.9
9		136.1		136.4
10	1.69 (3H, s)	16.2	1.68 (3H, s)	16.1
11	2.04 (2H, m)	39.8	2.05 (2H, m)	39.8
12	2.10 (2H, m)	26.7	2.12 (2H, m)	26.7
13	5.12 (1H, t, 5.9)	124.4	5.13 (1H, t, 7.6)	124.3
14		131.3		131.4
15	1.70 (3H, s)	25.7	1.70 (3H, s)	25.7
16	1.62 (3H, s)	17.7	1.62 (3H, s)	17.7
1'	4.15 (1H, d, 6.2)	43.3	3.98 (1H, dd, 11.3, 6.4)	42.8
2'	2.28 (1H, ddd, 13.9, 6.1, 2.9)	35.4	2.26, 2.19 (2H, m)	30. 5
3'		72.3	4.27 (1H, dd, 10.70, 3.69)	79.4
4'	1.33 (3H, s)	24.6		134.0
5'	5.80 (1H, d, 9.9)	131.7	1.77 (3H, s)	12.2
6'	5.97 (1H, dd, 9.9, 4.6)	134.0	5.53 (1H, t, 7.1)	126.4
7'	1.93 (1H, m)	40.8	2.79 (2H, t, 6.9)	26.7
8'	1.63, 1.37 (2H, m)	23.2	5.13 (1H, t, 6.8)	122.3
9'	1.66 (1H, m)	31.7		132.1
10'	0.93 (3H, d, 6.7)	20.9	1.66 (3H, s)	17.8
11'	0.98 (3H, d, 6.5)	21.0	1.72 (3H, s)	25.7
12'		173.4		174.1
13'	3.83 (3H, s)	51.9	3.77 (3H, s)	52.2

The inspection of HMBC and double quantum filter-correlation spectroscopy (DQF-COSY) spectra revealed that the gross structure of melissifoliane A (**1**) was based on a 2-(hydroquinone)acetic acid ester moiety flanked by two monoterpenoid units (**Figure 7**A). The connectivity between the cyclic terpenoid and 2-(hydroquinone) acetic acid ester groups was confirmed by the COSY correlation between H-1' (δ_H 4.15) and H-2' (δ_H 2.28), and the HMBC correlations between H-1' and C-8' (δ_C 23.2), and H-3 (δ_H 6.56) and C-1' (δ_C 43.3) (**Figure 7**A). The acyclic terpene unit was similarly connected to C-6 of the hydroquinone moiety based on the COSY correlation of H-7 (δ_H 3.31, 3.18) and H-8 (δ_H 5.28), and the HMBC correlations H-8 and C-6 (δ_C 131.2), H-7 and C-5 (δ_C 115.8), and H-7 and C-1 (δ_C 144.2) (**Figure 7**A). The configuration of melissifoliane A (**1**) was established by utilizing an ensemble of distinctive NMR chemical shift values, nuclear Overhauser effect (NOE) correlations, and QM calculation. The (*E*) C-8–C-9 olefin geometry was assigned based on a characteristic pair of carbon resonances for the C-10 methyl and the C-11 methylene at δ_C 16.2 and 39.8, respectively, and NOE correlations

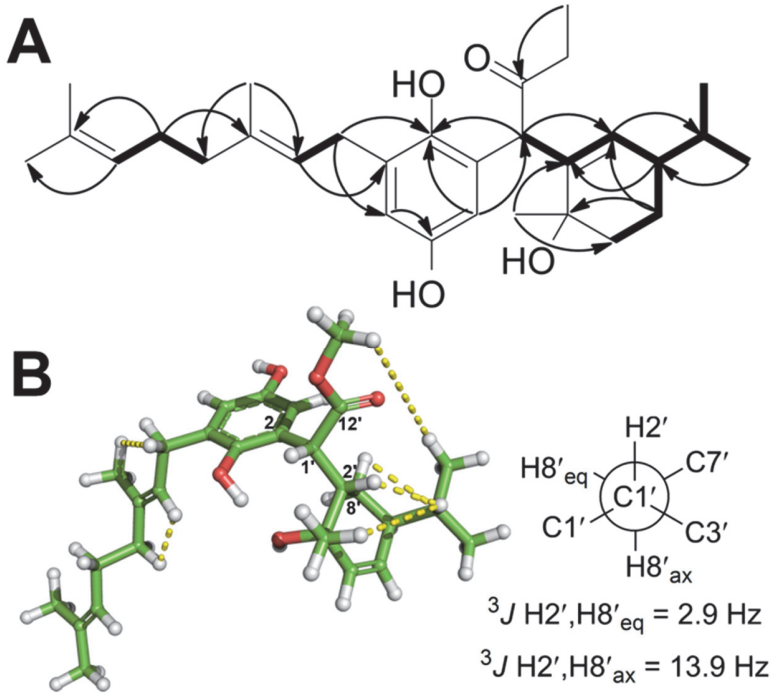

Figure 7. (A) Key HMBC (arrows) and COSY (bold lines) and (B) Key NOEs (dotted lines) of melissifoliane A (**1**)

between H_2-7 (δ_H 3.31, 3.18) and H_3-10 (δ_H 1.69), and H-8 (δ_H 5.28) and H_2-11 (δ_H 2.04) (**Figure 7**B).

The relative configuration of the hydroxylated monoterpenoid moiety was established based on the NOE correlations between H-2' (δ_H 2.28) and H-9' (δ_H 1.66), H-4' (δ_H 1.33) and H-9', and H-8' (δ_H 1.63, 1.37) and H-9'. $^3J_{H\text{-}2',H\text{-}8'ax}$ (13.9 Hz) and $^3J_{H\text{-}2',H\text{-}8'eq}$ values (2.9 Hz) suggested that the cyclohexene moiety predominantly occupies a half-chair conformation. The orientation of the isopropyl group was assigned by the NOE correlations between H-11' (δ_H 0.98) and the methyl ester group H-13' (δ_H 3.83). Thus, the relative configuration of the cyclic monoterpenoid unit was tentatively assigned 2′*S**, 3′*S**, 7′*S**.

The observed $^3J_{H1',H2'}$ value (6.2 Hz) indicated a significant conformational change associated with the C-1'–C-2' bond, thus indicating that the establishment of C-1' configuration would be challenging. The NMR and QM combined approach was utilized for the comparison between experimental and calculated spin-spin coupling constants (SSCCs) to establish the relative configuration of C-1'. Geometries were optimized in Jaguar (Schrödinger LLC.) using density functional theory (DFT) at the MPW1PW91/6-31G(d,p) level for all six staggered rotamers associated with the C-1′–C-2′ bond of diastereomers I and II having different C-1′ configurations (**Figure 8**). The SSCCs of each rotamer were calculated using the same theory and basis set in Gaussian09 (**Figure 8**, **Table 5**). To measure experimental homo- and hetero- coupling constants,

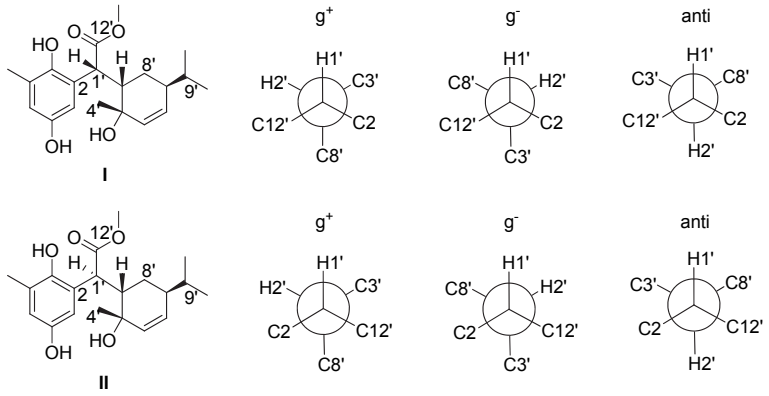

Figure 8. Diastereomers I and II, the plausible structures of melissifoliane A (**1**) with different C-1' configurations along with the Newman projections for all possible staggered rotamers associated with the C-1'–C-2' bond

^{1}H NMR, and heteronuclear long-range coupling (HETLOC) were employed. The total absolute deviation (TAD)[54,55] between the experimental and calculated values (**Figure 8**, **Table 5**) verified that the calculated SSCCs of diastereomer I in **Figure 8** with 1′*R**, 2′*S**, 3′*S**, 7′*S** showed a better agreement with the experimental *J* values.

Table 5. Calculated SSCCs (Hz) of the staggered rotamers of diastereomers I and II shown in **Figure 8** with the experimental values.

	Calculated SSCC [a]						Exp. [b]
	I			II			
	g^+	g^-	anti	g^+	g^-	anti	
$^3J_{H1', H2'}$	3.9	5.0	6.9	4.1	4.1	9.3	6.2
$^3J_{H1', C8'}$	5.9	1.4	4.6	5.3	2.8	1.9	6.5
$^2J_{H1',C2'}$	-4.6	-1.5	-5.2	-1.8	-3.8	-1.9	-5.0
$^2J_{C1',H2'}$	-3.9	-4.0	-4.3	-3.3	-3.8	-4.4	-5.0
TAD	**4.4**	10.8	**3.5**	8.2	8.2	11.4	

[a] MPW1PW91/6-31G(d,p) calculated *J* values. [b] Experimental *J* values (Exp.) observed from HETLOC and ^{1}H NMR spectra. TAD values calculated from ($\Sigma|J_{calc} - J_{exp}|$). The lowest TAD values in bold are found in diastereomer I.

The absolute configuration of melissifoliane A (**1**) was assigned by comparison of the calculated and experimental ECD spectra.[56-63] The major conformers were generated by selecting dihedral angles for the rotamers associated with the C-6–C-7, C-2–C1', C-1'–C-2', and C-1'–C-12' bonds. The conformation of the cyclohexene moiety was fixed as a half-chair conformation based on the coupling constants analysis described above. The Amber* force field was used to define the initial geometries of generated conformers followed by PM6[64] semi-empirical optimizations. These conformers were subsequently used in DFT B3LYP/6-31G(d,p) calculations to obtain more accurate geometries in the gas phase and in MeCN.[65,66] The 24 lowest-energy conformers within an energy window of 50 kJ/mol (conformers 1–24, for their coordinates see Supplementary Data 2 in the original article[67]) exhibited different intramolecular hydrogen bond interactions, involving

the C-1 and C-3' hydroxy groups and the C-12' ester oxygen atoms. Such hydrogen bonding partially restricted rotation of the C-12'–C-1', C-1'–C-2, and C-1'–C-2' bonds.

The full array of conformers was used for calculations of the excited state in the gas phase and in MeCN using time-dependent density functional theory (TDDFT). The excitation energies and rotational strengths of each conformer were Boltzmann-weighted according to the calculated Gibbs free energies and subsequently fitted to Gaussian 09 (Gaussian Inc.) functions to simulate ECD curves. The major conformers found at the B3LYP/6-31G(d,p) level were further optimized, and employed for ECD calculations at the B3LYP/6-311G++(2d,p) level to validate the initial ECD calculations at the B3LYP/6-31G(d,p) level. The experimental ECD spectrum of melissifoliane A (**1**) shows Cotton effects characteristic of the $n \rightarrow \pi^*$ electronic transition of the ester functionality at ca. 300 nm, the ^1L_b transition of the aromatic chromophore at ca. 260 nm, and the ^1L_a transition of the aromatic chromophore in the 220–240 nm region (**Figure 9**). **Figure 9** depicts overlays of the experimental ECD spectrum of melissifoliane A (**1**), the average calculated spectrum of the major conformers of melissifoliane A (**1**) at the B3LYP/6-31G(d,p) and B3LYP/6-311++G(2d,p) levels, respectively. The calculated ECD data employing the different

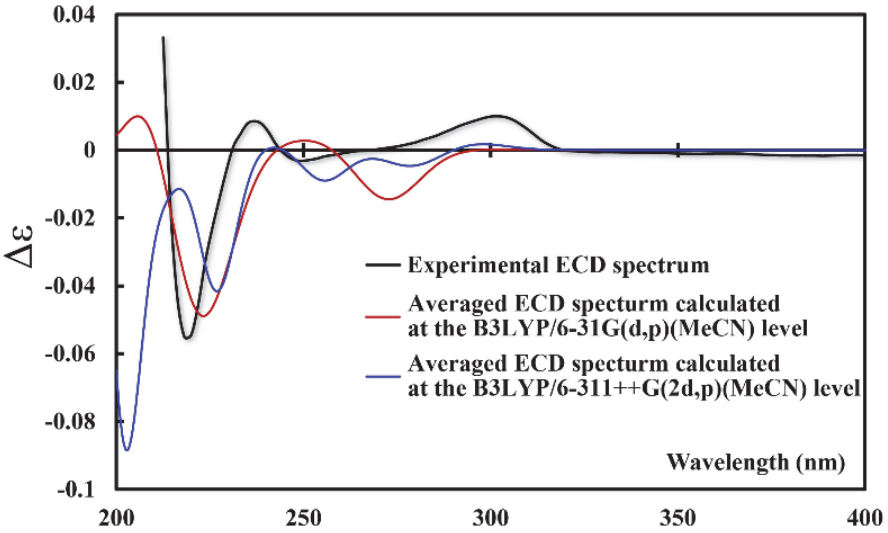

Figure 9. Overlaid experimental and averaged calculated ECD spectra of melissifoliane A (**1**) utilizing the two difference basis sets

basis sets shown in **Figure 9**, taken in conjunction with the experimental ECD curve, was sufficient to assign the absolute configuration as 1'*R*, 2'*S*, 3'*S*, 7'*S*.

The 1D NMR data of melissifoliane B (**2**) (**Table 4**) resembled those of melissifoliane A (**1**), which suggested that it shared structural similarities with the exception of the nature of the methyl groups of the C-1' substituent. The acyclic terpene and hydroxylated terpenoid moieties were connected to C-6 (δ_C 131.3) and C-1' (δ_C 42.8), respectively, using similar DQF-COSY and HMBC correlations as described for melissifoliane A (**1**). The C-8–C-9 olefin geometry was established as *E* based on the NOE correlations between H_2-7 (δ_H 3.27) and H_3-10 (δ_H 1.68), and H-8 (δ_H 5.30) and H_2-11 (δ_H 2.05). The *E* geometry of the C-4'–C-6' olefinic bond was assigned by the chemical shift values of C3' (δ_C 79.4) and C5' (δ_C 12.2) and NOE correlations between H_3-5' (δ_H 1.77) and H_2-7' (δ_H 2.79), and H-3' (δ_H 4.27) and H-6' (δ_H 5.53). Melissifoliane B was optically inactive which suggested a racemic mixture, which was confirmed by chiral chromatography (**Figure 19**). The attempt to assign the relative configuration of melissifoliane B (**2**) using *J*-based analysis failed because of the lack of a relevant model for phenyl substituents and infeasibility in measuring the $^3J_{CH}$ involving quaternary carbons of the hydroquinone moiety. Consequently, the relative configuration of melissifoliane B (**2**) was also established employing the identical manner as for **1**.[68] The gauche$^+$ conformer associated with C-1′–C-2′ exhibited the lowest TAD value and this conformer was assembled with the major conformer of the C-2′–C-3′ bond identified by *J*-based analysis (**Figure 10**). This collectively elucidated the relative configuration of melissifoliane B (**2**) as 1′*R** and 3′*R**.

CONCLUSIONS

Our study of the *Lindera melissifolia* metabolome exemplifies how new chemistry remains undiscovered among the numerous endangered plant species. This also demonstrates how analysis

by ECD and NMR techniques combined with various QM calculations is a valuable approach to support the stereochemical assignment of molecules possessing conformationally restricted bonds linking the different structural moieties. Utilization of the secondary metabolites obtained from other endangered plant species may serve as added justification for conservation of such plants given potential socioeconomic value they may generate.

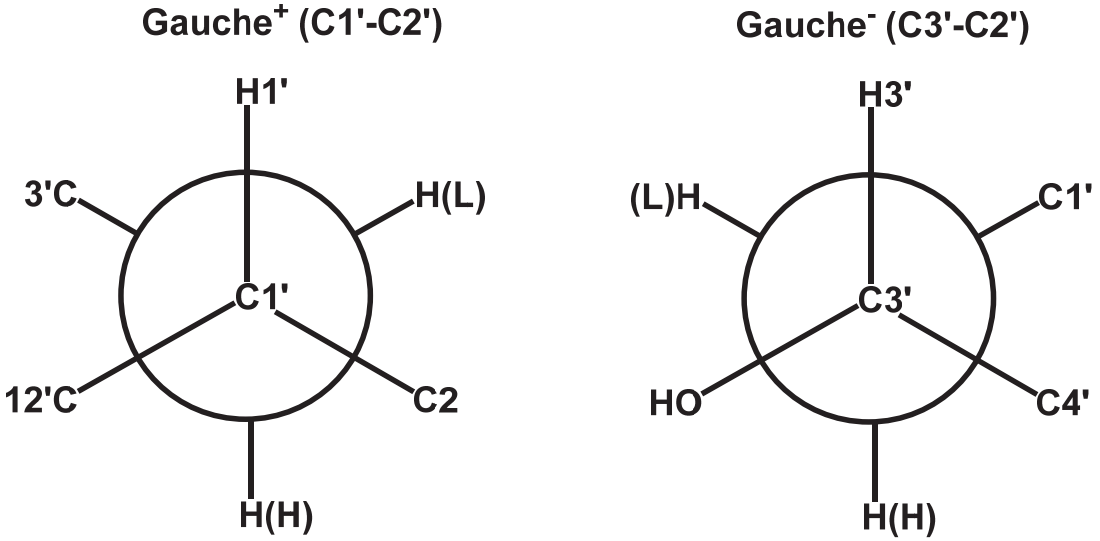

	Gauche^{+} (C-1'–C-2')	
	Calcd. SSCC [a]	Exp. [b]
$^{3}J_{H1', H(H)}$	11.3	11
$^{3}J_{H1', H(L)}$	3.2	5.2
$^{3}J_{H1', C3'}$	2.9	1.5
$^{2}J_{C1', H(H)}$	-3	-4
$^{2}J_{C1', H(L)}$	-3.1	-4
TAD	**5.6**	

Gauche^{-} (C-3'–C-2')	
	Exp. [b]
$^{3}J_{H(H), H3'}$	10.7
$^{3}J_{H(L), H3'}$	3.7
$^{3}J_{H3', C1'}$	3
$^{2}J_{H(H), C3'}$	-6
$^{2}J_{H(L), C3'}$	-4

Figure 10. The major conformers suggested by QM calculation (C-1′–C-2′, left) and *J*-based analysis (C-2′–C-3′, right). H(H) and H(L) indicate 2.26 and 2.19 ppm, respectively. [a] SSCCs were calculated at MPW1PW91/6-31G(d,p). [b] Experimental *J* values observed from HETLOC, exclusive COSY (E. COSY), and ^{1}H NMR spectra. TAD: See **Table 5**.

EXPERIMENTAL SECTION

General Procedures

NMR spectra were obtained using a Bruker Avance 400 MHz spectrometer referenced by residual dichloromethane and chloroform resonances. Homo- and hetero-nuclear coupling constants were measured using ^{1}H NMR, E. COSY, and HETLOC. Optical rotations were measured on a Rudolph Autopol V polarimeter. UV-vis spectra were recorded on an Agilent 1100 series diode array and multiple wavelength detectors. The LC-MS analyses were performed using an Agilent 1100 HPLC system equipped with a Phenomenex Luna 5 μm C_8(2) column (4.6 × 150 mm), an MeOH/H_2O (0.1% HCOOH) gradient solvent system, and a Bruker Daltonics microTOF mass spectrometer. For chiral chromatography, an Astec Chirobiotic R column (4.6 × 100mm) was utilized eluting with a 55% MeOH/H_2O isocratic solvent condition (20 mM NH_4Ac, 35 °C). HRESIMS spectra were obtained employing a Bruker Daltonics microTOF mass spectrometer with electrospray ionization. Column chromatography was conducted using silica gel 60 (40–63 μm particle size) and reverse phase (RP)-18 (40–63 μm particle size). Precoated TLC silica gel 60 F254 plates (Merck) were used for TLC. HPLC was performed on a Waters System equipped with Waters 2487 dual absorbance detector. Experimental ECD spectrum was acquired at 5 °C with an Olis CD spectrophotometer. The concentration of the sample was 500 μg/mL in MeCN and the path length was 5 mm.

Extraction and Purification

For the collection and authentication of the plant material, see **Plant Material** section in **Chapter 1**. The dried ripe drupes of *L. melissifolia* were coarsely ground and extracted with EtOAc, and the extract was dried under reduced pressure to give 100 g of crude extract. The extract was fractionated on silica gel eluted with hexanes-EtOAc (100:0, 80:20, 50:50 and 0:100) and then with EtOAc-MeOH (80:20, 50:50 and 0:100) to afford 10 fractions, respectively. Fractions 6–9

exhibited significant anti-infective activities and these active fractions were further chromatographed by normal phase HPLC [Phenomenex Luna silica, 50 × 250 mm, 10 μm, flow rate 30 mL/min] with a gradient elution of hexanes-EtOAc (1:0 to 8:2 over 120 min) and, finally, by RP HPLC [Waters C_{18} 20 × 250 mm, 10 μm, flow rate 10 mL/min; Phenomenex C_{18} 5 × 250 mm, 5 μm, flow rate 1 mL/min] using a gradient elution of H_2O-MeOH (1:1 to 0:1 over 110 min) to obtain the pure compounds.

- Melissifoliane A (**1**)

Melissifoliane A (**1**, t_R = 46 min), a pale yellowish oil, had the molecular formula $C_{29}H_{42}O_5$ deduced from HRESIMS data (obsd $[M+Na]^+$-H_2O at *m/z* 475.2842, calcd $[M+Na]^+$-H_2O at *m/z* 475.2819; obsd $[2M+Na]^+$-H_2O at *m/z* 927.5725, calcd $[2M+Na]^+$-H_2O = 927.5751). The specific rotation ($[\alpha]_D^{23}$) was established as +54.0 (*c* 0.2, MeCN). For ^1H and ^{13}C NMR data, see **Table 4**.

- Melissifoliane B (**2**)

Melissifoliane B (**2**, t_R = 45 min), a pale yellowish oil, had the molecular formula $C_{29}H_{42}O_5$ as deduced from HRESIMS results (obsd $[M+Na]^+$-H_2O at *m/z* 475.2852, calcd $[M+Na]^+$-H_2O at *m/z* 475. 2819; obsd $[2M+Na]^+$-H_2O at *m/z* 925.5530, calcd $[2M+Na]^+$-H_2O =927.5751). For ^1H and ^{13}C NMR data, see **Table 4**.

QM Computational Calculation

ECD calculation

Initial conformational analysis was conducted using the Amber* force field in the MacroModel program included in the Schrödinger software package (Schrödinger LLC.). The resulting structures were optimized using the PM6 semi-empirical method in the Gaussian 09 package (Gaussian Inc.). The PM6-optimized structures were further optimized using DFT gas-

phase calculations. The geometry optimizations and frequency calculations of the conformers 1–24 were implemented using the hybrid DFT method B3LYP with the 6-31G(d,p) basis set, specifying tight convergence. The major conformers (conformers 1, 3, 5, 6, 13, 14, 15, 16, 17 and 19) from the optimization process were further minimized at the B3LYP/6-311++G(2d,p) level with tight convergence in order to validate the effects of including a larger basis set. Separate optimizations were carried out starting from the PM6-optimized structures using the conductor-like polarizable continuum solvation model with a dielectric constant representing MeCN. The excited state calculations were performed using the TDDFT method with B3LYP with each of the two basis sets [i.e., 6-31G(d,p) and 6-311++G(2d,p)]. The generated excitation energies and rotational strengths were weighted using Boltzmann averaging based on the calculated Gibbs free energy of each conformer and then fitted with a Gaussian function to generate the computed ECD spectra. These raw computed data were visualized utilizing SpecDis[69] for comparison to the experimental ECD spectrum.

SSCC calculation

Geometries were optimized in Jaguar (Schrödinger LLC.) using DFT at the MPW1PW91/6-31G(d,p) level for all six staggered rotamers of each diastereomer associated with C-1'–C-2' of melissifolianes A and B (**1** and **2**). The SSCC of each rotamer was calculated using the same theory and basis set in Gaussian09.[70] The total absolute deviation (TAD)[54,55] between experimental and calculated values was used to suggest the most relevant conformers.

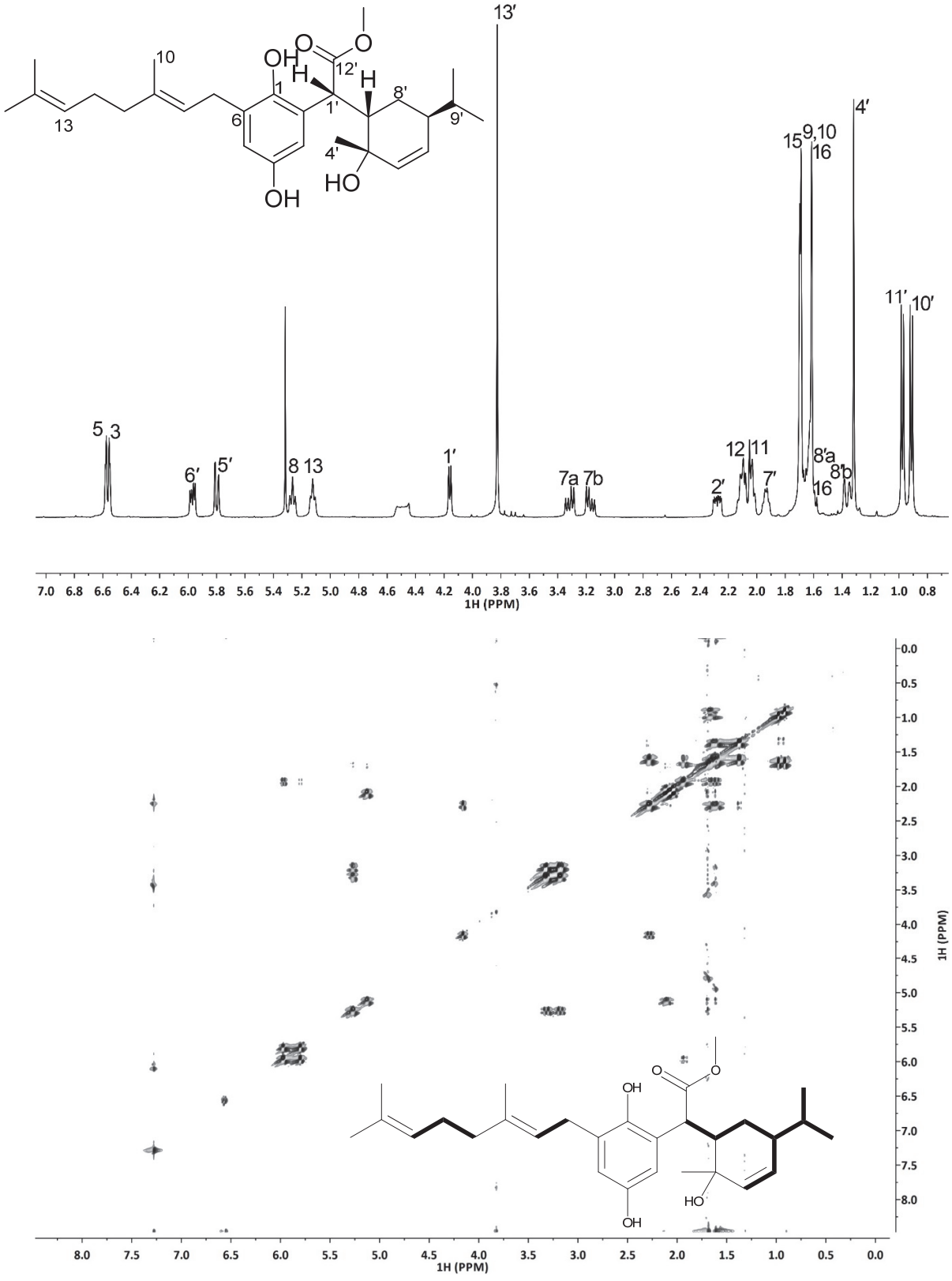

Figure 11. [1]H NMR (top) and DQF-COSY (bottom) spectra of melissifoliane A (**1**)

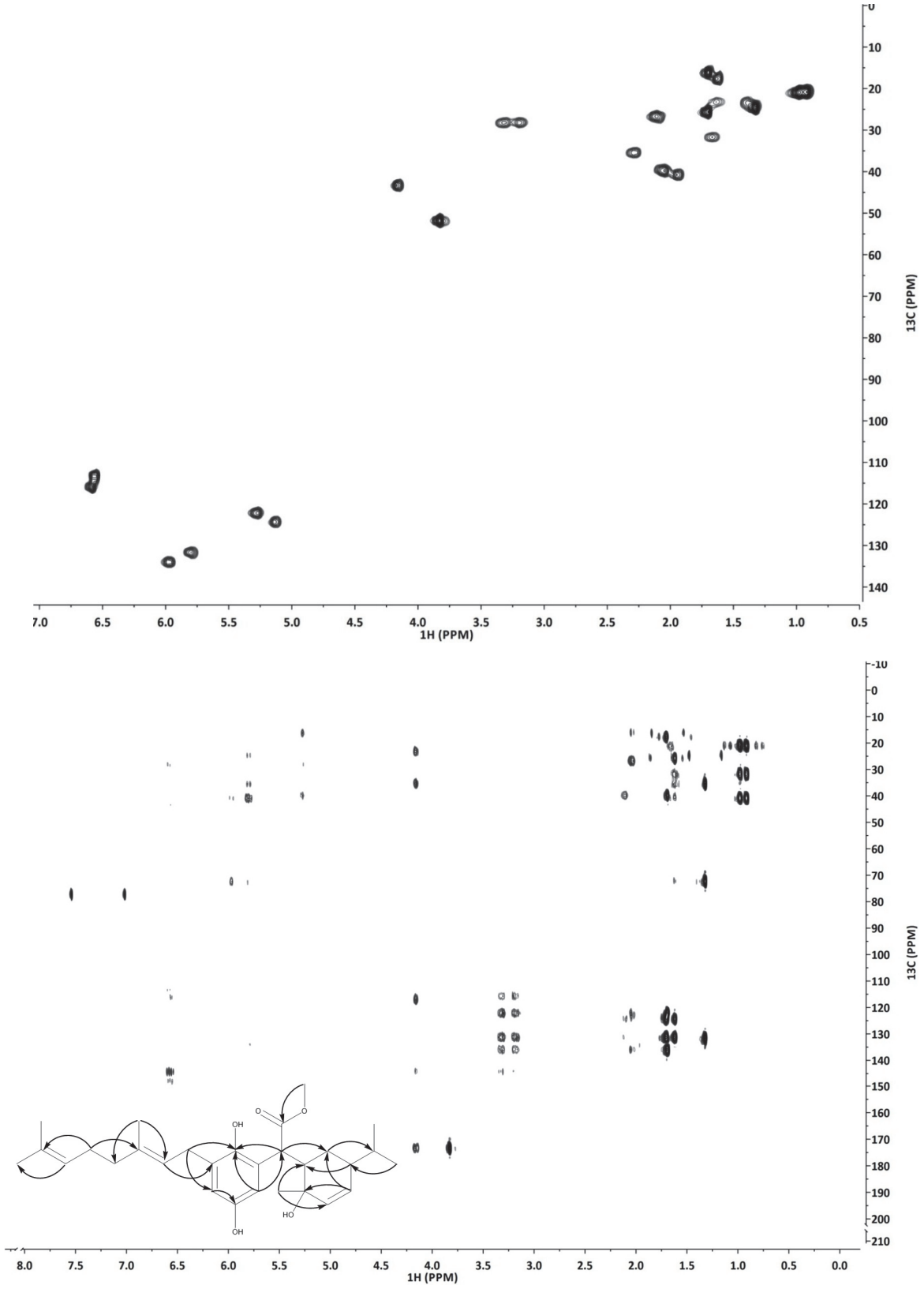

Figure 12. HSQC (top) and HMBC (bottom) spectra of melissifoliane A (**1**)

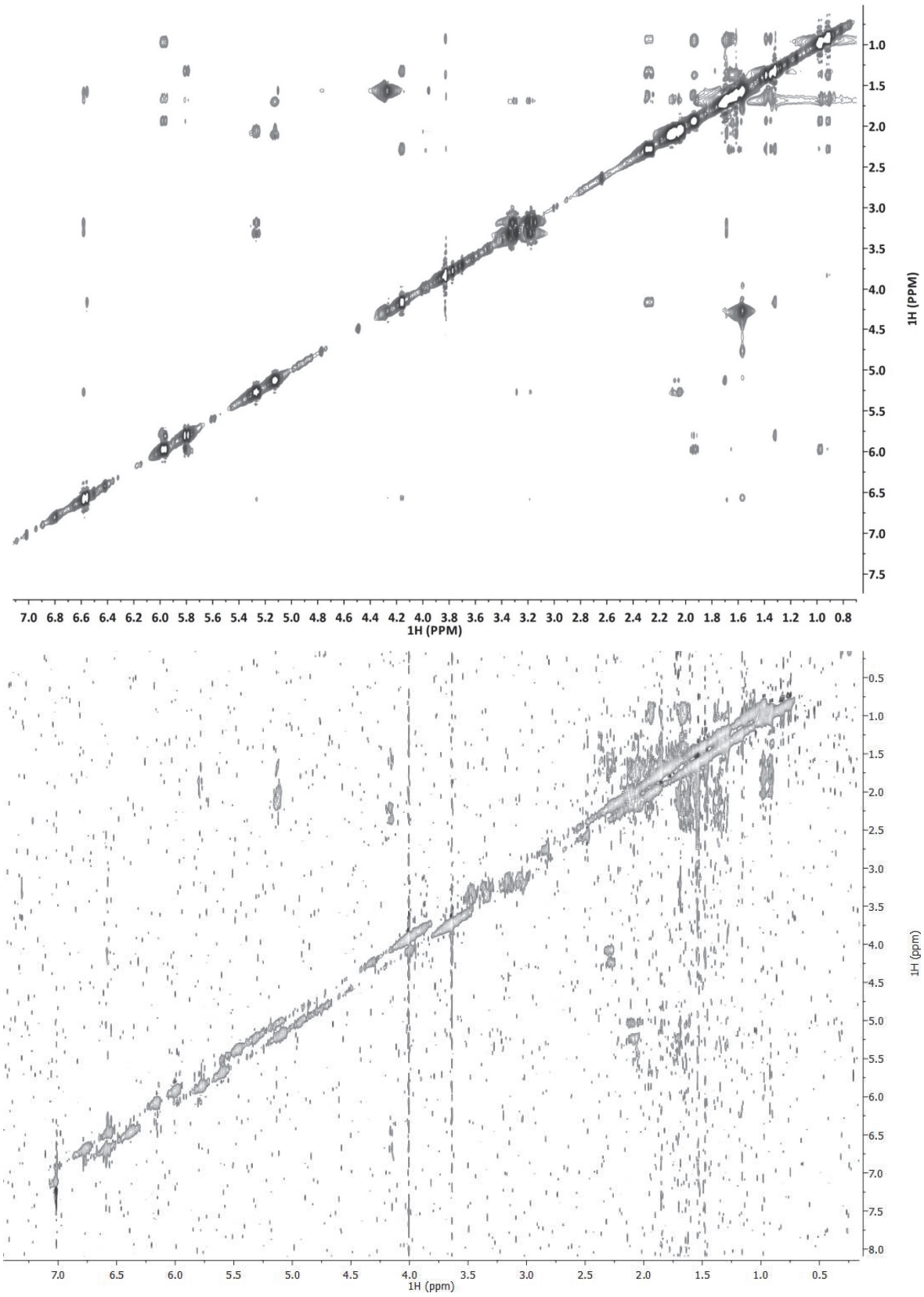

Figure 13. NOESY (top) and HETLOC (bottom) spectra of melissifoliane A (**1**)

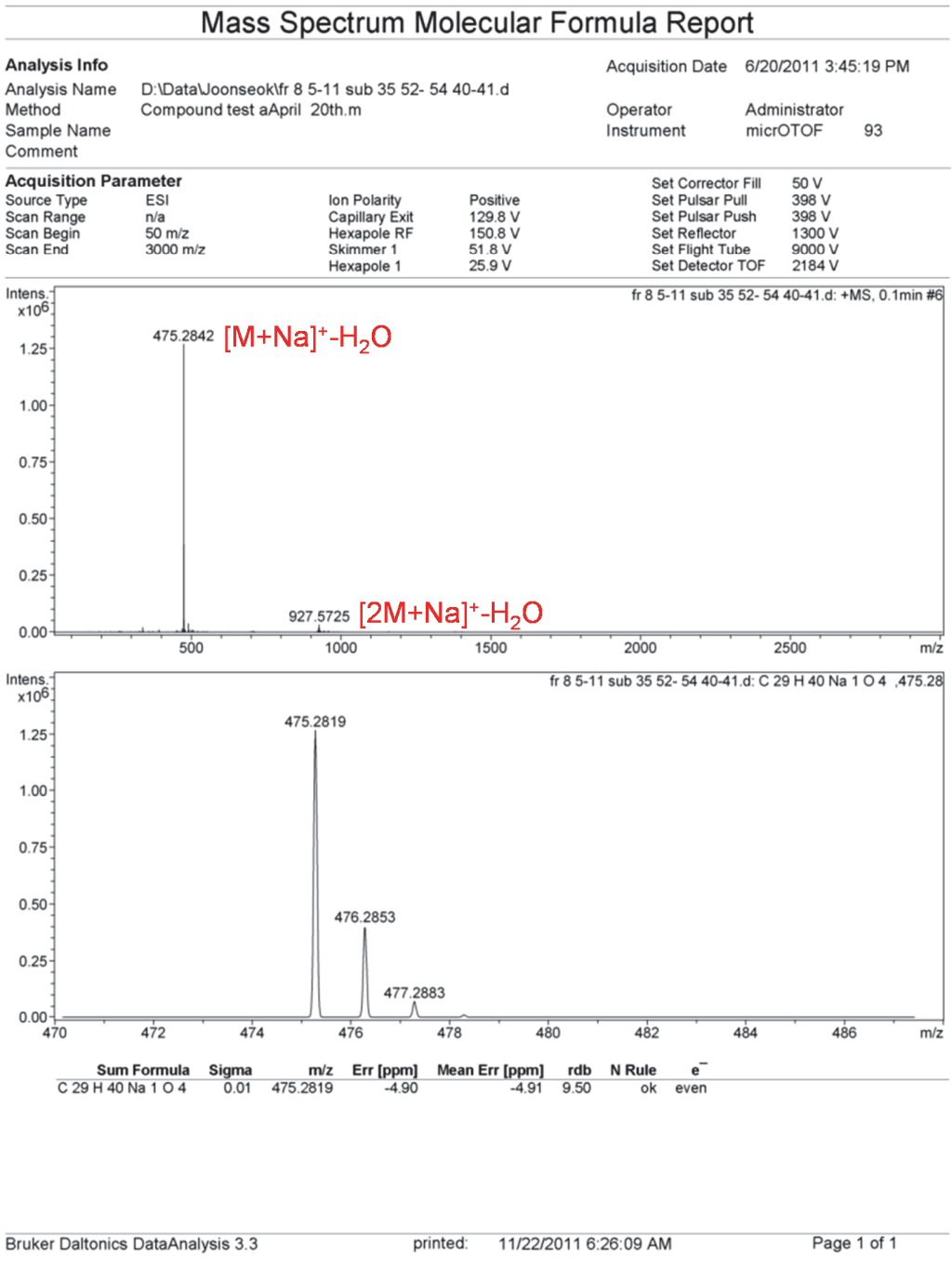

Figure 14. HRESIMS spectrum of melissifoliane A (**1**)

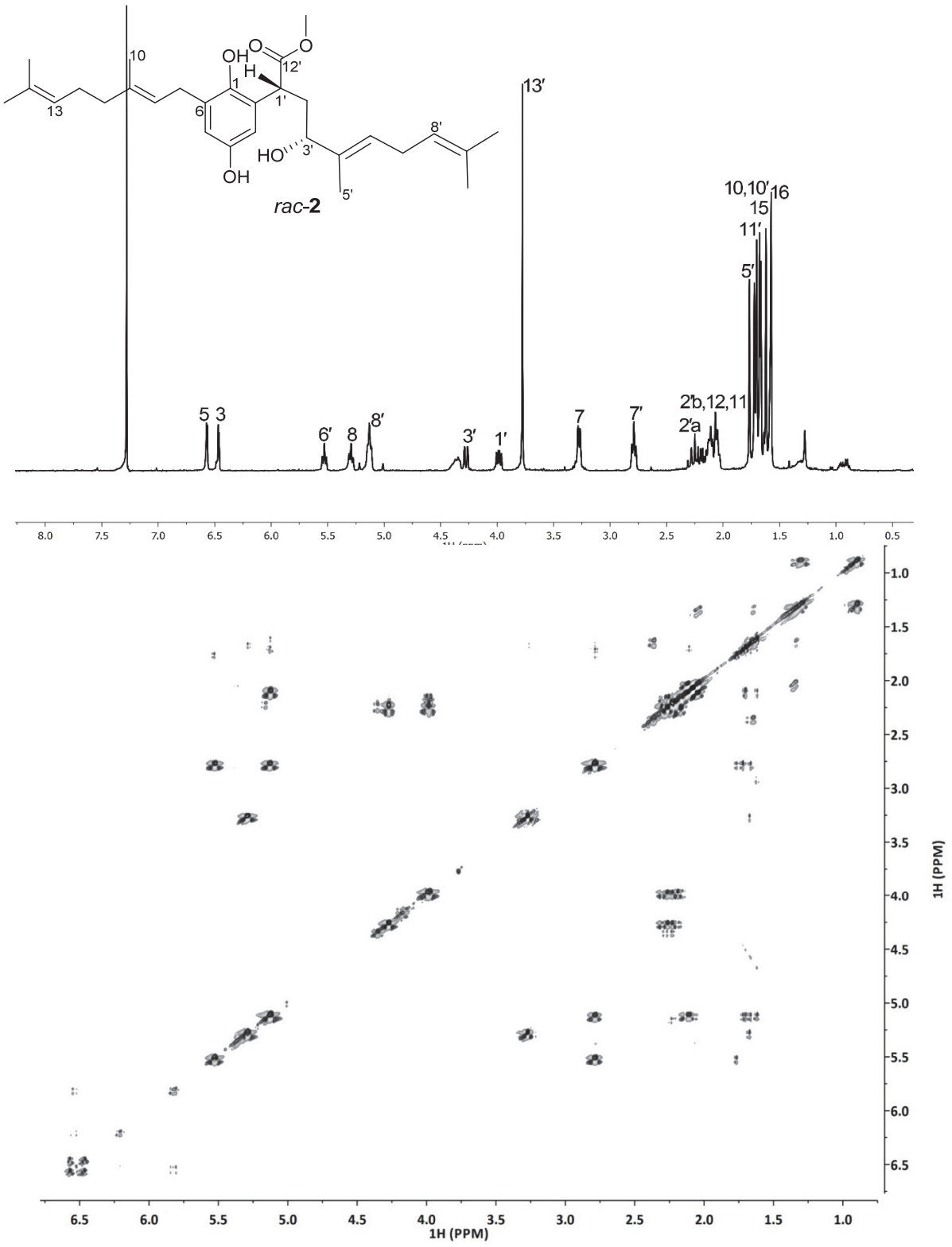

Figure 15 . ^{1}H NMR (top) and DQF-COSY (bottom) spectra of melissifoliane B (**2**)

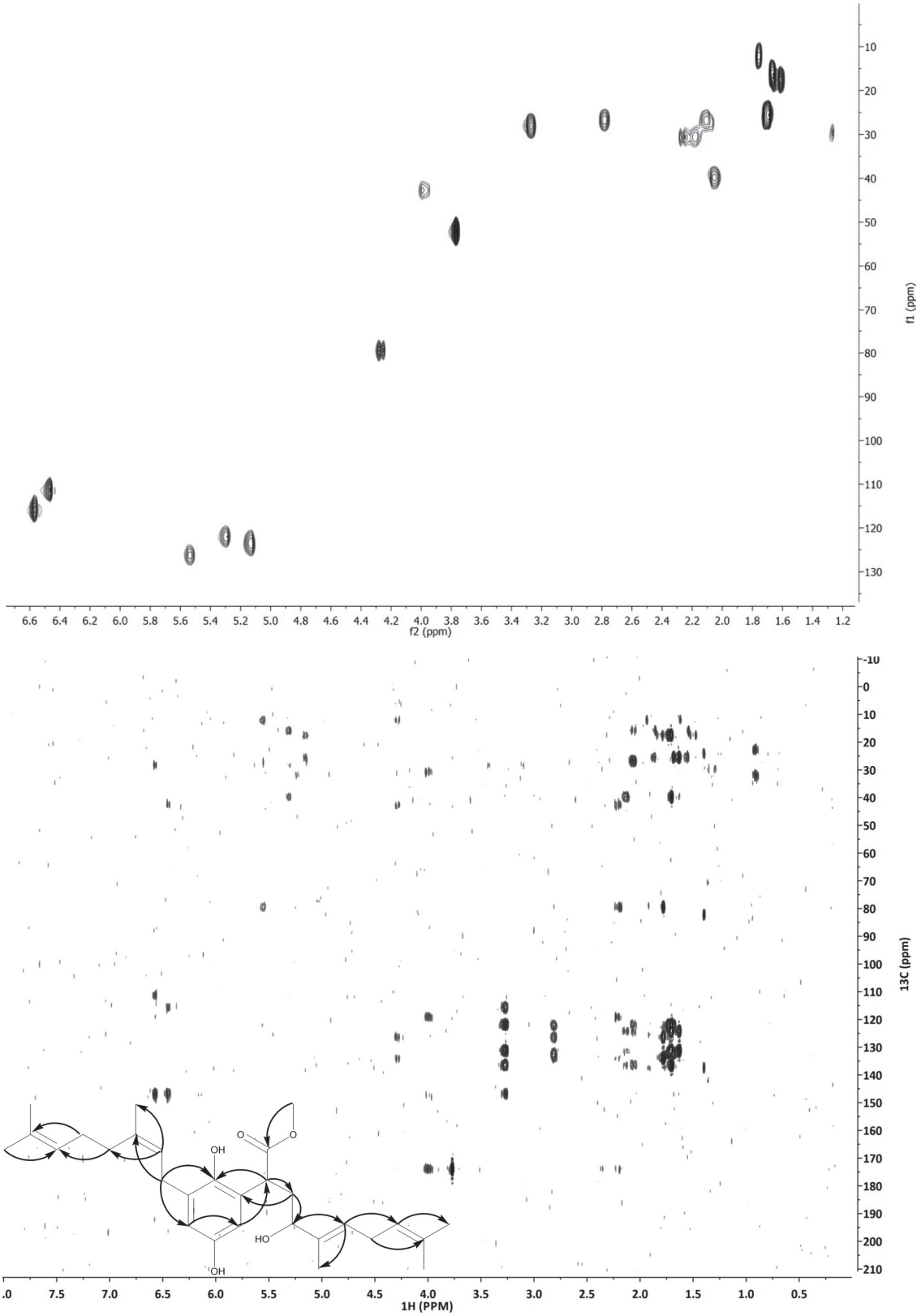

Figure 16. HSQC (top) and HMBC (bottom) spectra of melissifoliane B (**2**)

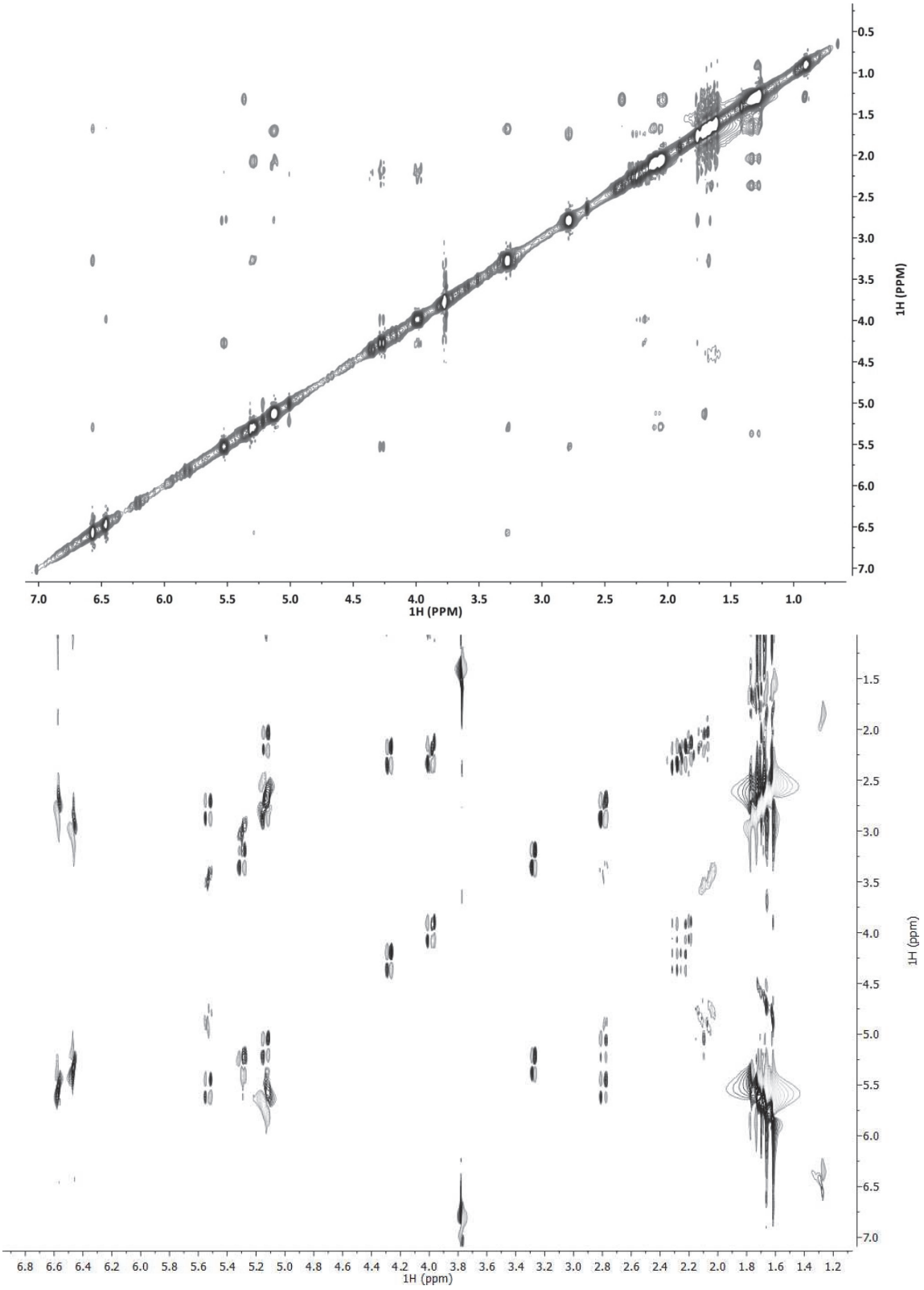

Figure 17. NOESY (top) and E.COSY (bottom) spectra of melissifoliane B (**2**)

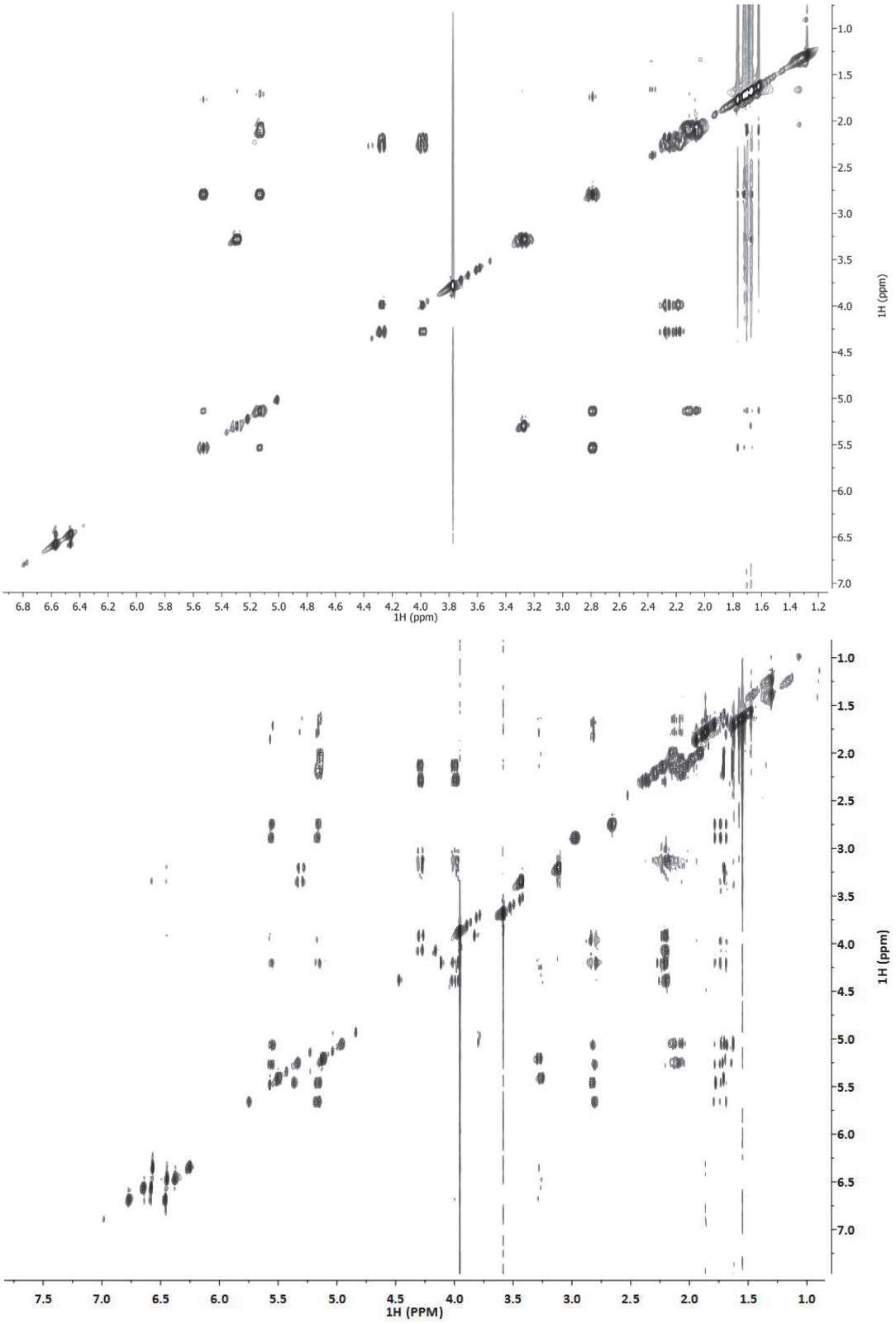

Figure 18. TOCSY (top) and HETLOC (bottom) spectra of melissifoliane B (**2**)

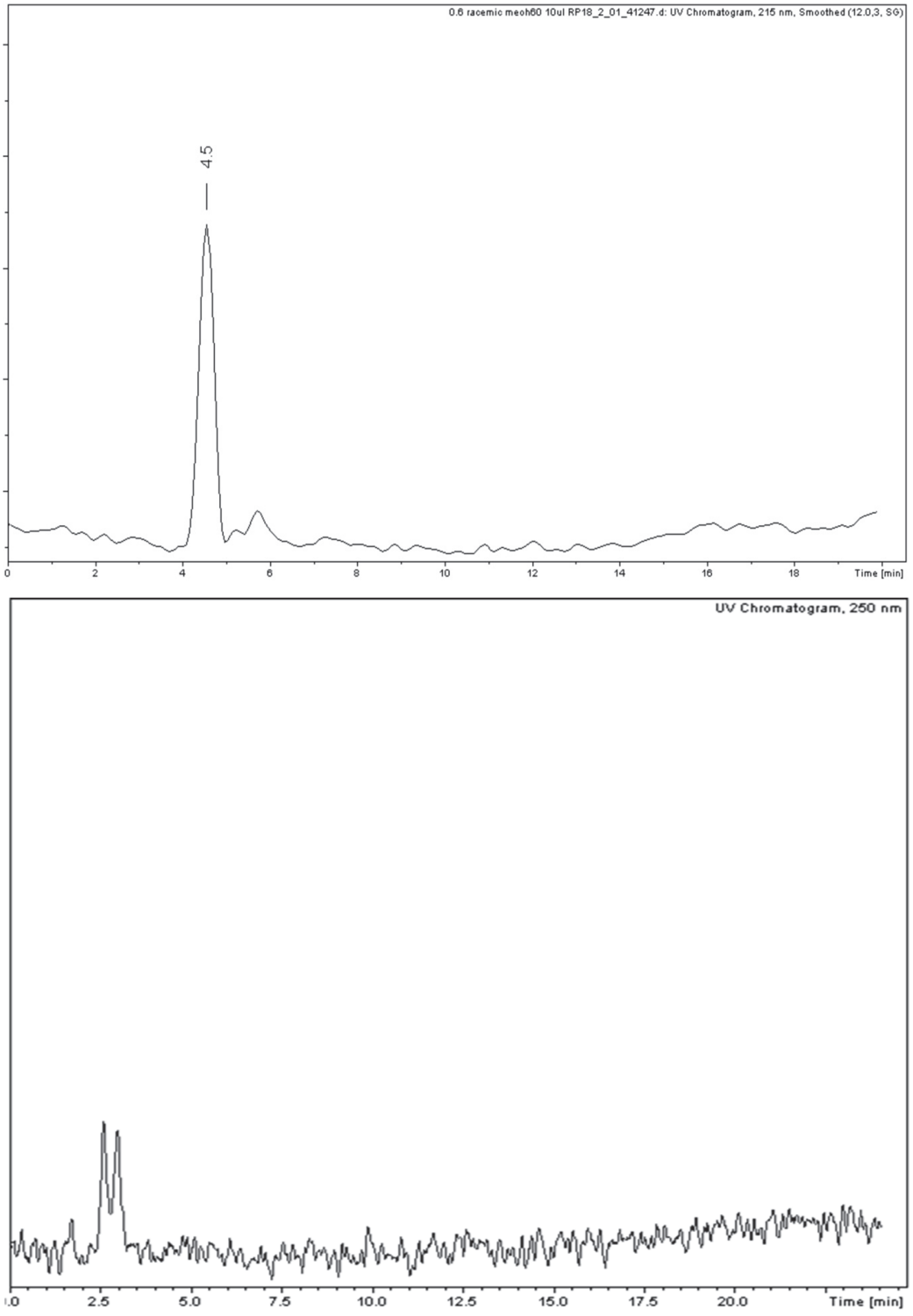

Figure 19. The RP chromatogram (Phenomenex C_8 5 × 150 mm, 5 µm, flow rate 0.6 mL/min using an isocratic elution of 70% MeOH in H_2O) (top) and chiral chromatogram (Astec Chirobiotic R 4.6 × 100mm, 5 µm, flow rate 0.6 mL/min with an isocratic elution of 55% MeOH in 20 mM NH_4Ac, pH 6, 35 °C) (bottom) of melissifoliane B (**2**)

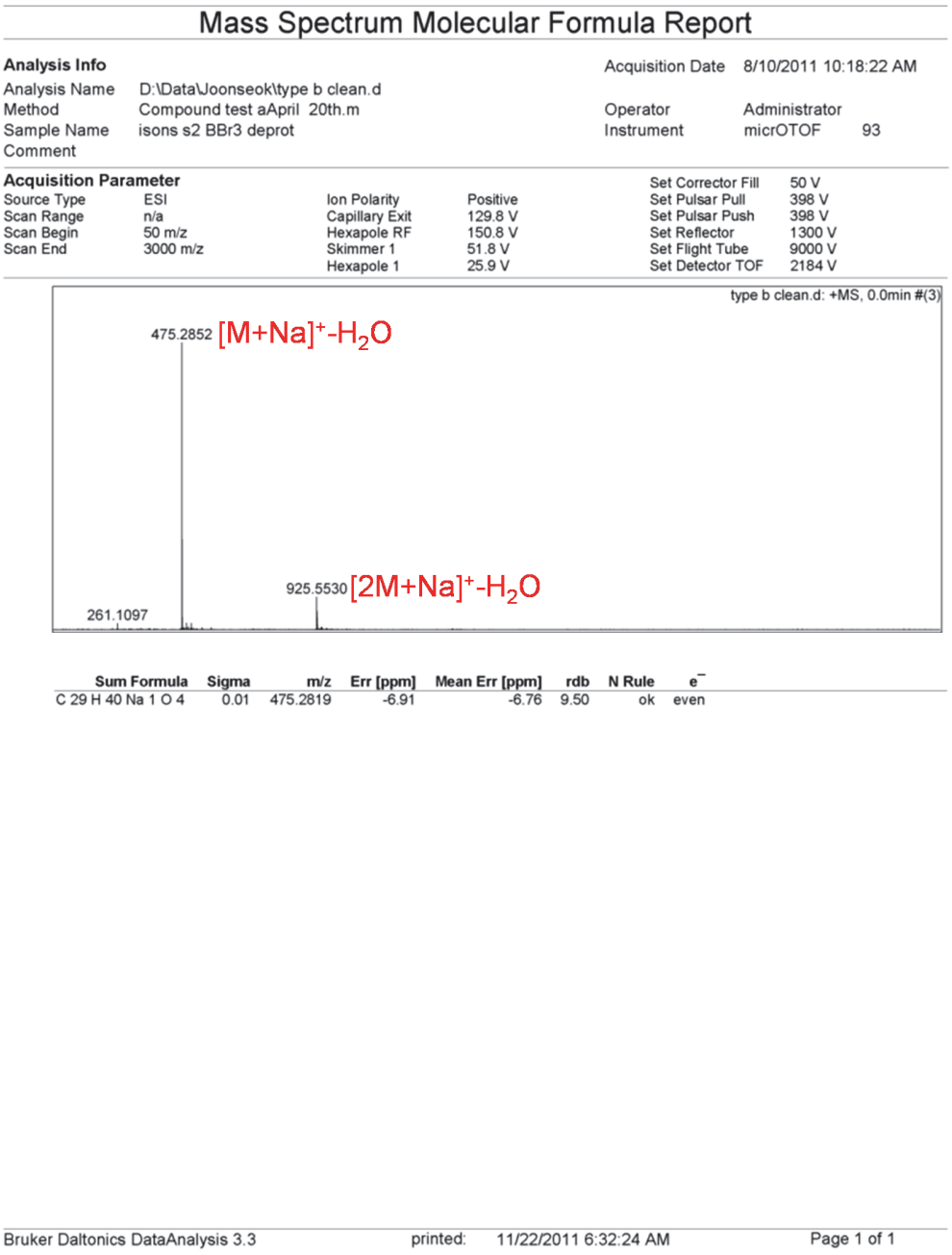

Figure 20. HRESIMS spectrum of melissifoliane B (**2**)

CHAPTER 3: DISCOVERY OF DRUG LEADS FOR TREATMENT OF SEPSIS FROM THE KOREAN ENDANGERED SPECIES *RHODODENDRON BRACHYCARPUM*

(The contents of this chapter were reproduced or edited from the original article published in *Biochim. Biophys. Acta, Gen. Subj.* with permission from the publisher via Rightslink® service, Copyright 2014 Elsevier B.V., Confirmation No. 11305580)

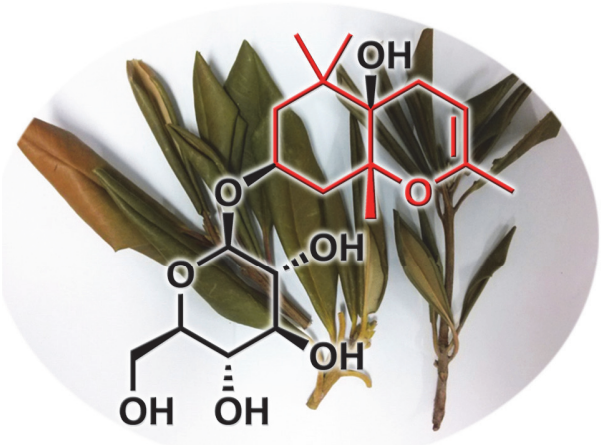

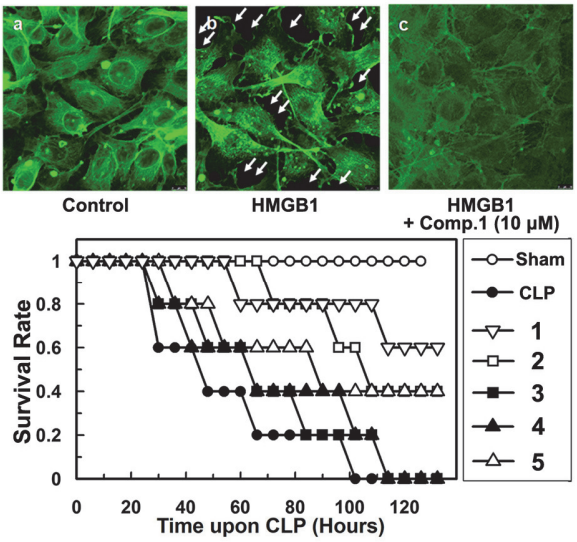

INTRODUCTION

Endangered plant species are an important resource for exploring novel drug prototypes[71] as discussed in the previous chapters. *Rhododendron brachycarpum* G. Don (Ericaceae) is a broad-leaved shrub native to northern Korean and central Japan.[72] The numbers of this species have been drastically diminished due to climate change, leading to its classification as an endangered and rare species in Korea.[72] Although *R. brachycarpum* is traditionally employed in the treatment of diseases including cardiovascular, diabetes, hypertension, hepatitis, rheumatoid arthritis, and headache,[73] only a limited number of studies have been carried out to validate these ethnopharmacological uses.[74,75]

Sepsis is a systemic and overwhelming inflammatory response of an organism to a local infection, potentially progressing to severe sepsis and septic shock with multiple organ failure and hypotension.[76] The mortality associated with the disease is as high as 50–70%, leading to its designation as the number one cause of death in intensive care units worldwide.[76] Comprehensive anti-inflammatory treatments have not alleviated the disease phenotypes during the last few decades.[76] The only FDA-approved antiseptic drug drotrecogin alfa (Xigris®) was withdrawn from the market due to its questionable efficacy,[77] thus stressing the necessity for the search of potential antiseptic prototypes with a novel mode of action (MOA). Among the therapeutic strategies targeting the mitigation of sepsis,[76] enhancement of the integrity of endothelial cells (ECs) has emerged as a sensible MOA for treatment of the serious disease.[78,79] Disruption of the integrity of ECs facilitates leucocytes to access inflamed tissue and hence initiating such vascular inflammatory manifestations.[78,79] In this regard, high mobility group box 1 (HMGB1) protein could be targeted specifically for the exploration of novel antiseptic agents capable of achieving

vascular barrier augmentation because of the significant role of the protein in disturbing the barrier integrity of ECs, and ultimately inducing severe sepsis and related fatalities.[78-80]

In continuing efforts aimed at discovering viable and new drug prototypes from endangered species,[71-73,81] the isolation and structural characterization of rhododendroside A (**1**), the first bicyclic megastigmane glycoside, is elaborated herein. It is also discussed whether this scaffold can be developed into a septic drug lead capable of mitigating HMGB1-induced vascular disruption.

RESULTS AND DISCUSSION

An extract of the leaves of *R. brachycarpum* was fractionated and purified employing various chromatographic techniques, leading to the purification of megastigmane glucosides (**1**–**5**) (**Figure** 21. (A) Structures **of 1–5** from *R. brachycarpum* and (B) key COSY (▬) and HMBC (→) correlations in **1**). Compound **1** was obtained as a yellow amorphous powder and the molecular formula was established as $C_{19}H_{32}O_8$ based on HRESIMS and ^{13}C NMR data (obsd $[M+Na]^+$ at *m/z* 411.1996, calcd $[M+Na]^+$ at *m/z* 411.1995). The ^1H NMR spectrum (**Table 6**) displayed resonances for an olefinic proton (δ_H 4.51), an anomeric proton (δ_H 4.43), an oxymethine proton (δ_H 4.16), an allylic (δ_H 1.66) and two tertiary and one oxygenated secondary methyl groups (δ_H 1.30, 1.07, 1.03). The ^{13}C NMR spectrum (**Table 6**) exhibited 19 resonances including six carbon resonances belonging to a glucopyranosyl moiety (δ_C 102.8, 75.1, 78.0, 71.6, 77.8, 62.7), two olefinic carbons (δ_C 149.4, 97.6), an oxymethine carbon (δ_C 73.2), one quaternary and two oxygenated tertiary carbons (δ_C 81.5, 72.0, 40.7), three methylene carbons (δ_C 44.7, 41.4, 29.9), one allylic (δ_C 20.0), and two tertiary and one oxygenated secondary methyl carbons (δ_C 27.4, 24.6, 22.7). These spectroscopic data are similar to those of icariside B_2 (**3**),[82] indicating the

presence of a megastigmane glucoside framework in **1**. Differences in the NMR data of **3** and **1** include the disappearance of the proton signals of the conjugated *trans*-olefinic group and a change of the nature of the acetyl methyl group in **3** compared to **1**. These differences are compatible with a structure of **1** generated from **3** via cyclization of the C-6 methyl vinyl ketocarbonyl functionality onto the oxirane moiety. This was confirmed by HMBC correlations between H-8 (δ_H 4.51) and C-6 (δ_C 72.0), C-7 (δ_C 29.9), C-9 (δ_C 149.4), and C-10 (δ_C 20.0), and between H-7 (δ_H 2.34, 1.99) and C-6 (δ_C 72.0), C-8 (δ_C 97.6), and C-9 (δ_C 149.4) (**Figure 21**). Such formation of a hexahydro-4*H*-chromene moiety leads to a unique cyclomegastigmane scaffold, which has not previously been observed in bisnorsesquiterpenoids. The connectivity of the aglycone and monosaccharide moieties was confirmed by an HMBC correlation between H-1' (δ_H 4.43) and C-3 (δ_C 73.2) (**Figure 21**). The coupling constant (J = 7.8 Hz) of the anomeric proton confirmed a β-glucosidic linkage. Acid hydrolysis followed by GC analysis confirmed the presence of D-(+)-glucose.

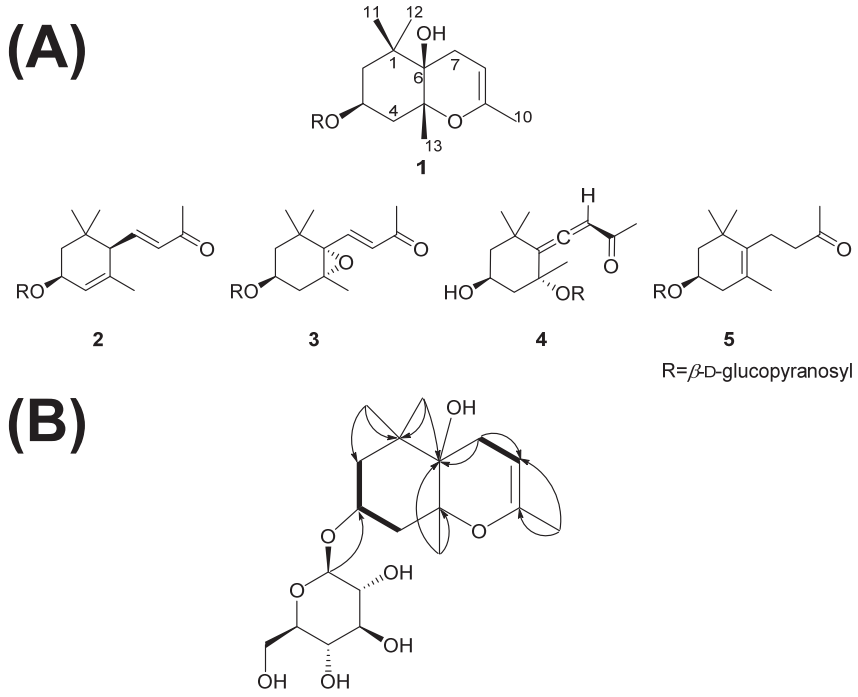

Figure 21. (A) Structures of **1**–**5** from *R. brachycarpum* and (B) key COSY (▬) and HMBC (→) correlations in **1**

Table 6. ^{1}H and ^{13}C NMR data (Exp.) of compound **1** in methanol-d_4 and calculated chemical shift values (Cal.) of diastereomers I and III

^{1}H NMR chemical shift values (δ_H)				^{13}C NMR chemical shift values (δ_C)		
position [a]	Exp.	Cal.		Exp.	Cal.	
	δ_H, multi, (*J* in Hz)	I [b]	III [c]		I [b]	III [c]
1				40.7	44.8	44.5
2ax.	1.76, t, (12.6)	1.90	1.75	44.7	47.7	45.7
2eq.	1.60, ddd, (12.6, 4.1, 2.4)	1.59	1.50			
3	4.16, tt, (12.6, 4.1)	4.35	4.33	73.2	68.6	69.0
4ax.	1.82, dd, (13 b.2, 12.6)	1.84	2.03	41.4	44.4	46.6
4eq.	2.12, ddd, (13.2, 4.1, 2.4)	2.07	2.19			
5				81.5	82.4	82.6
6				72.0	75.7	75.7
7α	1.99, m	1.99	1.94	29.9	33.5	33.9
7β	2.34, m	2.25	2.31			
8	4.51, m	4.61	4.60	97.6	96.5	96.5
9				149.4	146.6	146.8
		1.68	1.58			
10	1.66, m	1.77	1.73	20.0	21.0	21.0
		1.54	1.66			
		0.94	1.06			
11	1.03, s	0.97	1.27	27.4	28.0	28.2
		0.96	0.66			
		1.19	0.61			
12	1.07, s	1.46	1.59	24.6	25.2	25.3
		0.68	1.17			
		0.89	1.60			
13	1.30, s	1.63	0.98	22.7	25.2	24.8
		1.49	1.32			
1′	4.43, d, (7.8)	4.54	4.50	102.8	103.9	104.1
2′	3.18, dd, (9.1, 7.8)	3.51	3.51	75.1	76.5	76.6
3′	3.39, m	3.74	3.73	78.0	78.1	78.2
4′	3.35, m	3.60	3.56	71.6	72.3	72.2
5′	3.35, m	3.51	3.51	77.8	77.8	78.2
6′a	3.90, dd, (11.9, 2.1)	4.08	4.09	62.7	64.9	65.0
6'b	3.73, dd, (11.9, 5.1)	3.83	3.83			
DP4 (%)		96.3	3.7		70.9	29.1

[a] See **Figure 21**. [b,c] Calculated chemical shift values for diastereomers I and III shown in **Figure 22**

The relative configuration of the aglycone was established via coupling constants and NOE correlations. The coupling constants of H-3 (tt, 12.6, 4.1 Hz) suggest that the cyclohexane ring occupies either a chair or boat conformation. The relative configuration of C-5 was assigned based on the presence of a strong NOE correlation between H-3 (δ_H 4.16) and H-12 (δ_H 1.07) and the absence of an NOE correlation between H-3 (δ_H 4.16) and H-13 (δ_H 1.30) (**Figure 22**). Based on these findings, two plausible diastereomers (diastereomer I: 3*S,* 5*R*, 6*R*; diastereomer II: 3*S*, 5*R*,

6*S*) were proposed and minimized with the aforementioned conformational dihedral constraints and spatial distance information employing the MMFF94 force field (Schrödinger LLC.) (**Figure 22**A). The presence of an NOE correlation between H-12 (δ_H 1.07) and H-8 (δ_H 4.51) in diastereomer I and the absence of an NOE correlation between H-11 (δ_H 1.03) and H-13 (δ_H 1.30), but feasible in diastereomer II, support the relative configuration of diastereomer I and confirm its structural equivalence with compound **1** (**Figure 22**A). Owing to the mass limitations of **1**, definition of the absolute configuration was attempted utilizing GIAO NMR chemical shift calculations with accuracy improved by application of DP4 analysis that has been successfully applied for investigation of stereochemical details.[83-85] Having established the D-glucopyranosyl moiety in **1**, diastereomers I and III with enantiomeric aglycone moieties were considered (**Figure 22**). The major conformers of diastereomers I and III, generated by conformational searches employing Macromodel (Schrodinger LLC.), were subjected to gauge-invariant atomic orbital (GIAO) shielding constant calculations at the B3LYP/6-31G(d,p) level employing the Gaussian 09 package (Gaussian Inc.).

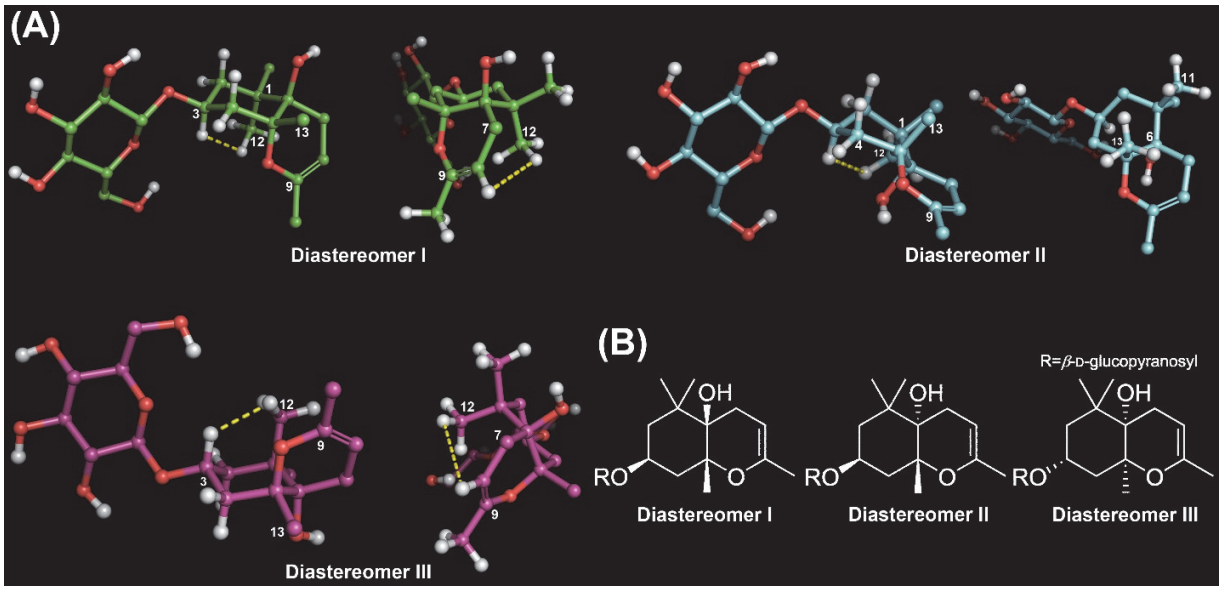

Figure 22. (A) Minimized stereostructures of plausible diastereomers of **1** (yellow dotted lines indicate NOE correlations) and (B) their 2D representations

The calculated chemical shift values were Boltzmann-averaged based on their relative MMFF94 potential energy and these averaged values were used for the calculation of DP4 probability. According to DP4 analysis (**Table 6**), Diastereomer I was supported with 98.4% probability when chemical shift values of the two nuclei were taken into consideration, permitting assignment of absolute configuration of compound **1** identical to that showed for Diastereomer I. Moreover, consistency regarding the 3*S*-configuration among analogues **2**–**5**[82,86,87] further supports the DP4 prediction of the 3*S* configuration of **1** when considered in conjunction with a similar biosynthetic pathway towards these bisnorsesquiterpenes. As shown in **Figure 23**, enzymatic epoxidation of **5** would stereochemically be directed by the 3*β*-equatorial substituent, leading to formation of oxirane **6** that would be susceptible to successive cyclization and dehydration via **7** to form **1**. On the basis of these findings, the structure of **1** was defined as (3*S*,5*R*,6*R*)-1,1,5,9-tetramethyl-3-*β*-D-glucopyranosyloxy-2,3,4,5-tetrahydro-7*H*-chromen-6-ol, named rhododendroside A (**1**). The known megastigmane glucosides, picrionoside A (**2**),[86] icariside B_2 (**3**),[82] citroside A (**4**),[87] and icariside B_6 (**5**)[82] were identified by 1D and 2D NMR analysis and confirmed by comparing the physical and spectroscopic data with those in the literature.

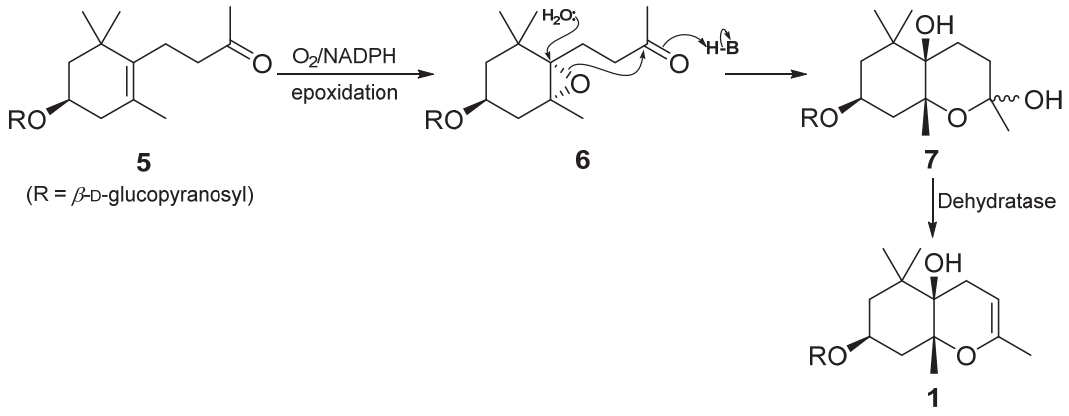

Figure 23. Plausible biosynthetic pathway for generation of rhododendroside A (**1**)

Compounds **1–5** were evaluated for their potential to hamper HMGB1-mediated vascular disruption as a cause of severe sepsis and associated manifestations.[78,79,88] To evaluate actin cytoskeletal arrangement activity of **1**–**5**, human umbilical vein endothelial cells (HUVECs) were treated with 10 μM of each compound employing immunofluorescence staining of HUVEC monolayers with the F-actin labeled fluorescein phalloidin (**Figure 24**A). The control displayed random F-actin distribution throughout cells with actin filament bundles localized at cell boundaries (**Figure 24**A) while vascular barrier disruption triggered by HMGB1 (1 μg/mL) was evidenced by the generation of paracellular gaps upon HMGB1 treatment (arrowed in **Figure 24**A). Pretreatment with **1**, **2**, and **5** eliminated HMGB1-induced paracellular gaps and facilitated the formation of dense F-actin rings (**Figure 24**A), protecting vascular barrier integrity from HMGB1-induced vascular stress. However, pretreatment with **3** and **4** did not recover the HMGB1-mediated paracellular gaps (**Figure 24**A). To further examine if compounds **1**–**5** enhance barrier integrity of HUVECs, a permeability assay was performed with various concentrations (1–10 μM). Pretreatment with **1**, **2**, and **5** (10 μM) restored the levels of permeability to those of the negative control (**Figure 24**B) in HMGB1-stimulated barrier integrity disruption while their pretreatment (10 μM) without the vascular stressor did not influence the barrier integrity, validating their strong supportive action of vascular barrier integrity (**Figure 24**B). To verify if the observed barrier protective action was associated with HMGB1 signaling through its receptors, expression of the associated receptors including toll-like receptors 2 and 4 (TLR2, TLR4) and receptor for advanced glycan endproducts (RAGE) was monitored upon pretreatment with compounds **1**–**5** (1–10 μM). Pretreatment of HUVECs with **1**, **2** and **5**, diminished the HMGB1 receptors in a dose-dependent manner, implying that the active compounds exerted the vascular barrier restorative action via the inhibition of HMGB1 interacting with the receptors (**Figure 24**C).

Phosphorylation of p38 mitogen-activated protein kinase (MAPK) was also evaluated employing enzyme-linked immunosorbent assay (ELISA) based on studies validating HMGB1 induces pro-inflammatory response by promoting phosphorylation of p38.[78,79] The treatment of HUVECs with HMGB1 significantly enhanced phosphorylation of p38 and this up-regulation was attenuated upon the pretreatment with **1**, **2**, and **5**, indicating that they averted HMGB1-induced pro-inflammatory reactions and consequently maintaining vascular barrier integrity (**Figure 24**D). Overall, these in vitro findings cohesively corroborated the active compounds exerted vascular protective potential via inhibition of HMGB1-induced pro- inflammatory response.

In vivo experiments employing murine models were conducted to confirm the observed in vitro vascular barrier protective effects of the examined compounds. Intravenous pretreatment of mice with **1**–**5** (7.7 μg/mouse) was carried out followed by HMGB1 [2 μg/mouse, intravenous (i.v.)]-induced barrier disruption in vivo. Compounds **1**, **2**, and **5**, protecting vascular barrier integrity in vitro, also restored vascular permeability in vivo upon HMGB1-induced pro-inflammatory stimuli based on the decreased dye leakage levels to near those of the negative control, while compounds **3** and **4** did not suppress the levels of dye leakage (**Figure 24**A). To corroborate in vitro anti-permeability effects of the active compounds, in vivo leukocyte migration was evaluated by counting the number of migrated leukocytes into peritoneal cavities upon HMGB1-challeged mice models. As shown in **Figure 25**B, i.v. pretreatment with **1**, **2**, and **5** inhibited migration of leukocytes based on the decreased peritoneal leukocytes counts, verifying their inhibitory action on leukocytes chemotaxis upon HMGB1-induced inflammatory environment.

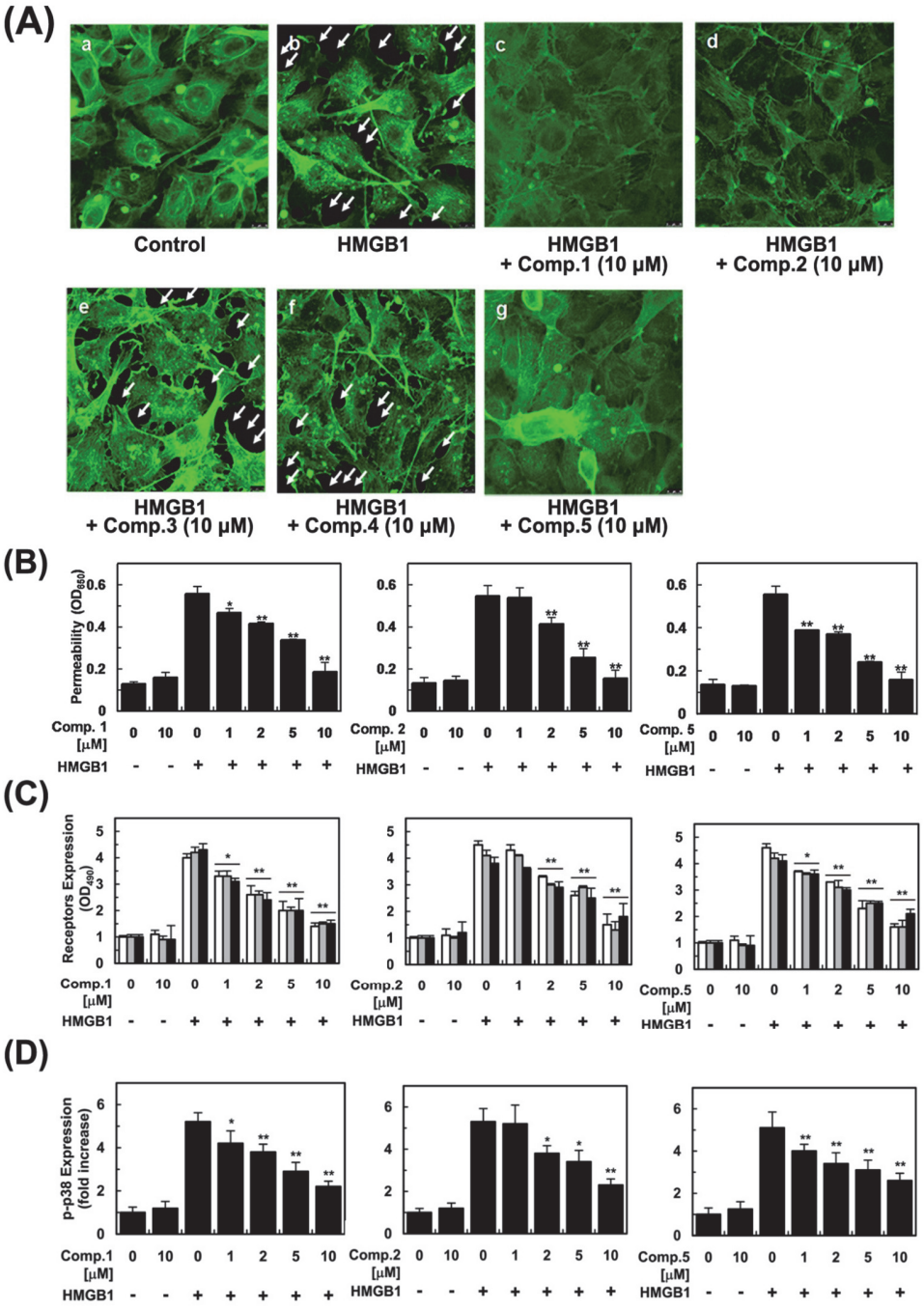

Figure 24. In vitro evaluation of vascular protective action of compounds **1**, **2**, and **5** against HMGB1 (1 μg/mL for 16 h)-induced vascular barrier disruption. Data were analyzed upon pretreatment of HUVECs with the indicated concentrations for 6 h. (A) Staining for F-actin upon pretreatment of **1**–**5**. (B) HMGB1-induced permeability was monitored by assessing the flux of Evans blue bound albumin across HUVECs. (C) Influence of **1**, **2**, and **5** on expression of HMGB1 receptors, and (D) phosphorylation of p38 was evaluated by ELISA. (C) White, gray, and black bars indicate expression of TLR2, TLR4, and RAGE. Results are indicated with the means ± standard deviations (SDs) of different of at least three experiments and *$p < 0.05$ and **$p < 0.01$ compared to cells only treated with HMGB1 (B–D).

To validate if the active megastigmane glucosides may be developed into practical prodrugs for treatment of septic fatalities, they were administered to mice (7.7 μg/mouse) upon cecal ligation and puncture (CLP) operation employed to simulate the late stage of severe sepsis.[89] According to the Kaplan–Meier survival analysis,[78,79] compounds **1**, **2**, and **5**, demonstrating potent vascular barrier protective activity in vitro and in vivo, improved the survival rate to 60, 40, and 40%, respectively, 132 h after the CLP operation (**Figure 25**C). In view of these biological findings, it is plausible that the megastigmane glucosides restore in vitro and in vivo vascular integrity with mitigating HMGB1-induced pro-inflammatory vascular stimuli, ultimately leading to alleviating septic lethality. Thus, megastigmane glucosides (**1**, **2** and **5**) could be a sensible starting point not only for conducting further structure-activity relationship studies but also developing an effective septic agent capable of inhibiting HMGB1.

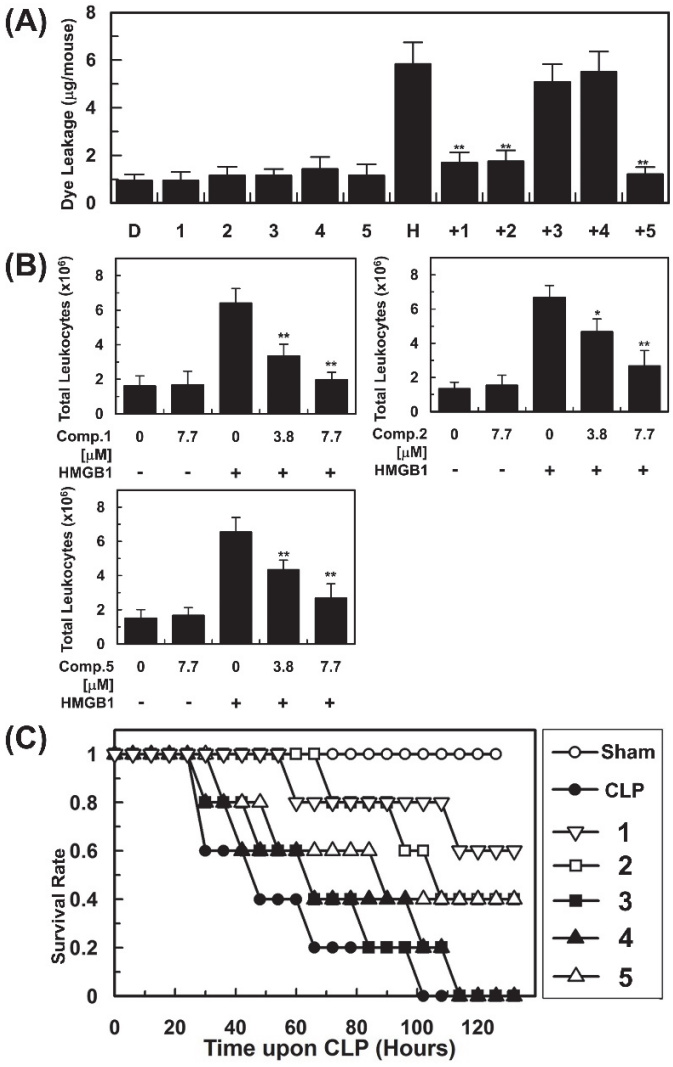

Figure 25. (A, B) In vivo vascular supportive and antiseptic action of **1**–**5** (7.7 μg/mL) upon HMGB1 (2 μg/mouse, i.v.)-mediated pro-inflammatory environment and (C) CLP operation. Effects of **1**–**5** on vascular permeability were measured by the amount of Evans blue in peritoneal washings (n=5). (A) H and D stand for mice groups administered with HMGB1 and DMSO, respectively. (B) Anti-migration potential (n=5) of **1**–**5** was evaluated by counting the number of migrated leukocytes into peritoneal cavities. (C) Anti-lethality activity (n=10) of those compounds was assessed using a CLP-induced septic shock mice model. Control CLP mice (●) and sham-operated mice (○) were administered sterile saline and survival was monitored every six-hour. Results are shown with the means ± SDs of three different experiments and $*p < 0.05$ and $**p < 0.01$ compared to mice only treated with HMGB1 (A,B).

CONCLUSION

This Chapter delineates that *R. brachycarpum* may be the source of a unique scaffold that can be developed into an antiseptic lead mitigating HMGB1-induced vascular pro-inflammatory stimuli. These results also reaffirm that rare and endangered plant species offer unique opportunities to explore novel drug leads, warranting conservation efforts especially in cases where modern-day disease challenges are intensifying.

EXPERIMENTAL SECTION

General Experiments

NMR experiments were conducted using a Bruker DMX 250 and Bruker DMX 600 spectrometers (Karlsruhe, Germany) referenced by residual pyridine and methanol signals. Specific rotations were recorded using a JASCO DIP-1000 (Tokyo, Japan) and mass spectrometric data were obtained utilizing a SYNAPT G2 Waters mass spectrometer (Manchester, U.K.). Medium-pressure liquid chromatography (MPLC) was carried out employing Biotage Isolera™ RP C_{18} SNAP Cartridge KP-C_{18}-HS and normal-phase SNAP Cartridge KP-Sil (340 g, Biotage AB, Uppsala, Sweden). The GC analysis was carried out on a Shimadzu-2010 with an SPB-1 column (0.25 mm × 30 m, temperature: 250 ˚C) employing FID and helium as carrier gas. HPLC separation was performed using a Gilson system with a UV detector and Phenomenex Luna C_{18} column (250 × 21.2 mm, 10 μm and 250× 4.60 mm, 5 μm). TLC was performed on glass plates precoated with silica gel 60 F_{254} and RP-18 F_{254} (Merck). Column chromatography was carried out using silica gel (Merck, 70 – 230 mesh).

Extraction and purification

Leaves of *R. brachycarpum* were purchased from a farm in Gongju Korea in 2011, identified by Prof. MinKyun Na (College of Pharmacy, Chungnam National University), and deposited at the Pharmacognosy Laboratory of the College of Pharmacy, Chungnam National University, Daejeon, Korea (CNU00195). Dried leaves (25 kg) were extracted with MeOH (2 × 250 L) at room temperature for one week and the extract was concentrated to yield a brownish slurry (6 kg). Half of the extract (3 kg) was suspended in H_2O (10 L) and partitioned three times with *n*-hexane (10 L), $CHCl_3$ (10 L), EtOAc (10 L), and BuOH (10 L) to afford four extracts amounting to 438, 140, 450, and 320 g, respectively. The BuOH-fraction (320 g) was further subjected to silica gel column VLC and eluted with CH_2Cl_2:MeOH:H_2O (10:1→2:1:0.1) to obtain six fractions (Fr. B1–B6). Fr. B1 (10 g) was purified by MPLC (C_{18} SNAP Cartridge KP- C_{18}-HS, 340 g) eluting with MeOH:H_2O (3:7 → 7:3) to afford seven sub-fractions (Fr. B11–B17). Fr. B14 (1.46 g) was further purified employing preparative HPLC (Luna C_{18} column: 250 × 21.20 mm, 20% MeCN, flow rate: 6 mL/min) to afford compounds **2** (26 mg, t_R 40.2 min) and **5** (3.8 mg, t_R 53.6 min). Fr. B2 (22 g) was fractionated into nine fractions (B21–B29) utilizing MPLC (C_{18} SNAP Cartridge KP-C_{18}-HS, 340 g) eluting with acetone:MeOH:H_2O (0:0:100→12:28:60). Fr. B26 (1.7 g) was subjected to silica gel MPLC (SNAP Cartridge KP-Sil, 120 g) and eluted with EtOAc:MeOH (98:2→90:10) to yield five fractions (B261–B265). Fr. B262 (92 mg) was chromatographed over a silica gel column (2 × 80 cm) and eluted with $CHCl_3$:acetone:H_2O (1:2:0.1) to obtain compound **1** (2 mg). Compound **4** (34 mg) was acquired from Fr. B264 (120 mg) using a silica gel column (2 × 80 cm) eluting with $CHCl_3$:MeOH:H_2O (6.5:1:0.1). Fr. B27 (2 g) was subjected to silica gel MPLC (SNAP Cartridge KP-Sil, 120 g) and eluted with $CHCl_3$:MeOH (94:6→85:15) to yield compound **3** (159 mg).

- Rhododendroside A (**1**)

Rhododendroside A (**1**): yellow amorphous powder; $[\alpha]_D^{20}$ = -15.4 (*c* 0.1, MeOH); HRESIMS (obsd $[M+Na]^+$ at *m/z* 411.1996, calcd $[M+Na]^+$ at *m/z* 411.1995). ^{1}H NMR (methanol-d_4, 600 MHz) and ^{13}C NMR (methanol-d_4, 150 MHz) data, see **Table 6**. With reference to a previous study,[90] the acid hydrolysis of compound **1** was performed as follows; the compound was heated in 10% HCl (1 mL) at 85 ˚C for 3 h and the residue was partitioned with EtOAc and H_2O. The aqueous layer was evaporated to yield a residue and the residue was dissolved in anhydrous pyridine (100 μL) followed by the addition of 0.1 M L-cysteine methyl ester hydrochloride (100 μL). After heating at 60 ˚C for 1.5 h, the residue was dried and trimethylsilylated with the addition of 1-trimethylsilylimidazole solution (500 μL), and heated at 60 ˚C for 5 min. The dried product was partitioned with *n*-hexane and H_2O, and the non-polar layer was analyzed using GC. The monosaccharide moiety was confirmed as D-glucose based on comparison of the retention time with that of a D-glucose standard (t_R 16.21 min) (**Figure 30**).

GIAO NMR chemical shift calculations[83,84]

All conformational searches were achieved employing Macromodel (Version 9.9, Schrodinger LLC.) program with "Mixed torsional/Low Mode sampling" in the MMFF force field. The searches were performed in the gas phase with a 50 kJ/mol energy window limit and 10,000 maximum number of steps to completely investigate all low-energy conformers. All minimization processes were accomplished utilizing polak-ribiere conjugate gradient (PRCG) method, 10,000 maximum iterations, and a 0.001 kJ (mol Å)$^{-1}$ convergence threshold. C-2–C-3 and C-3–C-4 bonds in compound **1** were constrained using a 1,000 force constant based on the associated coupling constants [$^3J_{H\text{-}2ax,H\text{-}3}$ (12.6 Hz), $^3J_{H\text{-}3,H\text{-}4ax}$ (12.6 Hz)]. Conformers within 10 kJ/mol of

each global minimum of the two diastereomers (diastereomers I and III shown in **Figure 22**) were selected for GIAO shielding constants calculation without geometry optimization employing Gaussian 09 package (Gaussian Inc.) at the B3LYP/6-31G(d,p) level in the gas phase. Calculated chemical shift values were obtained according to the following equation: $\delta_{calcd}^{x} = (\sigma^0 - \sigma^x)/(1 - \sigma^0/10^6)$ in which δ_{calcd}^{x} is the calculated chemical shift value for nucleus x (e.g., ^{1}H or ^{13}C), σ^x and σ^0 are the calculated isotropic constants for nucleus x and tetramethylsilane (TMS), respectively. The geometry of TMS was optimized utilizing the B3LYP/6-31G(d,p) level in the gas phase for unbiased comparison of calculated chemical shift values with those of other molecules according to the original authors' recommendation.[84] These calculated chemical shift values were Boltzmann-averaged based on their relative MMFF94 potential energy and these averaged values were used for the calculation of DP4 probability employing an applet available at http://www-jmg.ch.cam.ac.uk/tools/nmr/DP4/. All 3D images in this Chapter were rendered utilizing Pymol 1.6.x (Schrödinger LLC.).

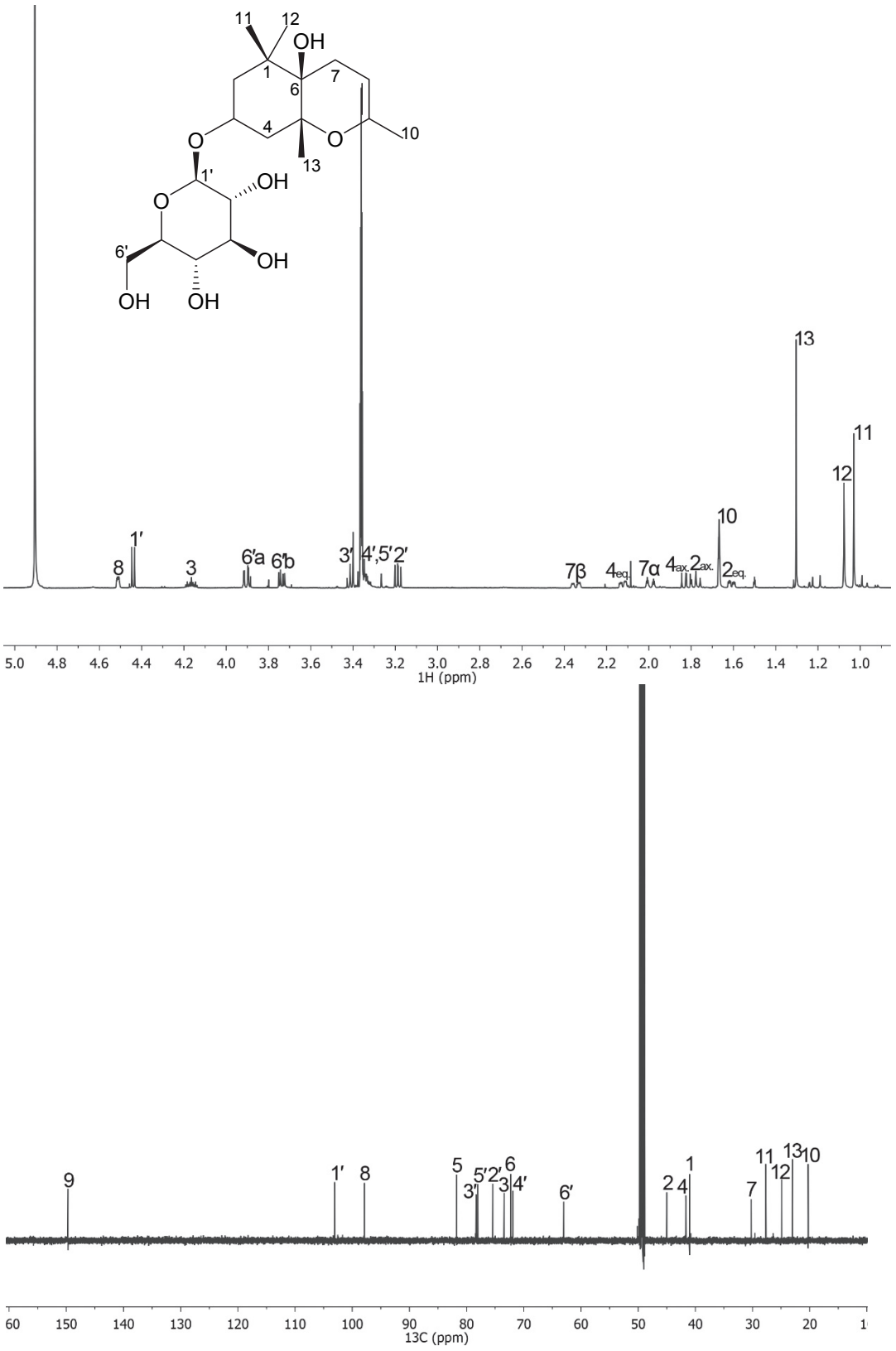

Figure 26. ^{1}H NMR (top) and ^{13}C NMR (bottom) spectra of rhododendroside A (**1**)

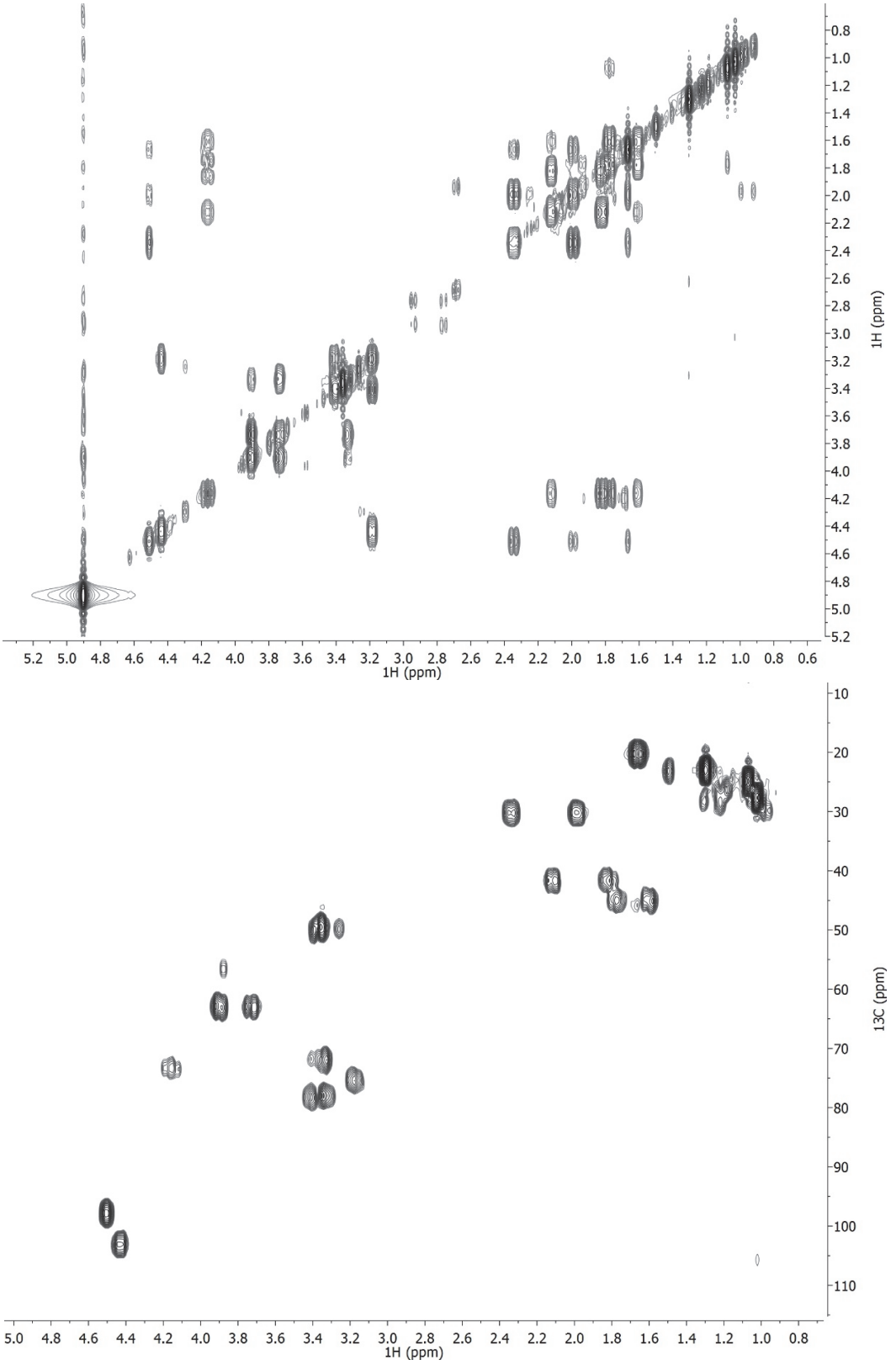

Figure 27. COSY (top) and HSQC (bottom) spectra of rhododendroside A (**1**)

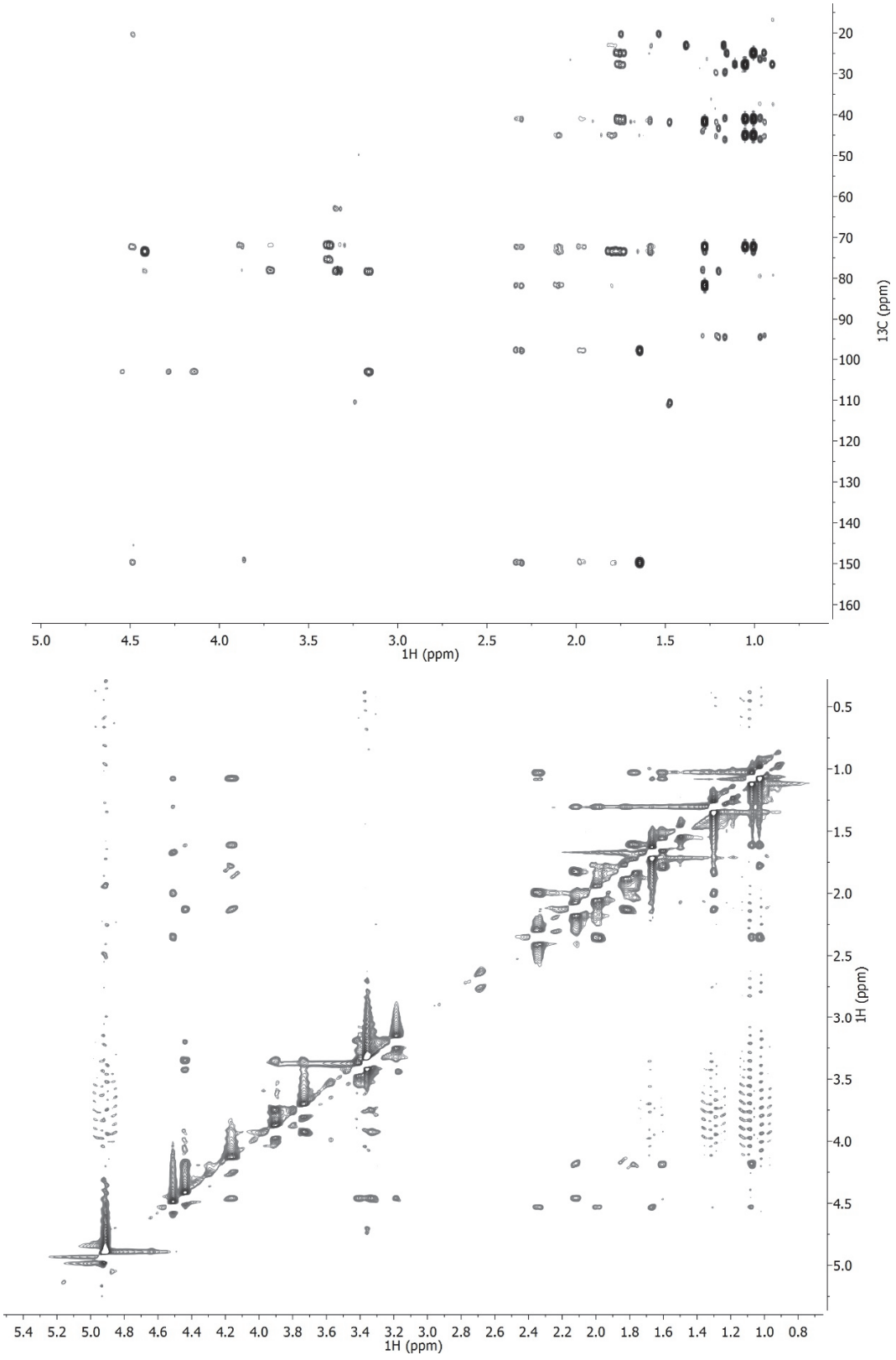

Figure 28. HMBC (top) and NOESY (bottom) spectra of rhododendroside A (**1**)

HR-ESI-MS Data Result

Sample : Rhododendron

Elemental Composition Report

Single Mass Analysis
Tolerance = 10.0 PPM / DBE: min = -1.5, max = 50.0
Element prediction: Off
Number of isotope peaks used for i-FIT = 3

Monoisotopic Mass, Even Electron Ions
83 formula(e) evaluated with 1 results within limits (up to 50 best isotopic matches for each mass)
Elements Used:
C: 0-500 H: 0-1000 O: 0-200 Na: 1-1

Minimum:				-1.5				
Maximum:		5.0	10.0	50.0				
Mass	Calc. Mass	mDa	PPM	DBE	i-FIT	Norm	Conf(%)	Formula
411.1996	411.1995	0.1	0.2	3.5	573.4	n/a	n/a	C19 H32 O8 Na

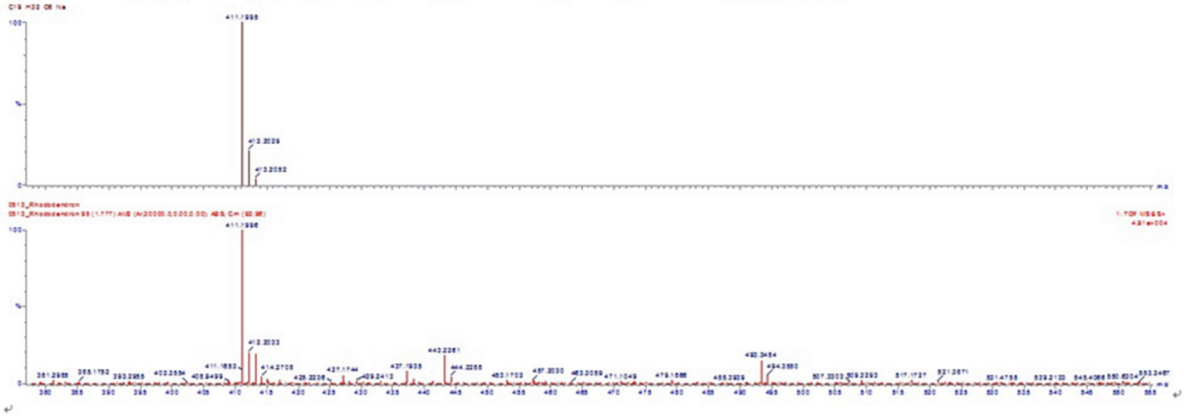

Figure 29. HRESIMS spectrum of rhododendroside A (**1**)

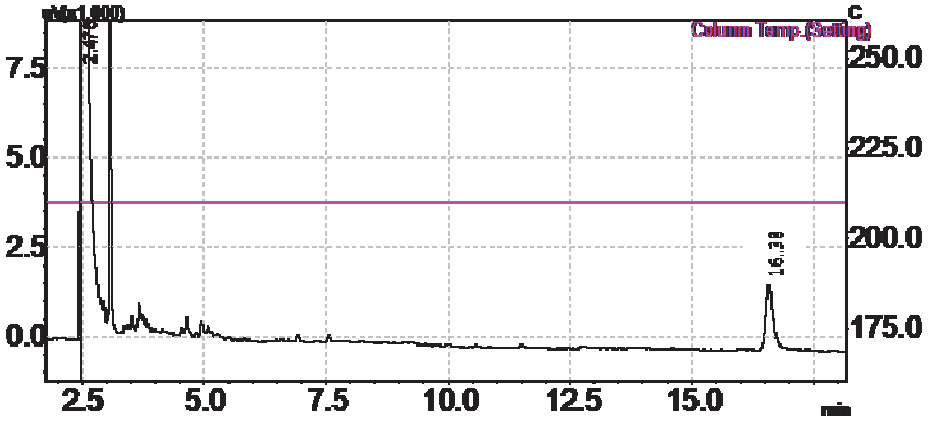

GC chromatogram of standard D-glucose (retention time: **16.38 min**)

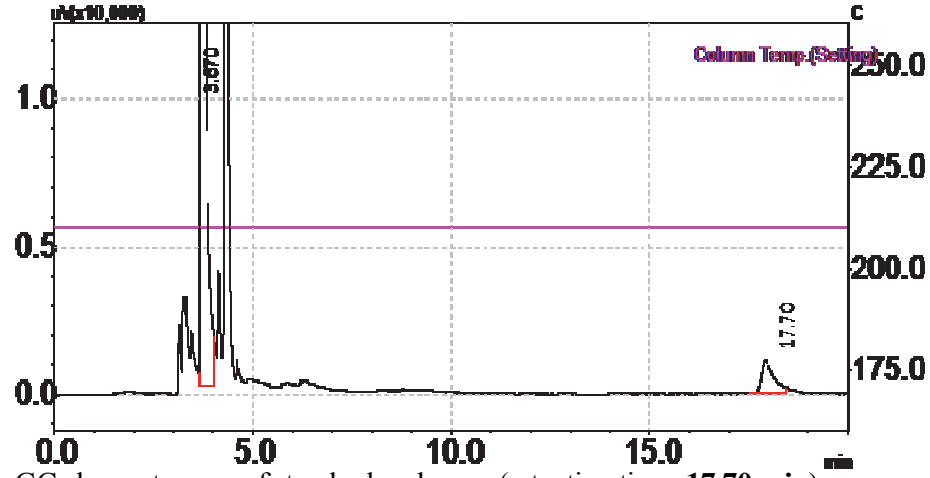

GC chromatogram of standard L-glucose (retention time: **17.70 min**)

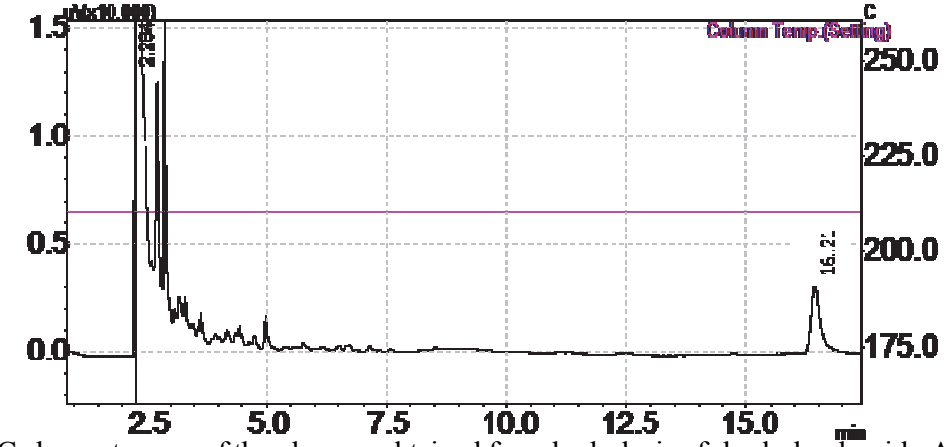

GC chromatogram of the glucose obtained from hydrolysis of rhododendroside A (**1**)

(retention time: **16.21 min**)

Figure 30. Identification of the glucose moiety in rhododendroside A (**1**) employing acid hydrolysis followed by GC analysis

CHAPTER 4: SCRUTINY OF THE SOUTH AMERICAN ENDANGERED SPECIES *DIPLOSTEPHIUM RHODODENDROIDES* FOR ANTIDIABETIC DRUG LEADS CAPABLE OF INHIBITING PROTEIN TYROSINE PHOSPHATASE 1B

(Some contents and figures in this chapter were reprinted from the original article published in *Proc. Nat. Acad. Sci. U.S.A.* with an appropriate citation. Permission requests have not been made based on the publisher policy item No. 3)

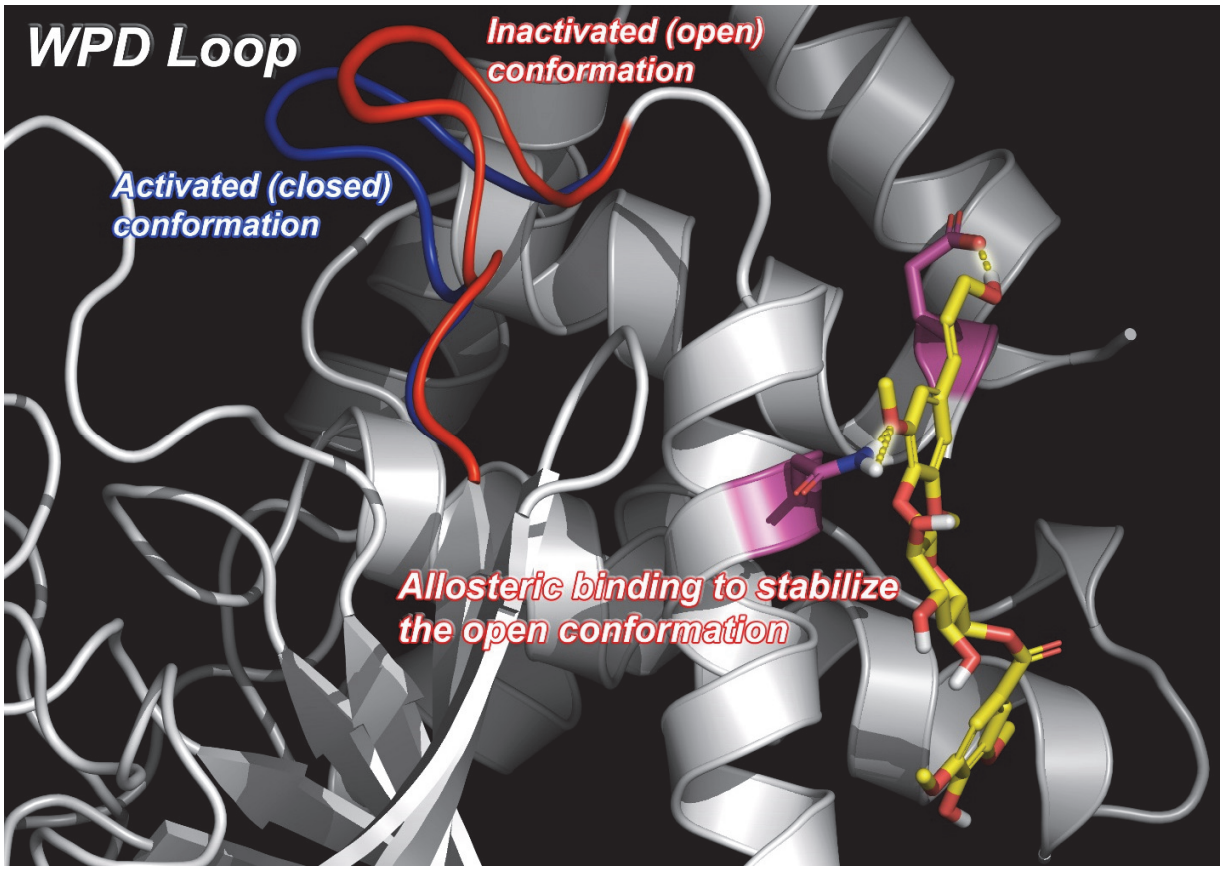

INTRODUCTION

The genus *Diplostephium* comprising ~110 species is a member of the Asteraceae family, one of the drug-producing families addressed in the aforementioned chapters. Previous studies on species in the genus *Diplostephium* have revealed the presence of only a few chemical constituents including diterpenoids, diterpene lactones, phenylpropanoids,[91,92] and flavonoids.[93] This implies that the genus may be an untapped resource for providing prodrug leads. The species *D. rhododendroides* Hieron. is a rare South American shrub native to the Andes and found at altitudes of 3000 – 4500 meter.[94,95] The genus *Diplostephium* is classified into three principal types based on the shapes of disk flowers[96] and *D. rhododendroides* belongs to one of those types featured with club-shaped disk flowers merely divided into two equal lobes.

Globally, elevated incidence of type 2 diabetes mellitus and obesity has prompted the search for new drug leads to alleviate metabolic diseases. Resistance to insulin and leptin is regarded as a common phenotype of type 2 diabetes mellitus and its related metabolic disorders.[97] In this regard, inhibition of protein tyrosine phosphatase 1B (PTP1B) has been regarded as a sensible approach to treat these metabolic manifestations. According to a previous study, PTP1B knock-out murine models demonstrated the reduced circulation of insulin, glucose, and triglyceride levels upon intravenous injection of insulin.[98,99] This phosphatase is comprised of 435 amino acids and the residues 177-185 construct a flexible loop called “WPD loop”. This loop is activated via its conformational change from “open” (inactivated) to “closed” (activated) upon substrate binding, leading to the formation of a tight binding pocket for the dephosphorylation catalytic reaction.[100] Wiesmann et al.[101] discovered a novel allosteric binding site ~20 Å away from the catalytic pocket in PTP1B and formulated several allosteric inhibitors capable of stabilizing

the inactivated open conformation, which thereby hampering the closure of the WPD loop. Owing to this allosteric binding site being poorly conserved among allosteric binding sites in other phosphatases, a specific inhibitor binding to the allosteric site of PTP1B may be developed into a highly selective antidiabetic agent. This is verified by the selective noncompetitive PTP1B inhibitor trodusquemine (MSI-1436) that has been advanced to phase I clinical trials as a potent hypoglycemic prodrug.[101,102]

Computational approaches using a wealth of PTP1B crystal structures (~100)[103] have been a crucial avenue for rational design and/or exploration of potent inhibitors[104-107] and successfully applied to the identification of an oxalylaminobenzoic acid moiety as a competitive inhibitor of PTP1B.[106,107] In particular, MD simulation could be an effective tool to search for PTP1B antagonists because the technique permits the investigation of dynamic changes of the WPD loop motility upon binding events.[104,108,109]

As a follow-up study of previous research on *D. rhododendroides*,[71] this chapter presents details of the isolation and structure elucidation of diplostephiosides A (**1**) and B (**2**) and their evaluation for PTP1B inhibitory potential. To expand a previous docking study,[71] molecular dynamics (MD) trajectory simulation was implemented for investigation of the conformational state changes of the WPD loop upon allosteric binding simulation of **1**, **2**, and the Wiesmann's allosteric inhibitor.[101]

RESULTS AND DISCUSSION

The molecular formula of diplostephioside A (**1**) was established as $C_{26}H_{32}O_{13}$ based on information gleaned from a sodium adduct ion at *m/z* 575.1694 $[M + Na]^+$ in HRESIMS and ^{13}C NMR data (**Table 7**).[71] The ^1H and ^{13}C NMR data of **1** (**Table 7**) exhibited the presence of two

symmetrical tetrasubstituted benzenoid moieties [δ_H 7.61 (H-2′, 6′), 6.85 (H-2, 6) and δ_C 154.4 (C-3, 5), 149.1 (C-3′, 5′), 143.9 (C-4′), 135.8 (C-4), 134.5 (C-1), 120.1 (C-1′), 108.6 (C-2′, 6′), 105.6 (C-2, 6)], a glucopyranosyl moiety [δ_H 5.75 (H-1″) and δ_C 105.1 (C-1″), 78.6 (C-2″), 76.2 (C-4″, 5″), 72.2 (C-3″), 65.4 (C-6″)], an ester carbonyl carbon [δ_C 167.1 (C-7″)], and an *E*-configured olefinic moiety [δ_H 6.84 (H-7, d, J = 15.6 Hz), 6.60 (H-8, dt, J = 15.6, 4.8 Hz) and δ_C 129.8 (C-7), 131.4 (C-8)].[71] The HMBC correlations between the proton resonances at δ_H 7.61 (H-2′, 6′) and the ester carbonyl carbon at δ_C 167.1 (C-7″) as well as between the 3′- and 5′-methoxy protons at

δ_H 3.74 and C-3′ and 5′ at δ_C 149.1 revealed the presence of a syringoyl moiety (**Figure 31**B).[71] The second 1,2,3,5-tetrasubstituted aromatic moiety was determined to be part of the sinapyl alcohol unit on the basis of the HMBC correlations from the oxymethylene proton resonances at δ_H 4.59 (H_2-9) to the olefinic carbon resonances at δ_C 131.4 (C-8) and 129.8 (C-7), from the olefinic proton resonances at δ_H 6.84 (H-7) and 6.60 (H-8) to the aromatic carbon resonances at δ_C 134.5 (C-1) and 105.6 (C-2), and from the C-3 and C-5 methoxy proton resonances at δ_H 3.77 to the aromatic carbon resonances at δ_C 154.4 (C-3, 5) (**Figure 31**B).[71] The syringoyl, sinapyl alcohol,

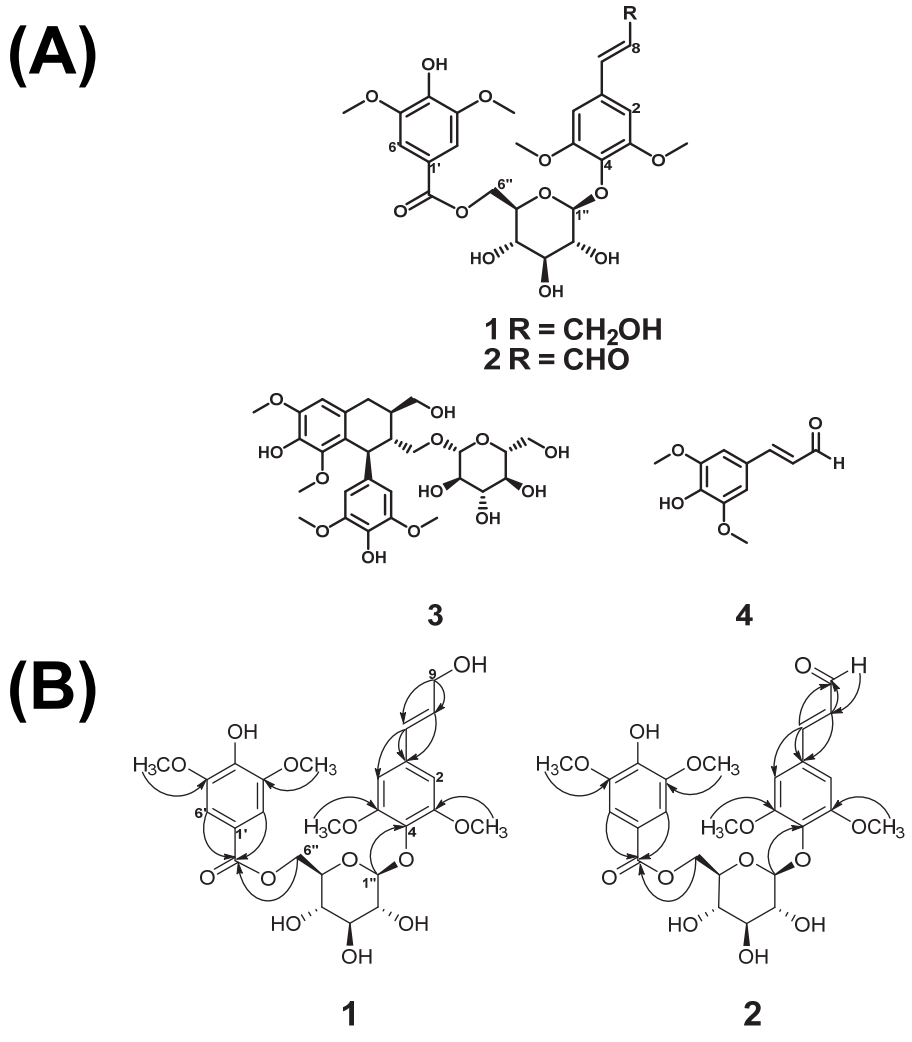

Figure 31. (A) Secondary metabolites from *D. rhododendroides* (**1–4**) and (B) Key HMBC (→) correlations for diplostephiosides A (**1**) and B (**2**)

and glucosyl moieties were connected based on HMBC correlations (**Figure 31**B).[71] The correlation from the anomeric proton resonance at δ_H 5.75 (H-1″) to the carbon resonance at δ_C 135.8 (C-4) indicated the acetalic linkage between C-1″ of glucose and C-4 of the sinapyl alcohol moiety. In addition, the deshielded resonances for the diastereotopic C-6″ protons of glucose at δ_H 5.22 and 4.97, and the carbon at δ_C 65.4 implied an ester linkage between C-6″ of the glucopyranosyl moiety and the ester carbonyl of the syringoyl moiety. This was confirmed by the HMBC correlation from the glucosyl C-6″ methylene proton resonances at δ_H 4.97 and 5.22 to the carbonyl carbon resonance of the syringoyl moiety at δ_C 167.1 (C-7″) (**Figure 31**B).[71] The coupling constant of the anomeric proton (H-1″, d, J = 7.2 Hz) confirmed a β-configured glucosidic linkage. Acid hydrolysis followed by GC analysis of the trimethylsilylated derivative confirmed the presence of the D-(+)-glucopyranosyl moiety in **1** (**Figure 37**). Thus, the structure of the compound **1**, diplostephioside A, was assigned as 4-[6-*O*-(4-hydroxy-3,5-dimethoxy-benzoyl)-β-D-glucopyranosyloxy]-3,5-dimethoxyphenylprop-7*E*-en-9-ol] based upon proper phenylpropanoid numbering and nomenclature in contrast to those followed in reference 71.

Table 7. NMR data of diplostephiosides A (**1**) (pyridine-d_5) and B (**2**) (methanol-d_4)

	1		**2**	
	δ_C	δ_H, mult. (*J* in Hz)	δ_C	δ_H, mult. (*J* in Hz)
1	134.5		130.5	
2	105.6	6.85 [a], s	106.1	6.80, s
3	154.4		153.4	
4	135.8		136.8	
5	154.4		153.4	
6	105.6	6.85 [a], s	106.1	6.80, s
7	129.8	6.84 [a], d (15.6)	153.5	7.42, d (16.0)
8	131.4	6.60, dt (15.6, 4.8)	127.6	6.65, dd (16.0, 7.6)
9	63.2	4.59, br d (4.8)	194.7	9.62, d (7.6)
1'	120.1		119.3	
2'	108.6	7.61, s	107.0	7.14, s
3'	149.1		147.5	
4'	143.9		141.5	
5'	149.1		147.5	
6'	108.6	7.61, s	107.0	7.14, s
1"	105.1	5.75, d (7.2)	102.7	5.04, d (7.6)
2"	78.6	4.37, m	74.2	3.56, m
3"	72.2	4.22, m	76.6	3.49, t (8.8)
4"	76.2	4.22, m	71.0	3.43, t (9.0)
5"	76.2	4.37, m	74.4	3.56, m
6"	65.4	5.22, d (11.2); 4.97, dd (11.2, 6.0)	63.5	4.53, dd (11.6, 7.6); 4.45, dd (11.6, 2.4)
7"	167.1		166.4	
3, 5-OMe	57.0	3.77, s	55.4[b]	3.80 [b], s
3′, 5′-OMe	56.6	3.74, s	55.6[b]	3.81 [b], s

[a] Signals partially overlapped
[b] Assignments may be interchanged

HRESIMS analysis of diplostephiosides B (**2**) identified a protonated ion at *m/z* 551.1745 $[M + H]^+$, which in conjunction with the ^{13}C NMR data led to its molecular formula being established as $C_{26}H_{30}O_{13}$.[71] The 1D NMR data (**Table 7**) for **2** were similar to those of **1** except for the NMR resonances at δ_H 9.62 (H-9) and δ_C 194.7 (C-9), diagnostic for the presence of a formyl functional group.[71] These distinctive NMR resonances along with the difference in two

mass unit in **2** implied that the C-9 hydroxymethylene group of diplostephioside A (**1**) was replaced by a formyl group in **2**. The HMBC correlations from the olefinic proton resonances at δ_H 7.42 (H-7) and 6.65 (H-8) to the C-9 formyl resonance at δ_C 194.7 and the C-1 aromatic resonance at δ_C 130.5, as well as from the formyl proton resonances at δ_H 9.62 to an olefinic carbon resonances at δ_C 127.6 (C-8) further supported the presence of a sinapyl aldehyde moiety (**Figure 31**).[71] The *β*-D-glucopyranosyl moiety of **2** was established on the basis of the coupling constant (J = 7.6 Hz) of the anomeric proton and acid hydrolysis followed by GC analysis of the trimethylsilylated derivative. The HMBC correlation of the anomeric proton resonance at δ_H 5.04 (H-1″) and aromatic carbon resonance at δ_C 136.8 (C-4) revealed the connectivity between C-1″ of glucose and C-4 of the sinapyl aldehyde moiety.[71] The HMBC correlations of the deshielded 6″-methylene proton resonances at δ_H 4.53 and 4.45 and the ester carbonyl carbon resonance at δ_C 166.4 (C-7″) indicated the linkage between C-6″ of the glucopyranosyl residue and the ester carbonyl of the syringoyl moiety (**Figure 31**B).[71] Consequently, the structure of compound **2**, diplostephioside B, was defined as 4-[6-*O*-(4-hydroxy-3,5-dimethoxy-benzoyl)-*β*-D-glucopyranosyloxy]-3,5-dimethoxyphenylprop-7*E*-en-9-al, the name being generated by appropriate application of phenylpropanoid numbering and nomenclature.

Compounds **3** and **4** were identified as (+)-lyoniresinol 3*α*-*O*-*β*-D-glucopyranoside and sinapyl aldehyde, respectively, based on comparison of experimental and reported spectroscopic and physico-chemical data.[110,111]

According to a previous study,[71] compounds **1** and **2** impeded PTP1B activity with half maximal inhibitory concentration (IC_{50}) values of 81.0 and 25.9 μM, respectively. These anti-PTP1B metabolites were investigated for their detailed molecular interactions with PTP1B using molecular docking studies, which suggested they bind to the allosteric site of the target

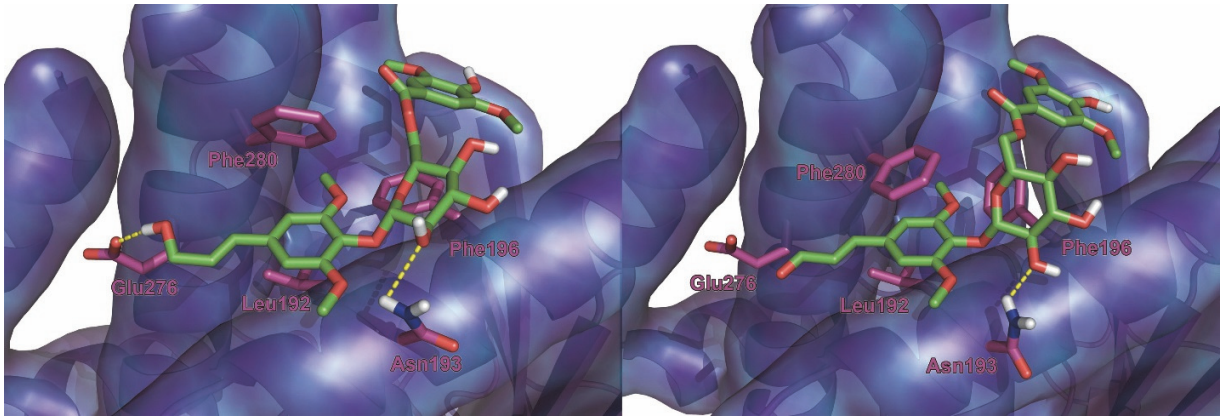

Figure 32.[71] Predicted binding poses of compounds **1** (left) and **2** (right) with key amino acid residues shown. Dotted lines indicate hydrogen bonds.

phosphatase (**Figure 32**).[71] To enhance this preliminary docking study, the conformational changes of the WPD loop were investigated utilizing MD trajectory analysis monitoring the distance between Trp179 and Arg221 upon the binding of **1** and **2**, and the Wiesmann's allosteric inhibitor as a control ligand (**Figure 33**).[101,104] The hydrogen bonding interaction between the aforementioned residues played an indispensable role in the activation of the WPD loop for the dephosphorylation catalytic reaction of PTP1B.[104] Thus, the distance between the carbonyl oxygen of Trp179 and the nitrogen of the guanidinium moiety of Arg221 (**Figure 33**A, see yellow-dotted lines) was examined using 1200 ps MD simulation (**Figure 33**B) upon binding of compounds **1** and **2**, and the Wiesmann's allosteric inhibitor to the allosteric site of PTP1B. The MD trajectory analysis displayed that the distances between the aforementioned residues was 3.67–6.45, 3.50–6.15, and 3.95–6.53 Å upon simulation of the allosteric inhibition by the Wiesmann's inhibitor and compounds **1** and **2**, respectively. The simulated distances of the two atoms generated upon allosteric docking of compounds **1** and **2** were similar with that of the Wiesmann's allosteric inhibitor, implying the binding of compounds **1** and **2** to the allosteric site stabilized and retained the inactivated (open) conformational state of the WPD loop. This observation indicated that their allosteric inhibition precluded the closure of the WPD loop for

formation of a tight binding pocket to implement the catalytic reaction of PTP1B for dephosphorylation. The MD trajectory analysis was also in accord with previous studies[101,104,105] demonstrating the distances of the aforementioned residues to be 4.15–5.22 Å for the open (inactivated) conformation of the WPD loop, and 2.35–3.19 Å for the closed conformation, validating our *in silico* investigation on the WPD loop flexibility.

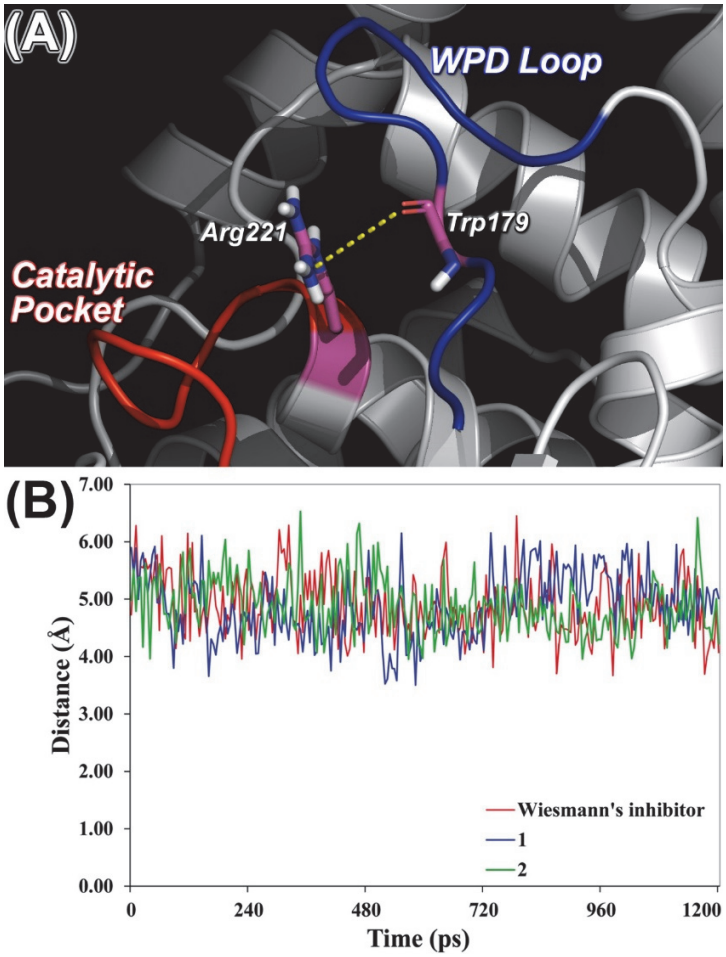

Figure 33. (B) MD trajectory analysis of distance between the carbonyl oxygen of Trp179 and the nitrogen of the guanidinium moiety of Arg221. The measured distance is indicated as yellow-dotted lines in (A). The MD software Desmond (Schrödinger, LLC) was employed with reference to previous studies.[101,104,105] The crystal structure was imported from the PDB data bank (PDB ID: 1T48), optimized, and minimized employing Protein Preparation Wizard and redrawn using Pymol (Schrödinger LLC.). Wiesmann's inhibitor indicates the allosteric inhibitor co-crystallized with 1T48[101,103]

CONCLUSIONS

This chapter elaborated details on the isolation and structure elucidation of diplostephiosides A and B (**1** and **2**) from a rare South American plant species, *D. rhododendroides*. Furthermore, MD analysis of **1** and **2** based on their docking simulation validated that a glucosyl moiety flanked by two aromatic groups may be a suitable template that

could be developed into selective PTP1B allosteric antagonists. Collectively, utilization of the metabolites obtained from endangered and rare plant species may warrant a strong and sustained emphasis on their conservation.

EXPERIMENTAL SECTION

General Experimental Procedures

See *General Experiments* sections in the previous chapters for routine experiment protocols.

The GC-MS data was recorded on a Hewlett Packard GC 6890 with an HP-5 column (cross-linked 5% phenyl methyl siloxane, 30.0 m × 250 μm × 0.25 μm) employing helium as carrier gas.

Plant Material

A *Diplostephium rhododendroides* Hieron. (Asteraceae) voucher sample was deposited in the National Herbarium at the Smithsonian Institution (code 0CJS1259) and the EtOH extract of the stems was obtained from Dr. D. Newman, Natural Products Repository, National Cancer Institute (NCI).

Extraction and Isolation

The EtOH extract (15 g) was subjected to Si gel VLC (1500 g, 40-75 μm) and eluted with a stepwise gradient of *n*-hexane/EtOAc [100:0, 75:25, 50:50, 25:75, 0:100 v/v (each 3 L)], EtOAc/MeOH [75:25, 50:50, 25:75, 100:0 v/v (each 3 L)], and MeOH/H_2O [75:25, 50:50, 100:0 v/v (each 3 L)] to give 12 fractions (Fr. 1 − 12). Fr. 6 (2.0 g) was further divided into 20 fractions (Fr. 6-1 to 6-20) using a C_{18} HPLC column (21.2 × 250 mm, 5 μm) with a gradient of MeOH/H_2O (35:65 → 60:40 v/v over 50 min, then 60:40 → 100:0 v/v for 5 min. Of these, Fr. 6-16 (99.0 mg) was resolved on a C_{18} HPLC column (10.0 × 250 mm, 5 μm) with a linear gradient of MeCN/H_2O (23:77 → 25:75 v/v for 60 min) to afford five sub fractions (Fr. 6-16-1 to 6-16-5). Fr. 6-16-3 was

further purified employing C_{18} HPLC [10.0 × 250 mm, 5 μm, MeCN/H_2O (17:83 v/v)] to yield compound **1** (t_R 20 min, 8.3 mg). Purification of Fr. 6-16-5 using a C_{18} HPLC column (10.0 × 250 mm, 5 μm) with a linear gradient of MeCN/H_2O (23:77 → 25:75 v/v for 60 min) afforded compound **2** (t_R 20 min, 16.6 mg). Fr. 6-8 (15.6 mg) was chromatographed using a C_{18} HPLC column [10.0 × 250 mm, 5 μm, MeCN/H_2O (17:83 v/v) for 30 min] to yield compound **3** (t_R 25 min, 15.3 mg). Compound **4** (t_R 38 min, 2.0 mg) was obtained from Fr. 6-18 (19.0 mg) employing a C_{18} HPLC column [10.0 × 250 mm, 5 μm, MeCN/H_2O (23:77 v/v) for 60 min].

Diplostephioside A (1): white amorphous powder; $[\alpha]_D^{25}$ −15 (*c* 0.2, MeOH); UV (DAD) λ_{max} 265.8 nm; ^{1}H and ^{13}CNMR see Table 1; HRESIMS *m/z*: 575.1694; $[M + Na]^+$ (Calcd. for $C_{26}H_{32}Na_1O_{13}$: 575.1735)[71]

Diplostephioside B (2): white amorphous powder; $[\alpha]_D^{25}$ −28 (*c* 0.2, MeOH); UV (DAD) λ_{max} 292.4, 315.6 nm; ^{1}H and ^{13}C NMR see Table 1; HRESIMS *m/z*: 551.1745 $[M + H]^+$ (Calcd. for $C_{26}H_{31}O_{13}$: 551.1765)[71]

Carbohydrate Analysis[90]

Compound **1** (1 mg) was dissolved in 0.5 mL of 1 N HCl, heated at 90 °C for 2 h, and partitioned with EtOAc and H_2O (3 × 1 mL). The aqueous layer was neutralized with Ag_2CO_3 and centrifuged. The dried supernatant was dissolved in anhydrous pyridine (1 mL) and 0.1 M L-cysteine methyl ester hydrochloride in pyridine (2 mL) was added. The mixture was kept at 60 °C for 1 hr. After the reaction mixture was dried in vacuo, the residue was trimethylsilylated with 1-trimethylsilylimidazole (0.5 mL) at 60 °C for 5 min. The resulting mixture was partitioned between *n*-hexane and H_2O (3 × 1 mL) and the *n*-hexane fraction was analyzed utilizing a GC column (HP-5ms, 5% phenyl 95% methyl polysiloxane, 30.0 m × 250 μm × 0.25 μm). The injector temperature

was set at 260 °C and the GC oven temperature was kept at 100 °C for 1 min and increased to 280 °C at a rate of 20 °C/min using helium as carrier gas. The retention times of the standard sugars were as follows: D-glucose (t_R 10.84 min) and L-glucose (t_R 10.95 min). In the hydrolysates of **1**, only D-glucose (t_R 10.83 – 10.85 min) was detected (Figure S14).

PTP1B Assay

PTP1B (human, recombinant) was purchased from BIOMOL® International LP (Plymouth Meeting, PA). The enzyme activity was evaluated utilizing *p*–nitrophenyl phosphate (*p*NPP), as described previously.[112] To each of 96 wells in a microtiter plate (final volume: 100 μL) was added 2 mM *p*NPP and PTP1B (0.05 – 0.1 μg) in a buffer containing 50 mM citrate (pH 6.0), 0.1 M NaCl, 1 mM EDTA, and 1 mM dithiothreitol with or without the test compounds. After incubation at 37°C for 30 min, the reaction was quenched with 10 M NaOH. The amount of *p*–nitrophenol was evaluated by measuring the absorbance at 405 nm. The non-enzymatic hydrolysis of 2 mM *p*NPP was adjusted assessing the increase in absorbance at 405 nm obtained in the absence of PTP1B enzyme.

Molecular Dynamics (MD) Simulation

All MD simulations were performed using Desmond ver. 3.0 (Schrödinger LLC.) based on protocols of previous PTP1B MD studies.[105,113] Compounds **1** and **2**, and 1T48 employed for previous docking studies[71,103] were minimized and solvated under the OPLS2005 force field with the explicit simple point charge (SPC) water model. The systems were neutralized by the addition of six sodium ions to replace SPC water molecules. MD simulations (1.2 ns) were carried out under 300 K and 1.0 atm. The coordinates were saved with every 1.2 ps of energy and 4.8 of trajectory.

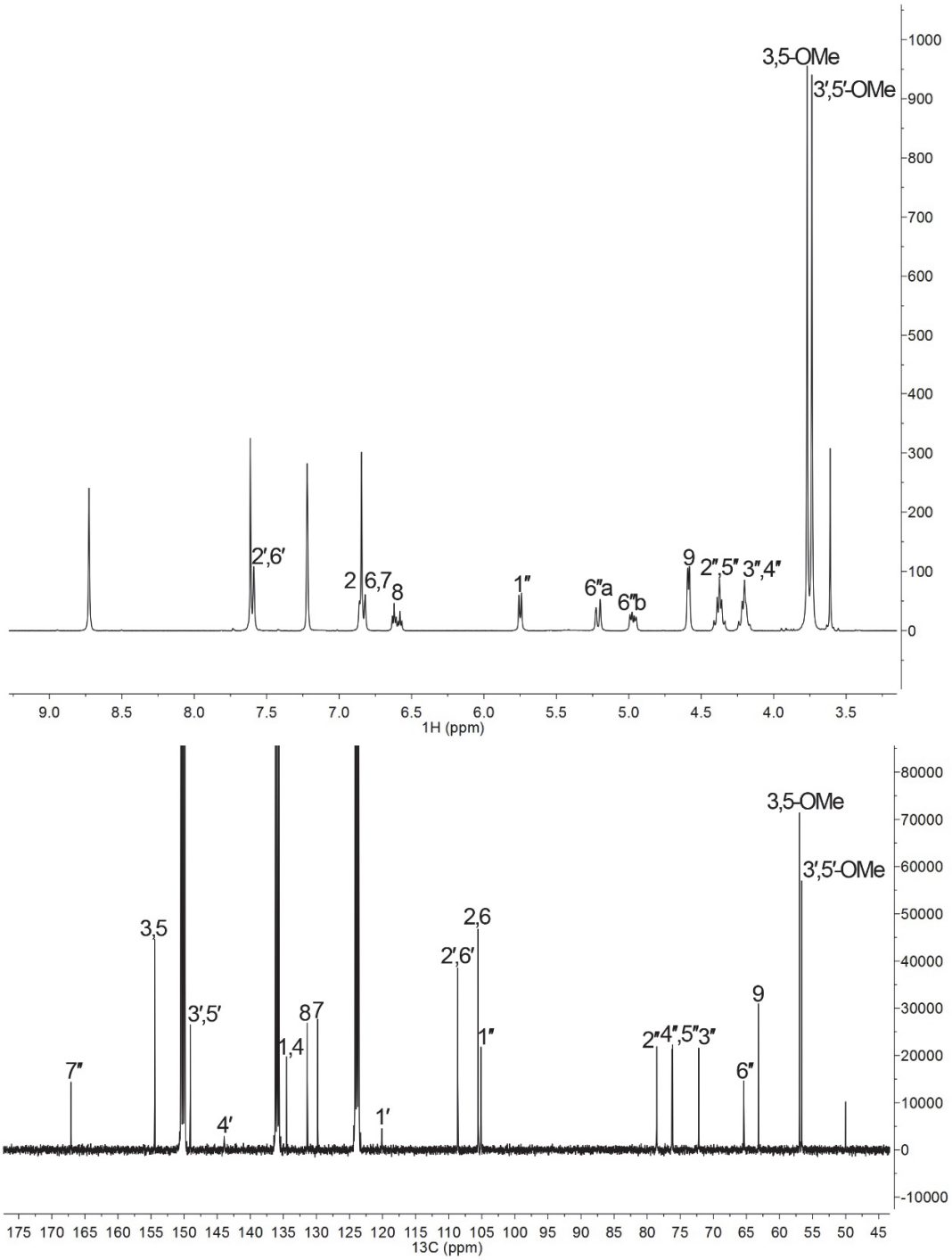

Figure 34. ^{1}H (top) and ^{13}C (bottom) NMR spectra (pyridine-d_5) of diplostephiosides A (**1**)

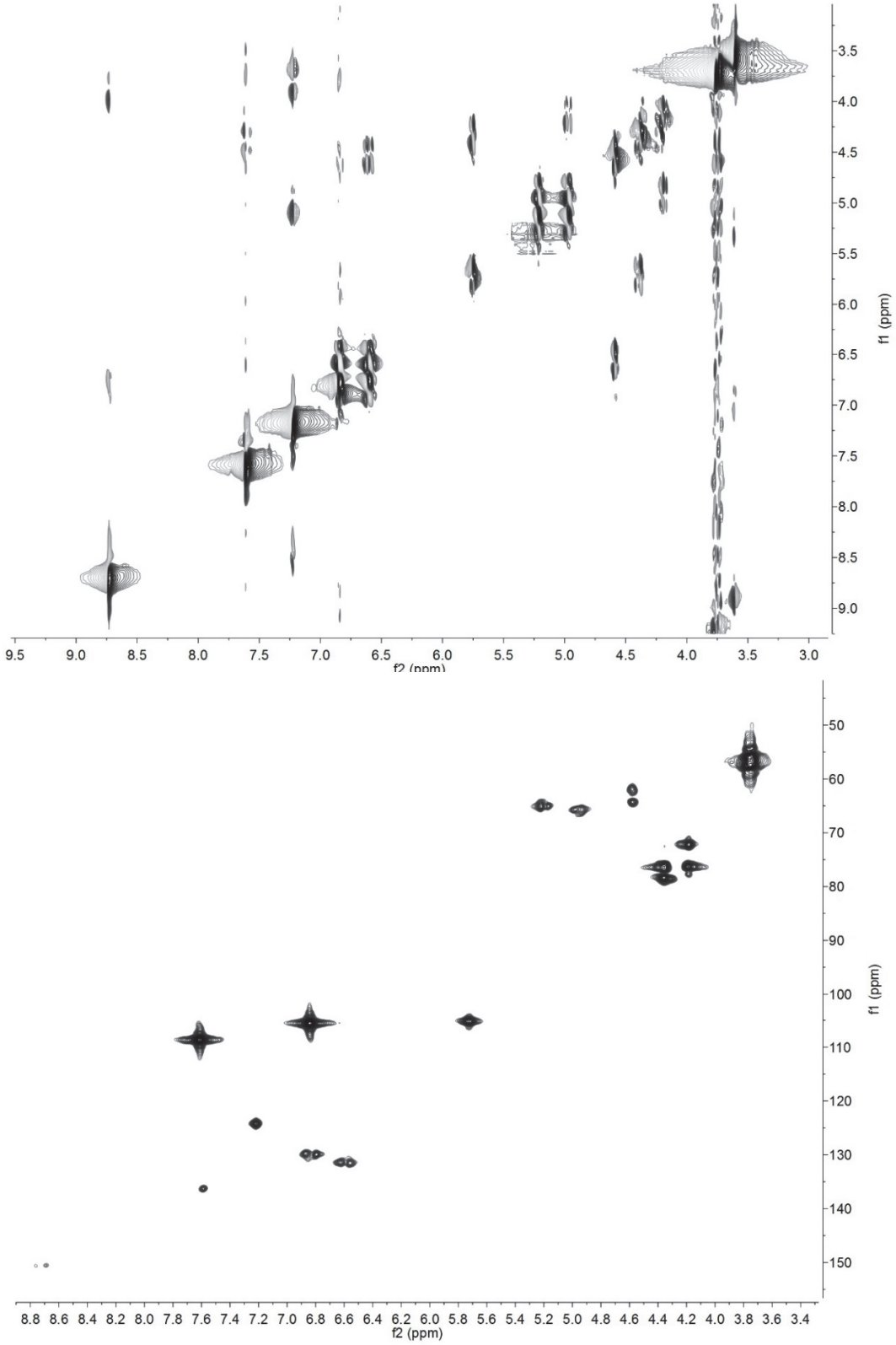

Figure 35. DQF-COSY and heteronuclear multiple-quantum correlation spectroscopy (HMQC) spectra (pyridine-d_5) of diplostephiosides A (**1**)

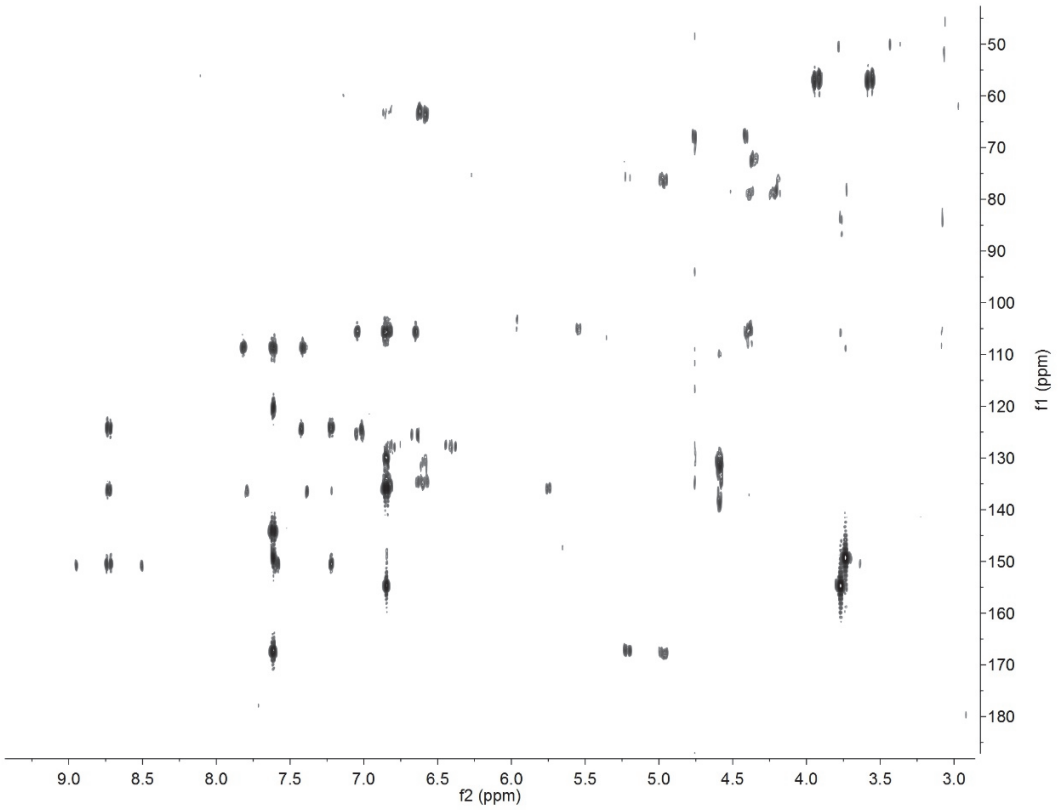

Mass Spectrum Molecular Formula Report

Analysis Info

Analysis Name	I:\N77951-6-16-3-4_5_01_11741.d	Acquisition Date	10/4/2007 7:35:13 PM
Method	LCMS-rutin-pos.m		
Sample Name	N77951-6-16-3-4	Operator	Administrator
Comment		Instrument	micrOTOF 93

Acquisition Parameter

Source Type	ESI	Ion Polarity	Positive	Set Corrector Fill	52 V
Scan Range	n/a	Capillary Exit	80.0 V	Set Pulsar Pull	402 V
Scan Begin	50 m/z	Hexapole RF	200.0 V	Set Pulsar Push	402 V
Scan End	3000 m/z	Skimmer 1	50.0 V	Set Reflector	1305 V
		Hexapole 1	21.9 V	Set Flight Tube	9000 V
				Set Detector TOF	2150 V

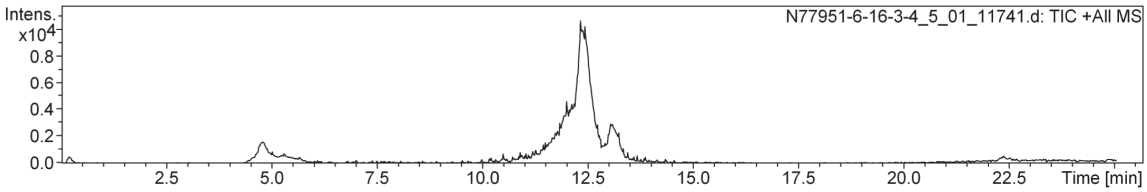

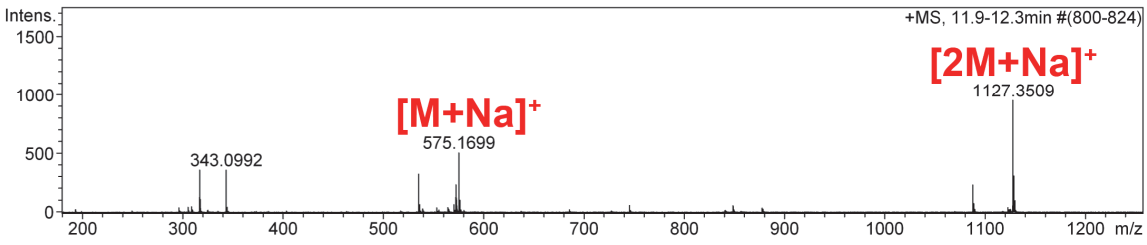

Sum Formula	Sigma	m/z	Err [ppm]	Mean Err [ppm]	rdb	N Rule	e⁻
C 26 H 32 Na 1 O 13	0.05	575.1735	6.25	5.48	10.50	ok	even

Figure 36. HMBC and HRESIMS spectra of diplostephiosides A (**1**)

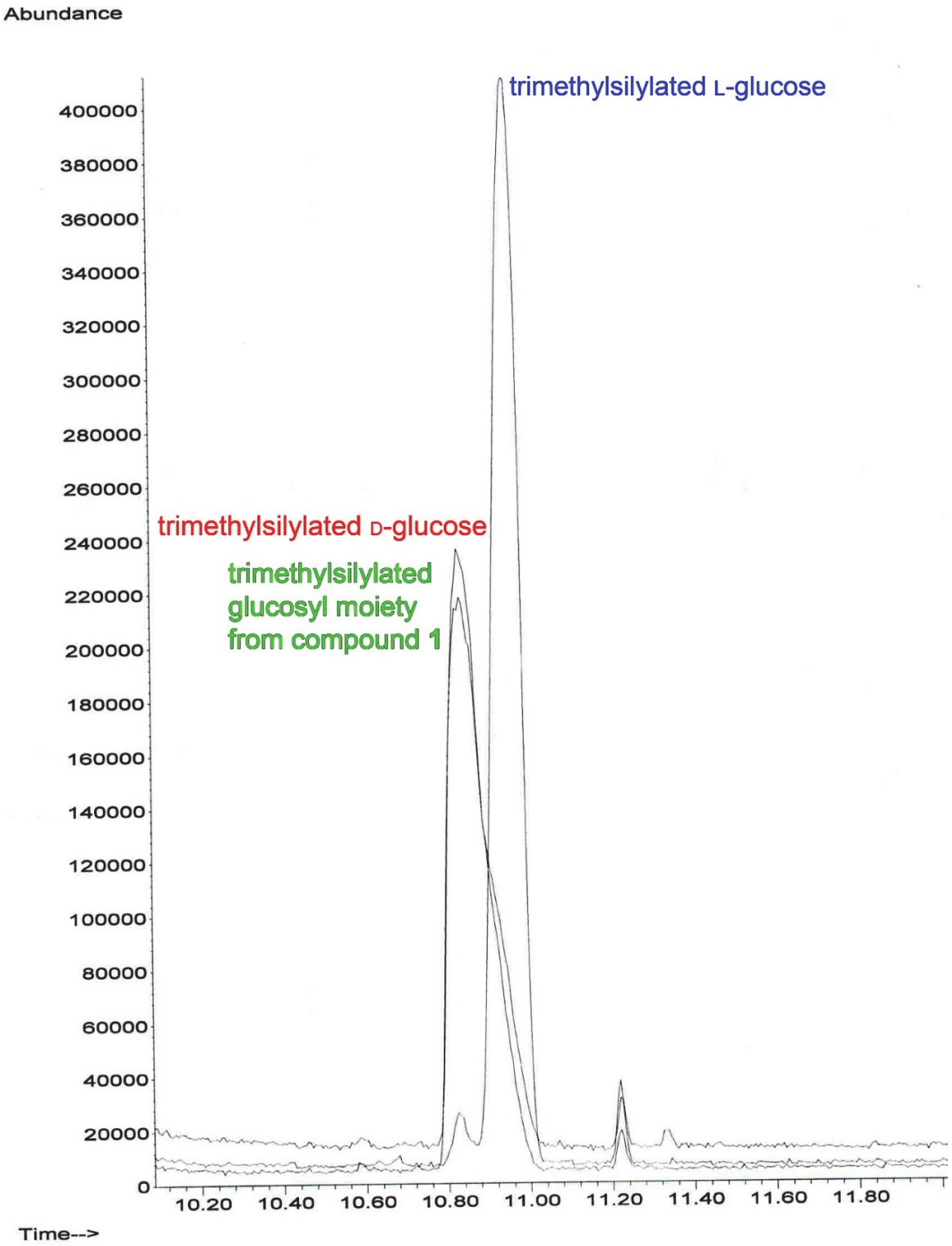

Figure 37. Overlaid GC spectra of trimethylsilylated glucosyl moiety of **1** and chiral glucose standards

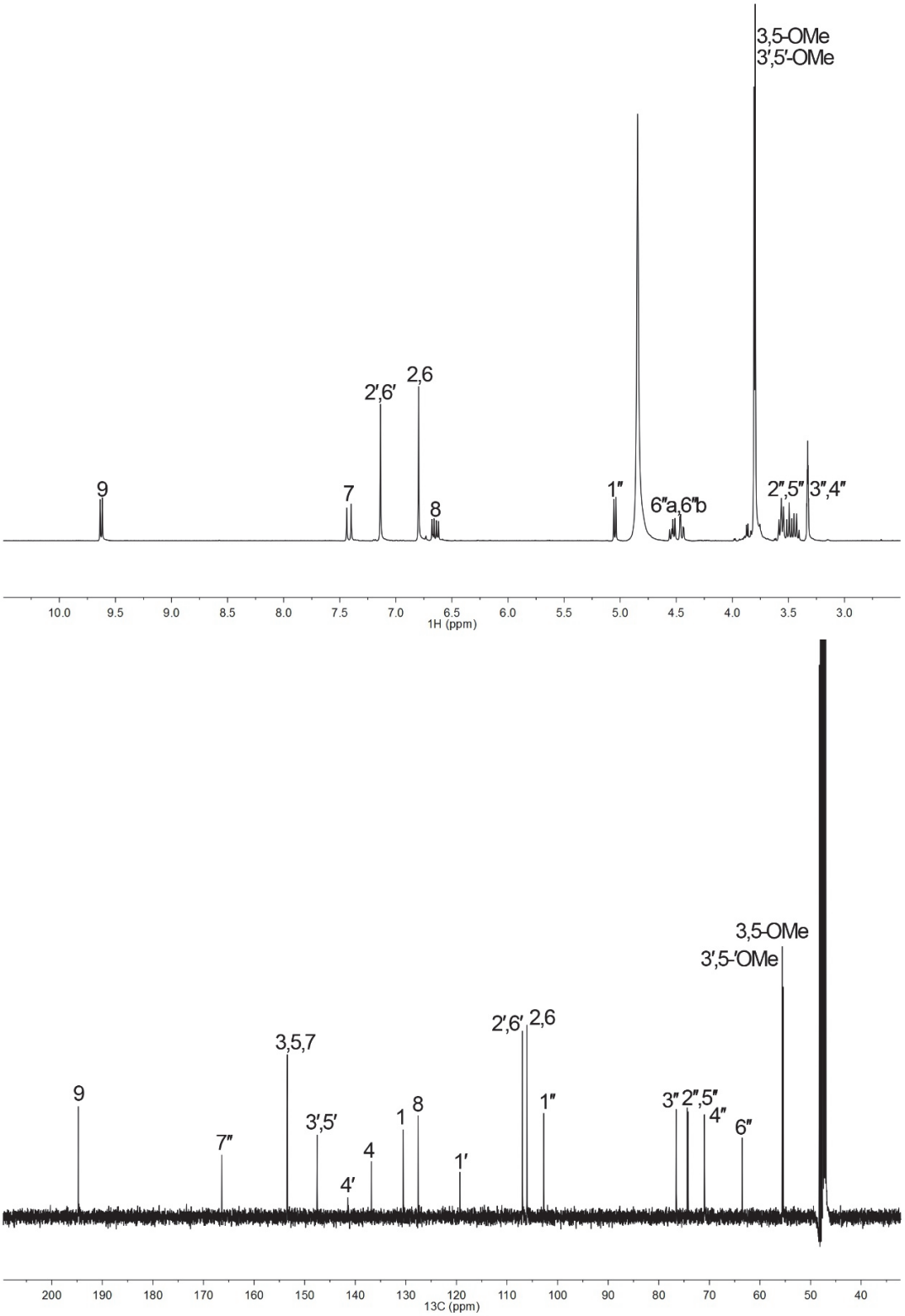

Figure 38. ^{1}H (top) and ^{13}C (bottom) NMR spectra (methanol-d_4) of diplostephiosides B (**2**)

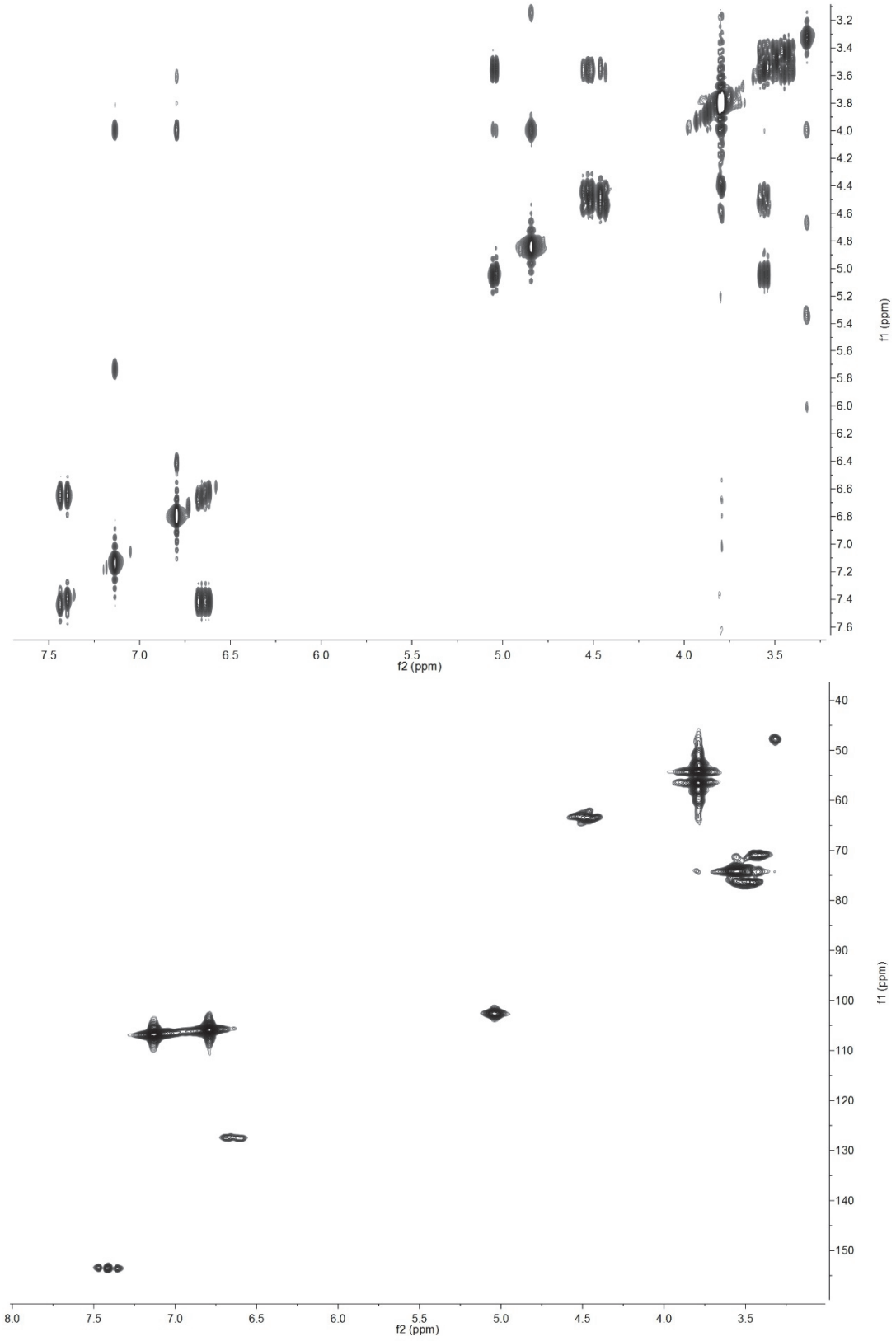

Figure 39. COSY (top) and HMQC (bottom) spectra of diplostephiosides B (**2**)

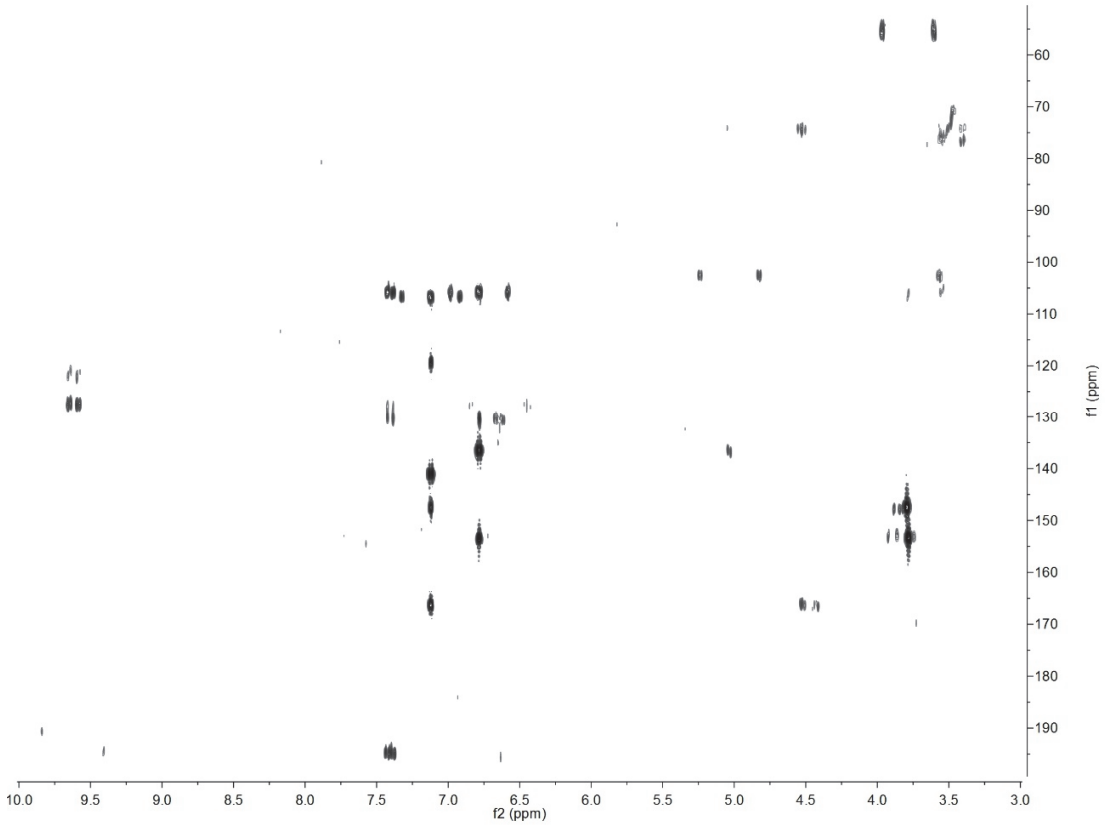

Mass Spectrum Molecular Formula Report

Analysis Info

Analysis Name	I:\N77951-6-16-5(1)_71_01_11541.d	Acquisition Date	9/25/2007 5:23:04 AM
Method	LCMS-rutin-pos.m		
Sample Name	N77951-6-16-5(1)	Operator	Administrator
Comment		Instrument	micrOTOF 93

Acquisition Parameter

Source Type	ESI	Ion Polarity	Positive	Set Corrector Fill	52 V
Scan Range	n/a	Capillary Exit	80.0 V	Set Pulsar Pull	402 V
Scan Begin	50 m/z	Hexapole RF	200.0 V	Set Pulsar Push	402 V
Scan End	3000 m/z	Skimmer 1	50.0 V	Set Reflector	1305 V
		Hexapole 1	21.9 V	Set Flight Tube	9000 V
				Set Detector TOF	2150 V

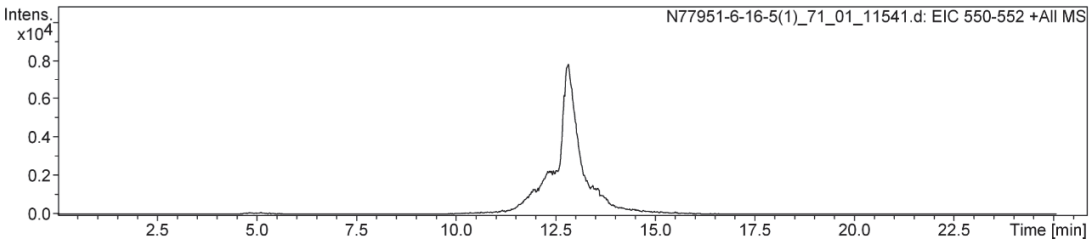

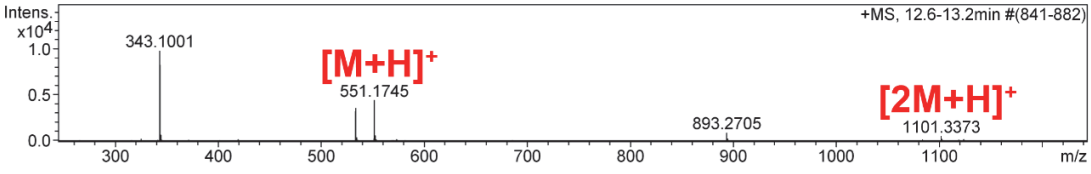

Sum Formula	Sigma	m/z	Err [ppm]	Mean Err [ppm]	rdb	N Rule	e⁻
C 26 H 31 O 13	0.09	551.1759	2.60	2.06	11.50	ok	even

Figure 40. HMBC and HRESIMS spectra of diplostephiosides B (**2**)

PART II: SYNTHETIC STRATEGY FOR PARTIAL SYNTHESIS OF SPONGE-DERIVED CYTOTOXIC DRUG PROTOTYPES AND STEREOSTRUCTURE OF BRCA1-IRIS INHIBITORY PEPTIDE EXHIBITING POTENT IN VIVO CYTOTOXIC ACTIVITY ON TRIPLE-NEGATIVE BREAST CANCER AND

CHAPTER 5

N-DEMETHYLATED MAKALUVAMINE A, A VERSATILE INTERMEDIATE FOR THE SYNTHESIS OF PYRROLOIMINOQUINONE-BASED CYTOTOXIC ALKALOIDS

CHAPTER 6

CHARACTERIZATION OF THE 3D STRUCTURE OF BRCA1-IRIS INHIBITORY PEPTIDE EMPLOYING THE ENSEMBLE OF A HIGH-FIELD NMR STUDY AND *IN SILICO* METHODS

CHAPTER 5: *N*-DEMETHYLATED MAKALUVAMINE A, THE VERSATILE INTERMEDIATE FOR SYNTHESIS OF PYRROLOIMINOQUINONE-BASED CYTOTOXIC ALKALOIDS

INTRODUCTION

Pancreatic cancer has been recognized as a major cause of death in the West along with breast cancer that will be addressed in Chapter 6. In 2015, an estimated 48,960 people in the US will be diagnosed with pancreatic cancer and about 20,710 will die from the serious disease.[114] These statistics render the malignancy to be the 4th leading cause of death from cancer in the US,[115] despite significant reductions in deaths and diagnoses of many other cancers.

Marine organisms harvested from global bodies of water have been validated as enriched resources for providing diverse and potent anticancer drug leads.[116] This is evidenced by the first anticancer drug to reach the market ecteinascidin-743 (ET-743/trabectedin) from the Caribbean tunicate *Ecteinascidia turbinate*,[117] a cytotoxic cyclic depsipeptide, didemnin B from the tropical *Tridemnum solidum*[118] and kahalalide F from the herbivorous Hawaiian opisthobranch *Elysia rufescens* and its prey *Bryopsis* spp.,[119] halichondrin B from the Japanese sponge *Halichondria okadai*[120] which was modified into the recently FDA-approved anticancer drug, eribulin mesylate,[121] and pyrroloiminoquinones such as the discorhabdins and makaluvamines, from diverse sponge sources worldwide, showing broad-spectrum antiproliferative effects and capable of inhibiting topoisomerase II, respectively.[122] Despite the extensive global investigations of marine resources during the last few decades,[116] the Aleutian Islands and invertebrate communities have been underutilized in investigation of antineoplastic leads presumably because of limited access. Consequentially, some marine environments in the Aleutian Islands remain unexplored, which may hold a promise for providing novel and prospective prototypes for anticancer chemotherapy. During our research group's sponge collection conducted in deep waters off the Aleutian Islands, more than 150 marine invertebrates were harvested and subjected to various bioassay screenings to search for antiproliferative pharmacophores.[123] Among the collected

diverse sponge materials, *Latrunculia* spp. produced discorhabdin X (unpublished) possessing intriguing ring systems based on a pyrroloiminoquinone architecture[122] and exhibiting selective cytotoxic activities in breast, brain, and pancreatic cancer cell lines (**Table 8**).

Table 8. Discorhabdin X and zones of inhibition (mm) against a wide range of cancer cell types. DMSO and ecdysone are employed as negative controls and discorhabdin A and karlotoxin 2 as positive controls.

Compound	Conc. (mg/mL)	L1210 (murine leukemia)	Colon 38 (murine colon cancer)	CFU-GM (human hematopoietic progenitor cell)	H-116 (human colon cancer)	H-125 (human lung cancer)	MCF-7 (human breast cancer)	LNCaP (human prostate cancer)	OVCAR-5 (human ovarian cancer)	U251N (human brain tumor)	MDA-MB-231 (human breast cancer)	PANC-1 (pancreatic cancer)	CCRF-CEM (human leukemia)
DMSO		0	0		0	0	0	0	0	0	0	0	
Ecdysone	2	0	0		0	0	0	0	0	0	0	0	
Discorhabdin X	2	950	>1000		>1000								
	1/4	700	>1000	**>1000**	950	>1000	**>1000**		900	**>1000**	>1000		900
	1/16	500	900	**>1000**	600	900	**>1000**	1000	700	**850**	800	**>1000**	750
	1/64	250	450	**750**	250	400	**600**	500	350	**700**	500	**650**	350
Karlotoxin 2	2	150	200		200	100	200	400	200	150	200	200	100
Discorhabdin A	2	1000	750		>1000								
	1/4	300	800	>1000	900	950	800		700	300	1000	450	450
	1/16	250	700	300	500	750	600	500	500	300	500	150	100
	1/64					400	350	250	200	200	300	100	50

The difficulty of developing prodrugs from marine invertebrates is evident because those materials are generally unculturable, which implies that the marine-derived secondary metabolites should be extracted and purified from specimens harvested by costly endeavors.[116] This poses a serious challenge to an adequate supply of marine natural products, which is a prerequisite for determining their clinical potential in vivo. Even though synthetic approaches have played a role in resolving the supply strain, large-scale synthesis demands a significant amount of time and resources, and often fail in generating an appropriate amount of target compounds. Thus, it is of great importance to fashion a viable synthetic route where each step comprising the synthetic strategy is well-established, and cost-effective starting materials and reagents are utilized.

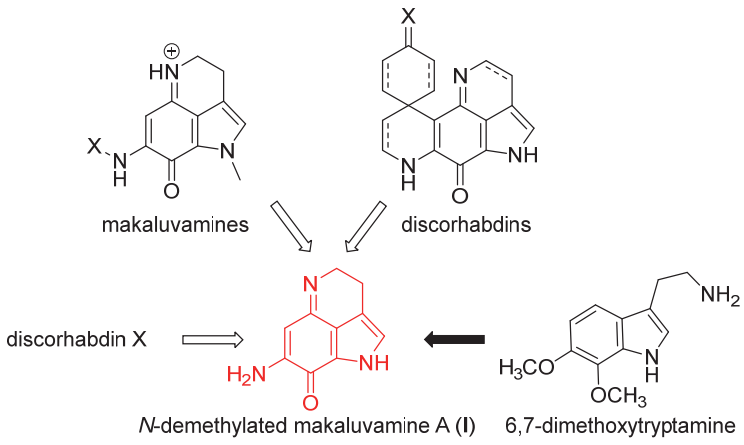

Scheme 1. The versatile intermediate **I** (*N*-demethylated makaluvamine A) for the synthesis of pyrroloiminoquinone-based cytotoxic alkaloids

Among the numerous pharmacophores identified from marine communities, pyrroloiminoquinone-based alkaloids such as discorhabdins and makaluvamines, briefly mentioned in the Introduction, have been recognized as a prospective antineoplastic scaffold due to the highly fused planar core structure.[122] There have been previous attempts to synthesize cytotoxic pyrroloiminoquinone alkaloids (Scheme 2). The core tricyclic indole architectures were prepared via condensation of tryptamines with the quinone residue,[124-127] or cyclization of 4-aminoindole,[128-131] 4-chlorotryptamine,[132] or 3-(azidoethyl)indole functionalities.[133,134] However, some of those strategies were developed based on costly starting materials, more than 10 reaction steps, and relatively small reaction scales (see Scheme 2 for details). This makes it impractical that those approaches are applied for a large scale synthesis of a marine-derived prodrug to address the supply strain. This chapter delineates the development of a practical and scalable synthetic approach (Hamann's group approach in Scheme 2) employing inexpensive starting materials with a large scale (230 mmol), and relatively short and straightforward reaction steps (eight steps) with stable intermediates aiming at the synthesis of a sufficient amount of the versatile intermediate **I**

for discorhabdin X and the related pyrroloiminoquinone-based cytotoxic alkaloids (Scheme 1).

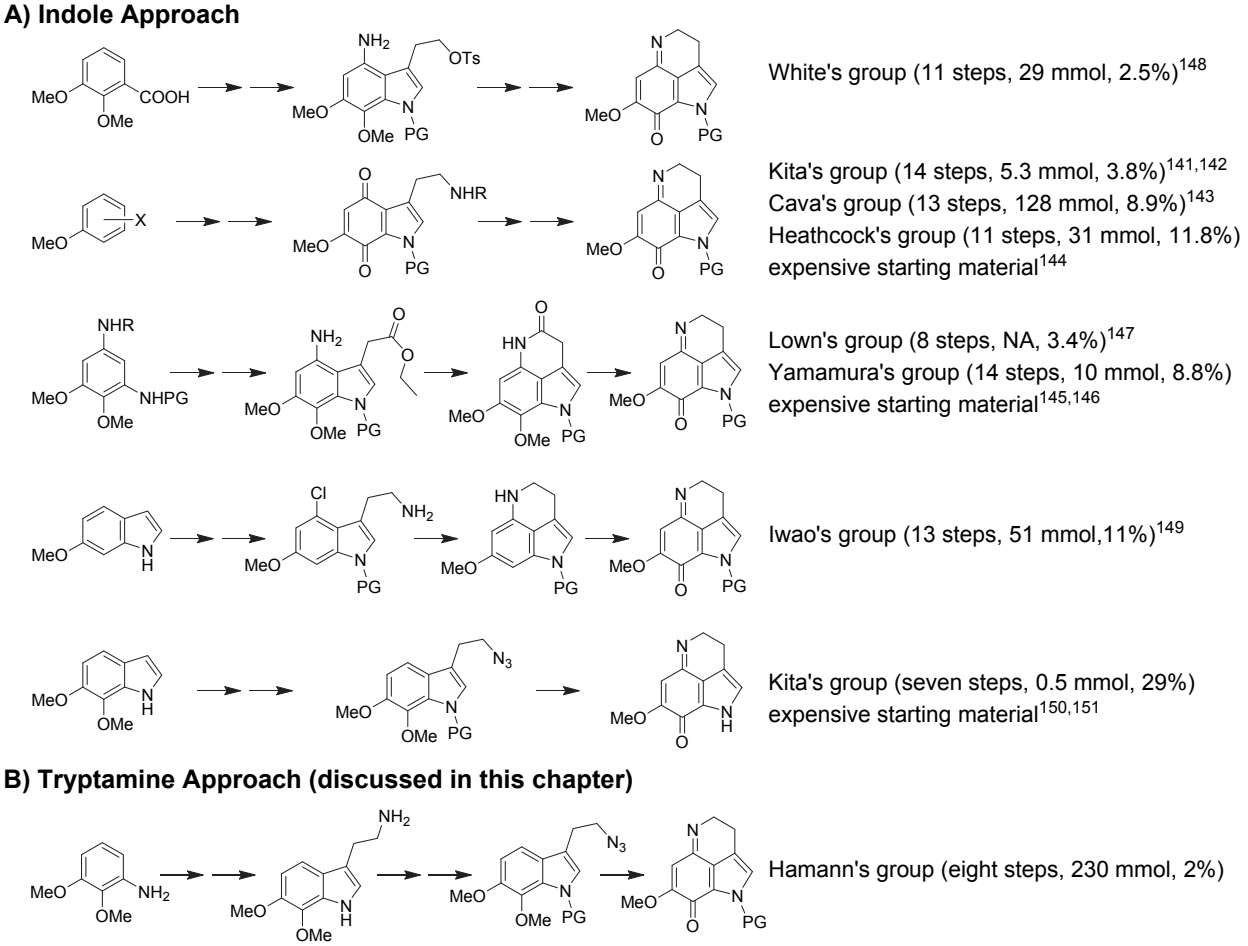

Scheme 2. Previous protocols for the synthesis of pyrroloiminoquinones. Part of this scheme was adopted with permission from Hu, J.-F.; Fan, H.; Xiong, J.; Wu, S.-B. *Chem. Rev.* 2011, 111, 5465-5491. Copyright 2011 American Chemical Society. Reaction steps, scales, and overall yields for each synthetic approach are shown in parentheses; PG: Protecting Group; NA: Not Available

RESULTS AND DISCUSSION

Unlike the previous protocols for synthesis of pyrroloiminoquinones (Scheme 2), the current strategy in this chapter employs a tryptamine framework in **I** as the key intermediate. In order to cost-effectively synthesize it, a one-pot synthesis approach utilizing palladium-catalyzed annulation of *o*-iodoaniline **2** and aldehyde **5** was employed.[135] With reference to reported procedures, commercially available aniline **1** was iodinated employing iodine monochloride in a

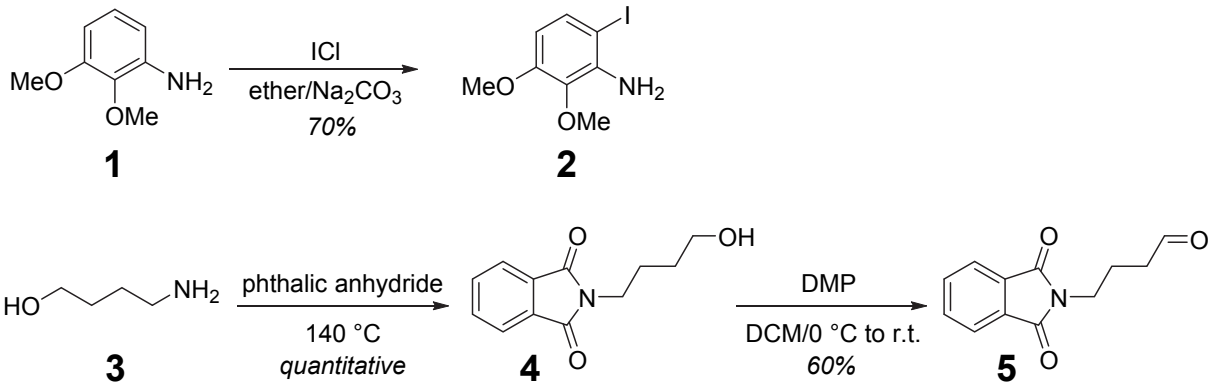

Scheme 3. Preparation of coupling partners for the generation of dimethoxytryptamine via pd-catalyzed annulation

biphasic solution to generate 6-iodo-2,3-dimethoxyaniline (**2**) (70%, 66 mmol-scale) (Scheme 3) for the Pd-catalyzed coupling reaction.[136] Using Dess–Martin periodinane (DMP) oxidation, the other aldehyde (**5**) partner was prepared from 4-phtalimidobutanol **4** (60%, 36 mmol-scale)[137,138] that was synthesized simply by heating a mixture of phthalic anhydride and 4-aminobutanol **3** (quantitative, 230mmol-scale) (Scheme 3).[139]

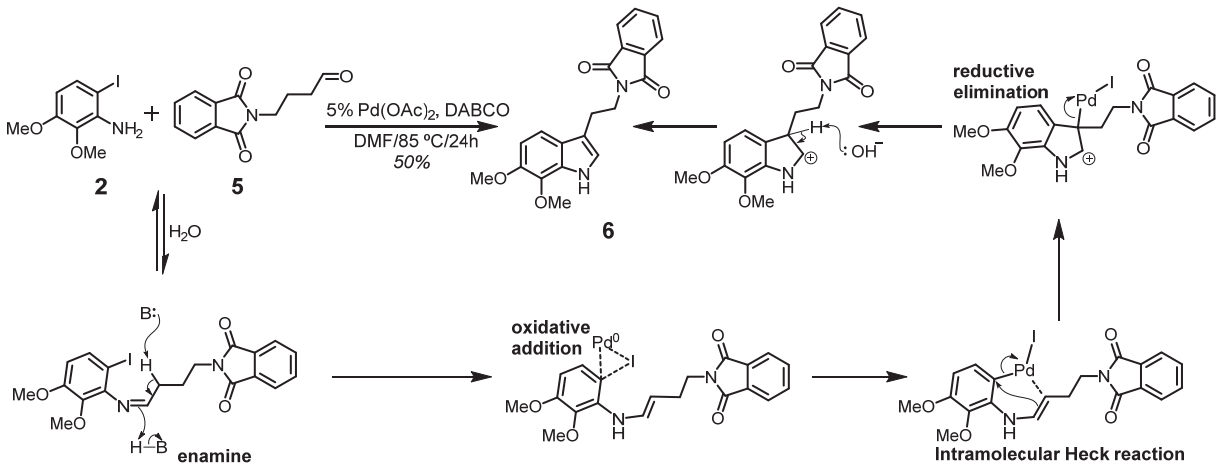

Scheme 4. Pd-catalyzed cyclization via intramolecular Heck reaction and its mechanism. Pd: $Pd(OAc)_2$, DABCO: 1,4-diazabicyclo[2.2.2]octane

The coupling reaction was implemented with **2** and **5** via the intramolecular Heck reaction catalyzed by the relatively inexpensive palladium source $Pd(OAc)_2$ (50%, 10.5 mmol-scale)

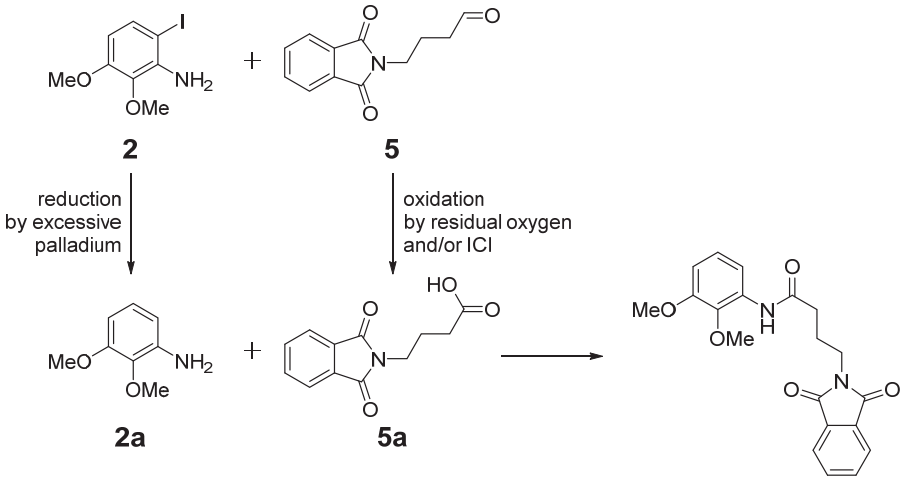

Scheme 5. Side reactions dropping the yield of the palladium-catalyzed cyclization reaction

(Scheme 4) to generate *N*-protected 6,7-dimethoxytryptamine **6**.[135,140] The Pd-catalyzed reaction should be performed carefully in terms of the purity of the coupling partners, reaction concentrations, and an accurate amount of the catalyst used since the reaction was involved with an intermolecular reaction to produce enamine and an intramolecular reaction to generate the pyrrole functionality (Schemes 4 and 5). Indeed, residual ICl used to generate **2** rapidly oxidized phthalamic aldehyde **5** into its corresponding carboxylic acid **5a** (Scheme 5). This unexpected oxidation was also effected by residual oxygen in dimethylformamide (DMF), which stresses the necessity of the solvent being rigorously degassed for the annulation reaction. Moreover, an excessive amount of $Pd(OAc)_2$ led to the dehalogenation of **2** to form **2a** and this deiodinated product subsequently reacted with **5a**, leading to a significant reduction in yield of the Pd-catalyzed reaction (Scheme 5). The phthalimide-protected **6** was deprotected utilizing 85% hydrazine monohydrate to obtain

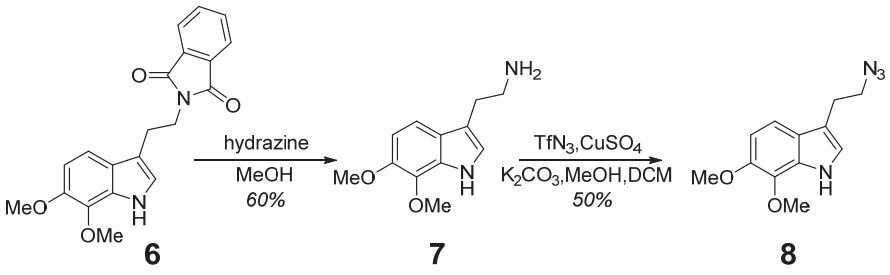

Scheme 6. Deprotection of the phthalimide group and successive formation of azide **8**

6,7-dimethoxytryptamine **7** (60%).[140] Next, Cu^{2+}-catalyzed azido group transfer using trifluoromethanesulfonyl azide (TfN_3) was implemented to convert amine **7** to azide **8** (50%)[141] (Scheme 6) that would play a key role in constructing a pyrroloiminoquinone template in later steps. This azido transferring strategy, which has been predominantly used in aminosugar synthesis, was also applicable for generating a target azide from a terminal amino group comprising a tryptamine moiety, which verifies the substrate tolerance of such a reaction application.

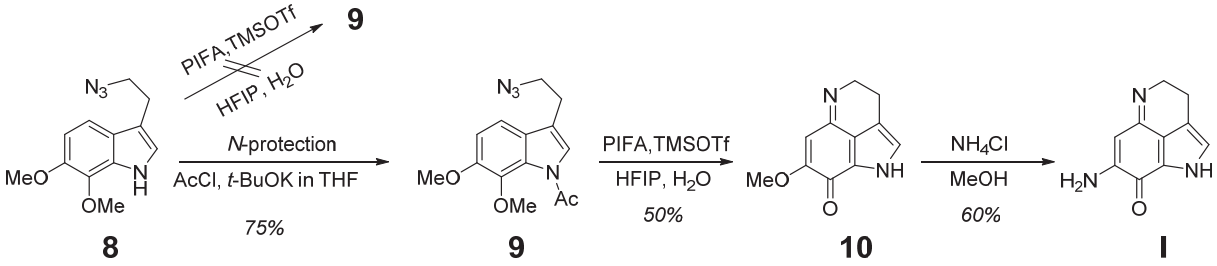

Scheme 7. Activated PIFA-mediated formation of the indole-based tricyclic structure followed by transamination for synthesis of the end product **I**. *t*-BuOK: potassium *tert*-butoxide

The indole alkaloid bearing an ethylazido side chain **8** was used to attempt cyclization into pyrroloiminoquinone **9** utilizing the hypervalent iodine (III) reagent [bis(trifluoroacetoxy)iodo]benzene (PIFA) activated by trimethylsilyl trifluoromethanesulfonate (TMSOTf) in a mixture of $(CF_3)_2CHOH$ (1,1,1,3,3,3-hexafluoroisopropanol, HFIP) and H_2O.[133] The reaction resulted in complex mixtures presumably because of side reactions occurring with the activated PIFA at the nucleophilic centers in **8**, i.e., N-1, C-2, and C-3 as discussed in previous studies.[133,142] Alternatively, the N-1 position of indoles was protected with electron-withdrawing groups including an acetyl group (**9**, 75%) and treated with the activated PIFA in a mixture of HFIP and H_2O (50:1) to establish the formation of the corresponding pyrroloiminoquinone **10** as

found in previous studies (50%) (Scheme 7).[133,143] The transamination approach, which was employed for such transformation from *N*-methylated **10** to makaluvamine A, was adopted to convert **10** to **I**, the end product (60%) (Scheme 7).[144]

Even though some reaction steps in this chapter were validated to be scalable and versatile with diverse substrates, those protocols were not successful in terms of the overall yield (2%) as compared to a similar synthetic scheme developed by Kita's group to generate the key intermediate **10** (Scheme **8**, 29%).[143] Thus, the Kita's protocols are currently attempted to be reproduced and optimized to synthesize **8**. The commercially available starting material **11**[145] was treated with oxalyl chloride in dry Et_2O to synthesize **12** (85%), which was reduced into **13** using $LiAlH_4$ in dry THF (50%). The current yields are lower than the reported ones, which implies that optimization of the currently performed reactions is necessary.

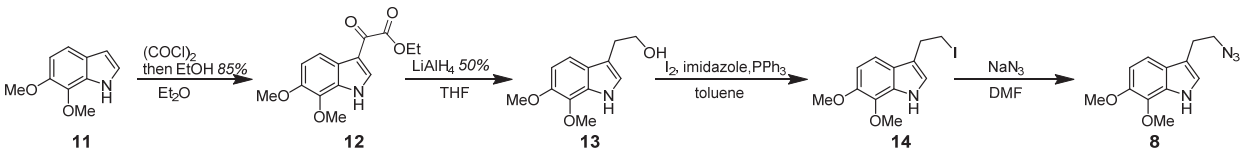

Scheme 8. Alternative synthetic route for the generation of **8**; Yields in parentheses are the reported ones.[143]

CONCLUSION AND FUTURE WORK

This chapter aimed to establish a scalable synthetic protocol comprised of well-established synthesis protocols with low-priced starting materials to provide a sufficient amount of the versatile intermediate **I**. A large amount of pyrroloiminoquinone **I** may resolve the supply strain of pyrroloiminoquinone-based antineoplastic alkaloids such as discorhabdins, makaluvamines, and discorhabdin X from deep waters off the Aleutian Islands to investigate their antineoplastic potentials in vivo. Even though the current yields and scales of some steps need to be improved for a large-scale synthesis of **I**, this chapter may serve as a stepping stone for the design of a cost- and time-effective synthetic strategy for the challenging synthesis of the indole-based tricyclic

architectures and further examination of their therapeutic potentials for control of various cancer types and related complications. Besides, further reproducing efforts and optimization of Kita's approach will be required.

EXPERIMENTAL SECTION

General Experiments

See *General Experiments* sections in the previous chapters for routine experiment protocols. Chemicals were purchased from Sigma-Aldrich (St. Louis, MO), Fischer Scientific (Pittsburgh, PA), J & W PharmLab (Levittown, PA), Oakwood Chemical (West Columbia, SC), and Waterstone Technology (Carmel, IN).

Synthesis Details

*6-Iodo-2,3-dimethoxyphenylamine (**2**).*[136]

A biphasic mixture composed of 440 mL of ether and 60 mL of saturated Na_2CO_3 was prepared and 10.0 g (66 mmol) of 2,3-dimethoxyaniline was stirred in the dark. To this biphasic mixture was added slowly 17 g (108 mmol) of iodine monochloride in 72 mL of ether. The reaction mixture was stirred for 4 h and the layers were separated using a separation funnel. The ether layer was washed five times with saturated Na_2SO_3 or $Na_2S_2O_3$ to thoroughly remove residual iodine monochloride and the combined ether layer was dried over anhydrous MgSO4 and concentrated. The residue was purified using gravity silica gel chromatography to give 13 g (70%) of **1** as a yellow solid; ^{1}H NMR (400 MHz, $CDCl_3$) δ_H 3.83 (s, 3H), 3.84 (s, 3H), 4.25 (brs, 2H), 6.19 (d, 1H, J = 9.0 Hz), 7.31 (d, 1H, J = 9.0 Hz); ^{13}C NMR (100 MHz, $CDCl_3$) δ_C 56.0, 60.1, 74.0, 104.4, 133.3, 135.4, 141.8, 153.2.

*4-Phthalimidobutanol (**4**).*[139]

A mixture of phthalic anhydride (36 g, 240 mmol) and 4-aminobutanol (20 g, 240 mmol) was heated to 145 °C. Nitrogen gas was streamed to remove water vapor. After cooling to r.t., the reaction residue was dried and the product was obtained as a pale yellow oil (quantitative); ^{1}H NMR (400 MHz, $CDCl_3$) δ_H 1.5 (p, 2H, *J* = 6.0 Hz), 1.6 (p, 2H, *J* = 7.6 Hz), 3.5 (t, 2H, *J* = 6.5 Hz), 3.7 (t, 2H, *J* = 7.2 Hz), 7.6 (m, 2H), 7.8 (m, 2H); ^{13}C NMR (100 MHz, $CDCl_3$) δ_C 24.9, 29.7, 37.6, 61.6, 123.0, 131.8, 133.8, 168.3.

*4-Phthalimidobutanal (**5**).*[137,138]

Compound **4** (5 g, 23 mmol) was dissolved in 50 mL of dichloromethane (DCM) in an ice bath and Dess-Martin periodinane (15 g, 33 mmol) was added to the solution under argon. The reaction mixture was stirred overnight, diluted with DCM, and added with saturated $Na_2S_2O_4$ and $NaHCO_3$. The organic layer was dried over $MgSO_4$ and concentrated. The residue was chromatographed over gravity column chromatography to furnish **5** (60%) as a white power. ^{1}H NMR (400 MHz, $CDCl_3$) δ_H 1.9 (p, 2H, *J* = 7.0 Hz), 2.5 (t, 2H, *J* = 6.9 Hz), 3.7 (t, 2H, *J* = 7.0 Hz), 7.6 (m, 2H), 7.8 (m, 2H), 9.7 (s); ^{13}C NMR (100 MHz, $CDCl_3$) δ_C 21.0, 37.0, 40.9, 123.1, 131.8, 133.9, 168.2, 200.9.

*3-(2-Phthalimidoethyl)-6,7-dimethoxyindole (**6**).*[140]

A mixture of **2** (3 g, 11 mmol), **5** (2.3 g, 11 mmol), and DABCO (3.7 g, 33 mmol) in dry dimethylformamide (DMF) (55 mL) was degassed using freeze-thaw-pump technique. $Pd(OAc)_2$ (120 mg, 0.55 mmol) was added to the reaction mixture and it was heated at 85 ˚C for 12 – 24 h. The reaction was monitored using TLC and additional palladium source was added to completely consume **5**. Upon the completion of the reaction, the mixture was cooled to room temperature and diluted with water. The aqueous layer was extracted with EtOAc and the combined organic phases

were washed with brine, dried using ($MgSO_4$), and evaporated under reduced pressure. Purification of crude product by gravity column chromatography provided the desired product (50%) and starting material **2** (10%). ^{1}H NMR (400 MHz, $CDCl_3$) δ_H 3.1 (t, 2H, J = 7.8 Hz), 3.9 (s, 3H), 4.0 (s, 3H), 4.0 (t, 2H, *J* = 7.1 Hz), 6.86 (d, 1H, *J* = 7.0 Hz), 7.0 (s, 1H), 7.4 (d, 1H, *J* = 7.0 Hz), 7.7 (m, 2H), 7.8 (m, 2H); ^{13}C NMR (100 MHz, $CDCl_3$) δ_C 24.5, 38.4, 57.5, 60.8, 108.3, 112.7, 113.8, 121.7, 123.2, 124.2, 130.8, 132.2, 133.9, 134.5, 147.2, 168.3.

*6,7-Dimethoxytryptamine (**7**).*[140]

To a solution of **6** (900 mg, 0.4 mmol) in 90 mL of MeOH, 60% hydrazine monohydrate (9 mL, 180 mmol) was added and the mixture was proceeded for 2 h. After addition of saturated aqueous $NaHCO_3$ solution (100 mL), the solvent was evaporated and the aqueous phase was extracted sufficiently with EtOAc (8 × 20 mL). The collected organic phase was dried over $MgSO_4$ and evaporated under reduced pressure, and the resultant residue was chromatographed on gravity silica column chromatography using a mixture solvent ($MeOH:CH_2Cl_2:NH_4OH$ = 10:100:1) to afford a light yellow oil **7** (28 mg) (60%). ^{1}H NMR (400 MHz, $CDCl_3$) 2.8 (t, 2H, *J* = 6.2 Hz), 3.0 (br t, 2H), 3.9 (s, 3H), 3.9 (s, 3H), 6.8 (d, 1H, *J* = 8.2 Hz), 6.9 (s, 1H), 7.2 (d, 1H, *J* = 8.4 Hz); ^{13}C NMR (100 MHz, $CDCl_3$) 28.6, 41.6, 57.1, 107.5, 112.9, 113.4, 121.9, 124.2, 130.7, 134.2, 146.6.

*3-(2-Azidoethyl)-6,7-dimethoxyindole (**8**).*[141]

A triflyl azide solution was freshly prepared with reference to a previous study.[141] Compound **7** (200 mg, 0.93 mmol) was dissolved in 3 mL of H_2O and treated with potassium carbonate (192 mg, 1.39 mmol) and $CuSO_4$ hydrate (1.4 mg., 8.8 mmol). To this solution was added MeOH (6 mL) and the triflyl azide solution. Additional MeOH was added for homogeneity of the reaction mixture and the reaction mixture was stirred for 18 h. The mixture was filtered through cotton, extracted with DCM three times and the organic layer was concentrated. The residue was applied

to gravity silica column chromatography to obtain compound **8** (50%) as a pale yellow oil. ^{1}H NMR (400 MHz, $CDCl_3$) 3.0 (t, 2H, *J* = 7.2 Hz), 3.6 (t, 2H), 3.9 (s, 3H), 4.0 (s, 3H), 6.9 (d, 1H, *J* = 8.5 Hz), 7.0 (br s, 1H), 7.2 (d, 1H, *J* = 8.4 Hz); ^{13}C NMR (100 MHz, $CDCl_3$) 25.1, 51.6, 57.5,60.8, 108.3, 112.5, 113.5, 122.0, 124.0, 130.9, 134.6, 147.2.

*1-Acetyl-3-(2-azidoethyl)-6,7-dimethoxyindole (**9**).*[143]

A solution of **8** (0.50 mmol) in dry THF (5.0 mL) was added dropwise to a stirred suspension of potassium *t*-butoxide (1.0 mmol) in dry THF (1.25 mL) under argon at an ice bath and stirred at 0 °C for 1 h. Acetyl chloride was added to the solution at 0 °C and the reaction mixture was stirred for overnight at r.t. The mixture was quenched with H_2O and extracted with CH_2Cl_2. The organic layer was dried over $MgSO_4$, evaporated, and subjected to gravity column chromatography to give **9** (75%). ^{1}H NMR (400 MHz, $CDCl_3$) 2.6 (s, 3H), 2.8 (t, 2H, *J* = 7.2 Hz), 3.5 (t, 2H), 3.9 (s, 3H), 3.9 (s, 3H), 6.9 (d, 1H, *J* = 8.5 Hz), 7.1 (d, 1H, *J* = 8.4 Hz), 7.3 (br s, 1H); ^{13}C NMR (100 MHz, $CDCl_3$) 24.6, 25.2, 50.5, 56.9,60.7, 110.4, 113.7, 117.5, 124.6, 127.5, 128.9, 137.8, 151.3, 168.7.

*7-Methoxy-3,4-dihydropyrrolo[4,3,2-de]quinolin-8(1H)-one (**10**).*[133,143]

To a stirred solution of **9** (0.20 mmol) in HFIP/H_2O (10 mL:0.20 mL), TMSOTf (0.500 mmol) was added dropwise at 0 °C under argon and PIFA was added successively (0.24 mmol). After stirring for 1.5 h at 0°C, the mixture was quenched with $NaHCO_3$ and the solvent was evaporated. The residue was extracted with CH_2Cl_2 and concentrated to be used for the next reaction without purification due to its structural instability. ^{1}H NMR (400 MHz, $CDCl_3$) 2.8 (t, 2H, *J* = 8.3 Hz), 3.8 (s, 3H), 4.2 (t, 2H, *J* = 8.1 Hz), 6.1 (s, 1H), 6.9 (s, 1H)

*7-Amino-3,4-dihydropyrrolo[4,3,2-de]quinolin-8(1H)-one (**I**).*[144]

A mixture of **10** (113 mg, 0.5 mmol) and NH_4Cl (270 mg) in MeOH (25 mL) was stirred r.t. overnight. The mixture was concentrated and the resultant residue was purified utilizing gravity

silica gel (CH_2Cl_2/MeOH/NH_4OH = 80:20:1 → 70:30:1) to garner **I** (60%). The purified compounds was treated with TFA in MeOH, resulting in the formation of its corresponding TFA salt. ^{1}H NMR (400 MHz, methanol-d_4) 2.9 (t, 2H, J = 7.5 Hz), 3.8 (t, 2H, J = 7.7 Hz), 5.7 (s, 1H), 7.1 (s, 1H).

*6, 7-Dimethoxy-3-(2-hydroxyethyl)indole (**13**)*[143]

To a solution of 6,7-dimethoxyindole (**11**) (100 mg, 0.564 mmol) in dry Et_2O (10 mL) a solution of oxalyl chloride (0.064 mL, 0.734 mmol) in Et_2O (8 mL) was added dropwise under argon at 0 °C and stirred for 2 h at 0 °C. EtOH (0.12 mL) was added to the reaction mixture at 0 °C and this was stirred for 3 h r.t. $NaHCO_3$ was added to quench the reaction and the mixture was extracted with EtOAc. The organic layer was evaporated and proceeded to the next step without purification to provide **12** (85%). ^{1}H NMR (400 MHz, $CDCl_3$) 1.3 (t, 3H, J = 7.2 Hz), 3.9 (s, 3H), 3.9 (s, 3H), 4.4 (q, 2H, J = 7.2 Hz), 7.0 (d, 1H, 8.9 Hz), 8.0 (d, 1H, 8.9 Hz), 8.4 (br d, 1H); ^{13}C NMR (100 MHz, $CDCl_3$) 14.0, 56.9, 61.1, 62.1, 111.0, 114.6, 117.4, 121.8, 130.8, 134.4, 137.2, 148.6, 162.8, 178.2. A solution of **12** (70 mg, 0.25 mmol) in THF (1 mL) was added dropwise to a suspension of LiA1H4 (98 mg, 2.5 mmol) in THF (4 mL) under an argon atmosphere at 0 °C, and the mixture was stirred in the ice bath for 20 mins. The mixture was carefully quenched with EtOAc, MeOH. and brine. After filtration was performed through Celite, the filtrate was concentrated in vacuo. The residue was dissolved with EtOAc and then evaporated to give pure 6 (1.13 g, quant) as a colorless oil. ^{13}C NMR (100 MHz, $CDCl_3$) 28.7, 57.4, 60.8, 62.5, 108.1, 112.4, 113.7, 122.3, 124.1, 130.9, 134.4, 147.1.

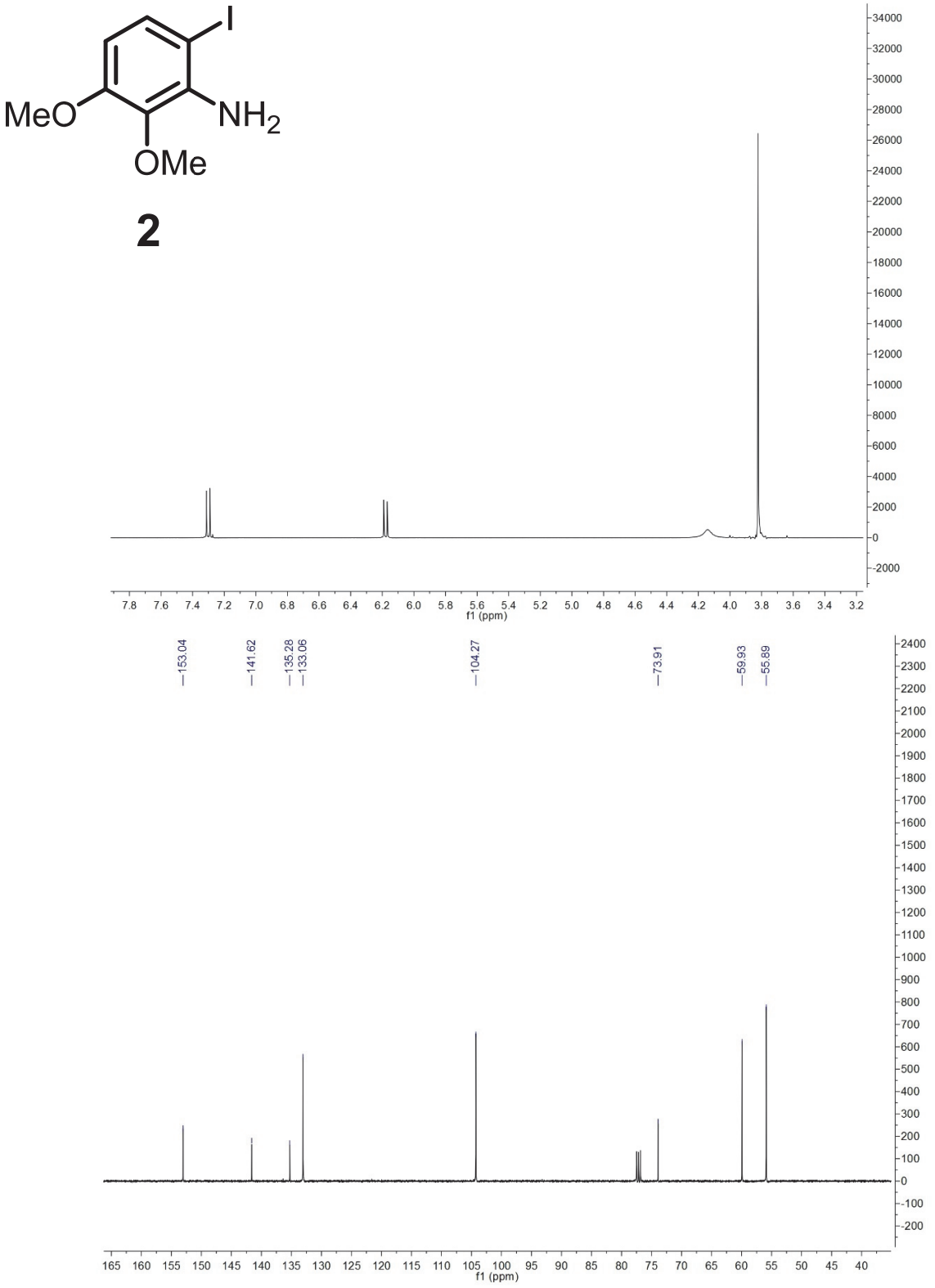

Figure 41. ^{1}H and ^{13}C NMR spectra of **2** ($CDCl_3$)

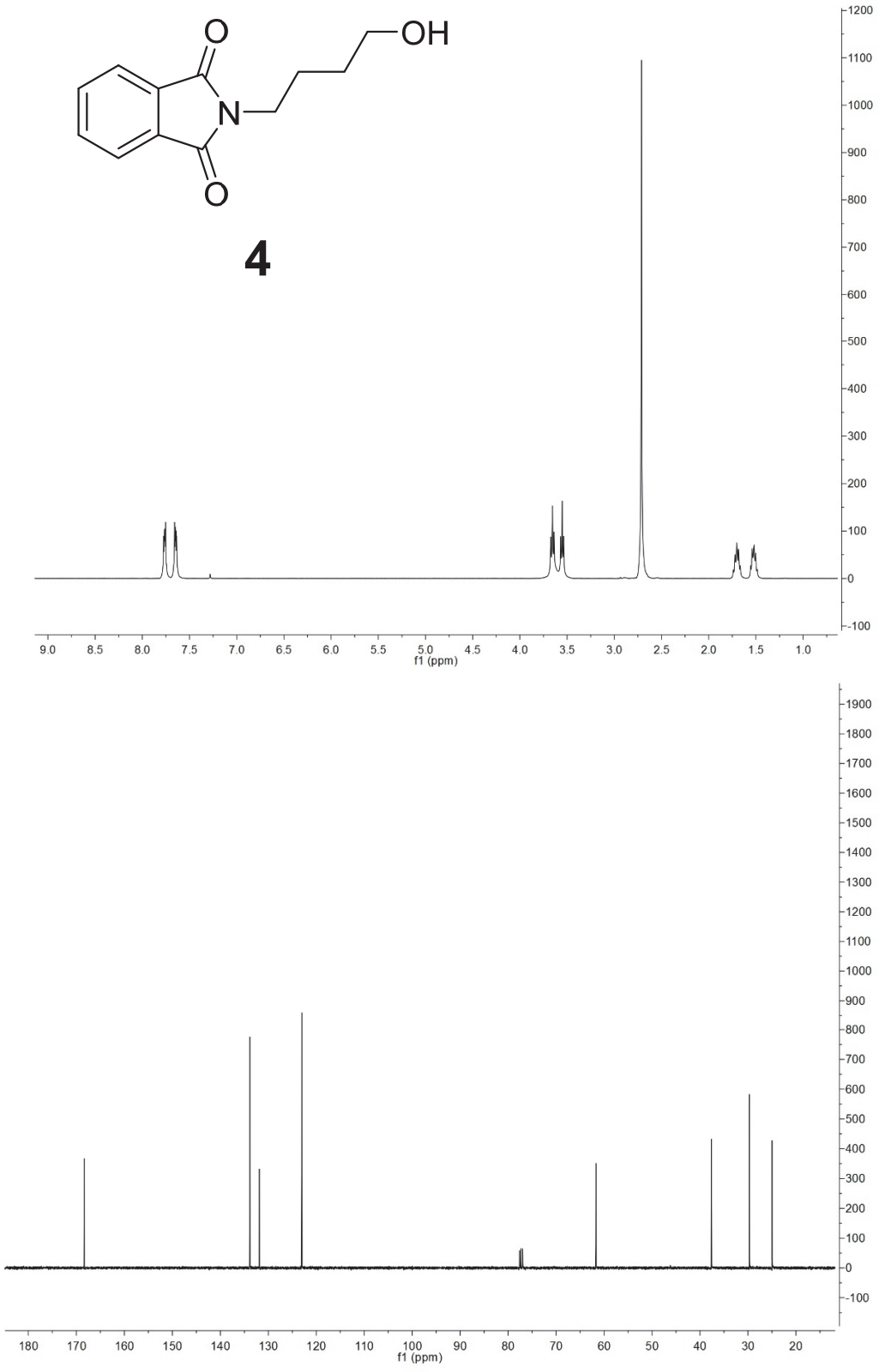

Figure 42. ^{1}H and ^{13}C NMR spectra of **4** ($CDCl_3$)

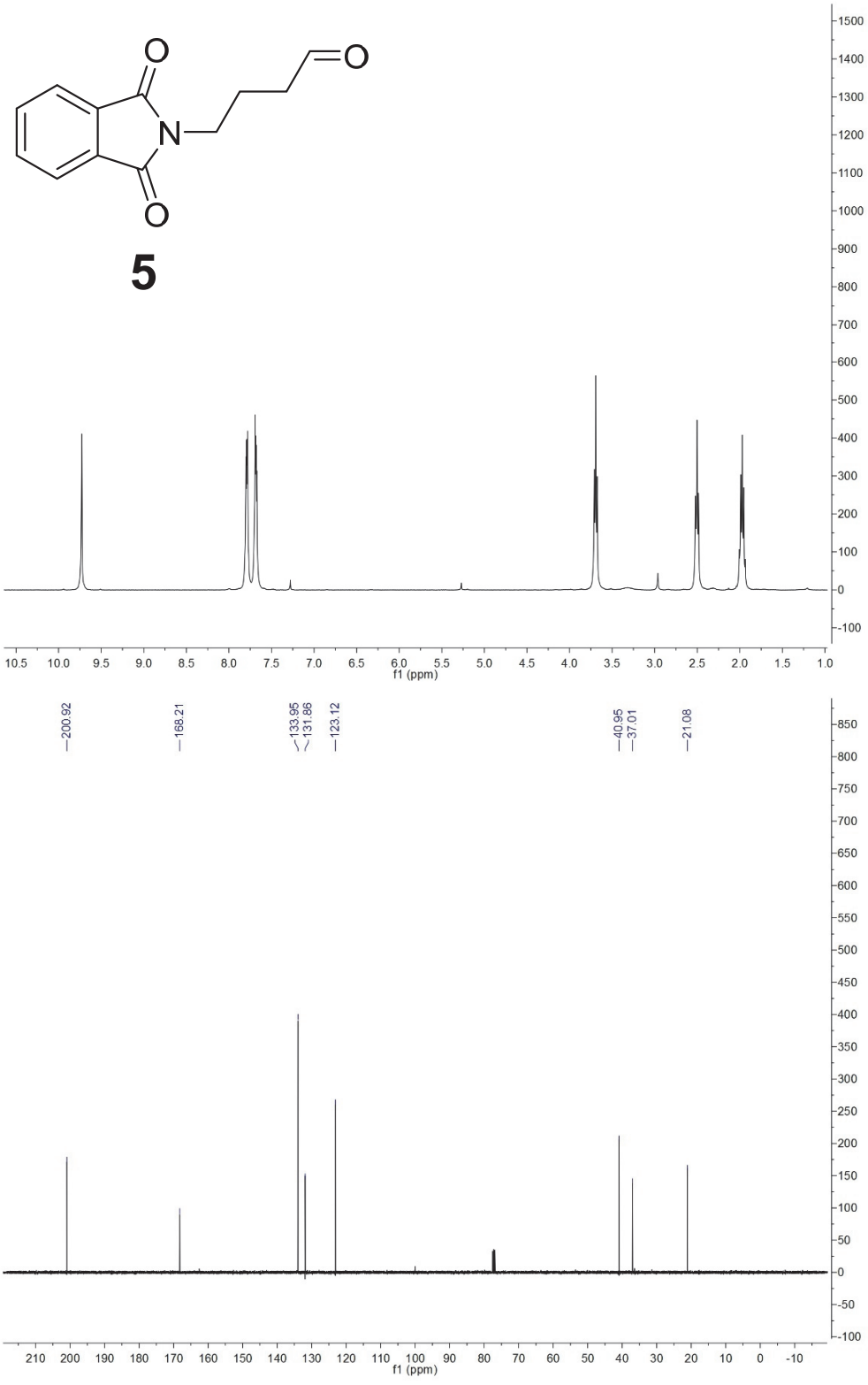

Figure 43. ^{1}H and ^{13}C NMR spectra of **5** ($CDCl_3$)

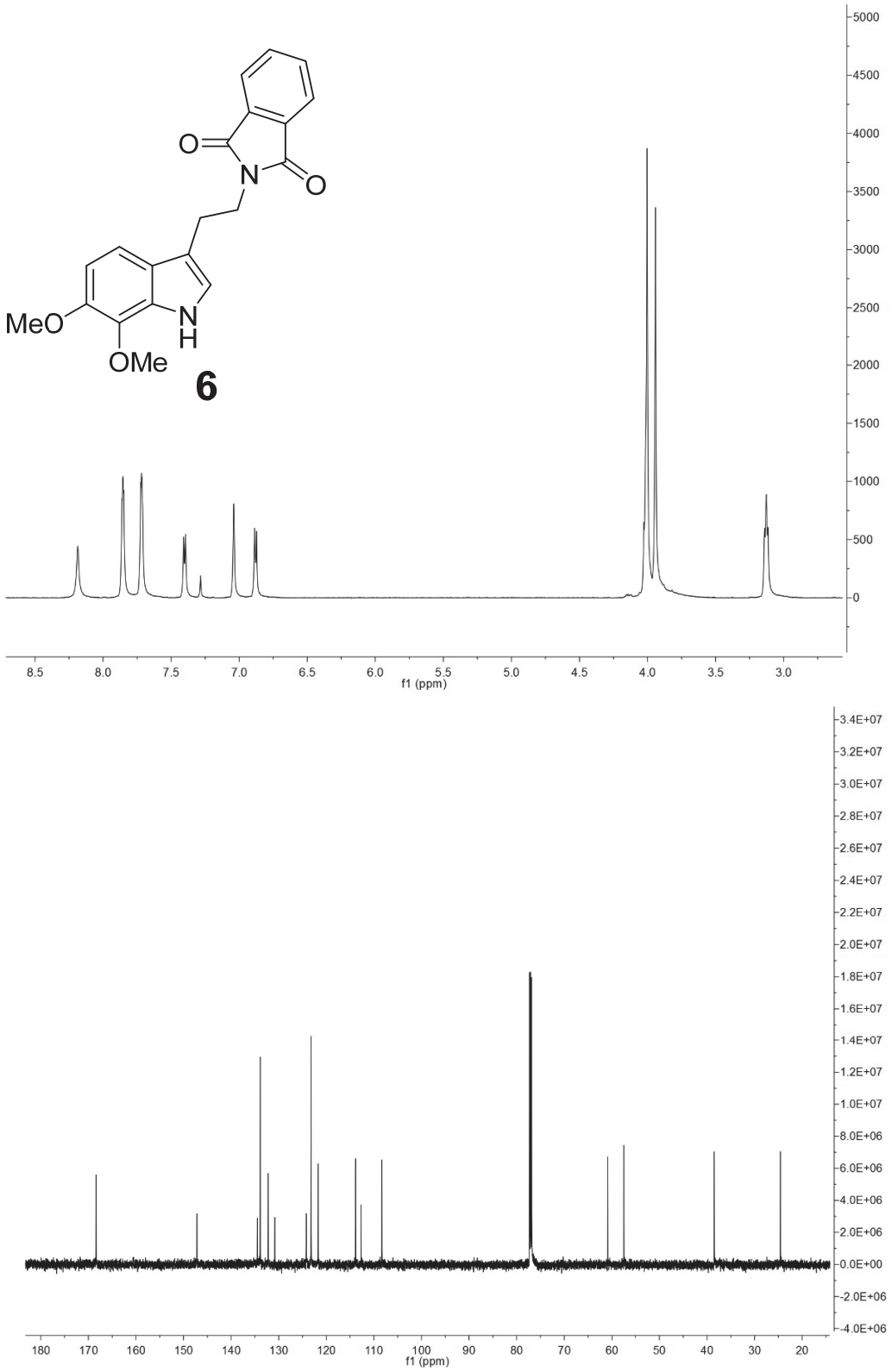

Figure 44. ^{1}H and ^{13}C NMR spectra of **6** ($CDCl_3$)

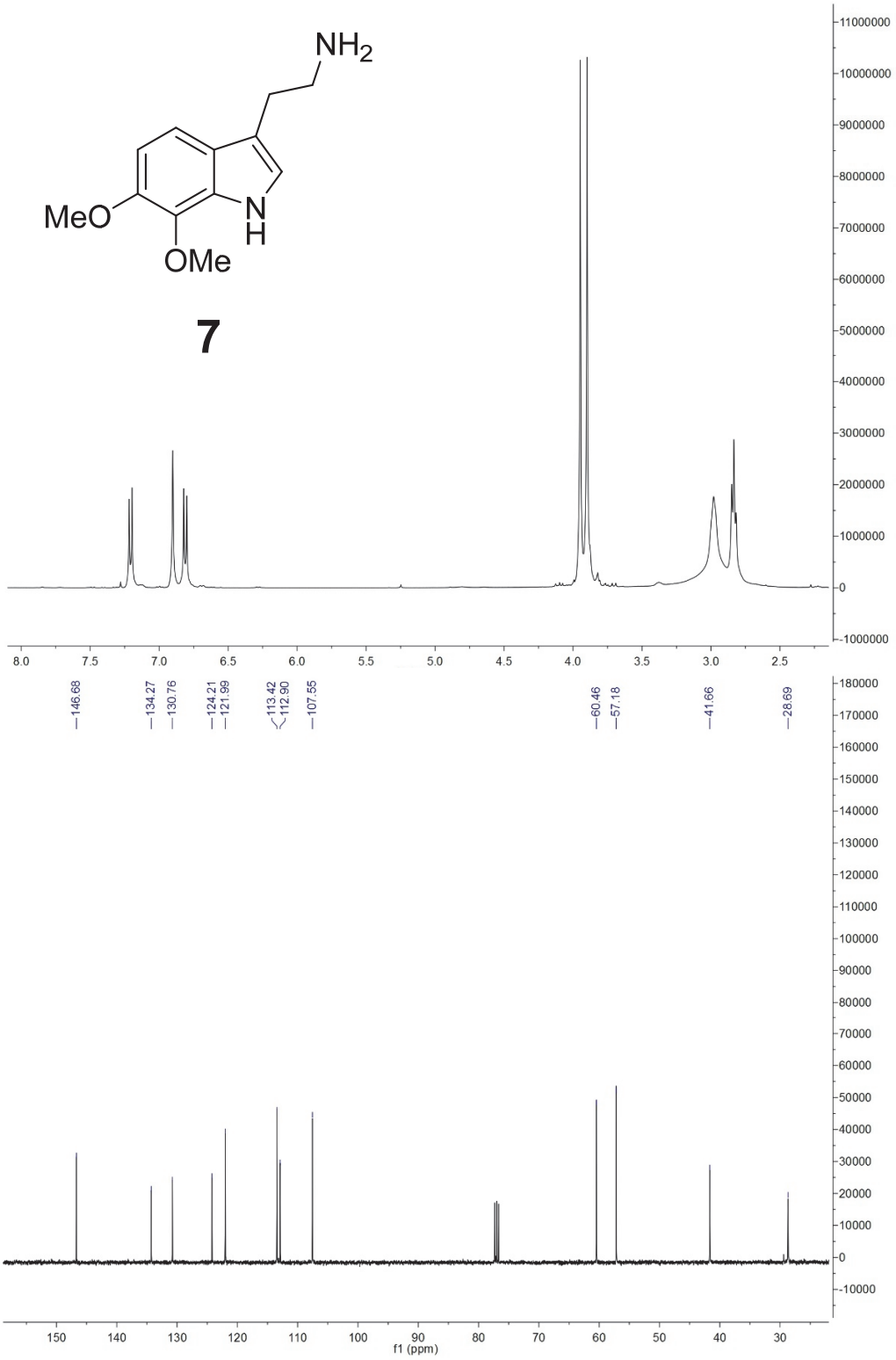

Figure 45. ^{1}H and ^{13}C NMR spectra of **7** ($CDCl_3$)

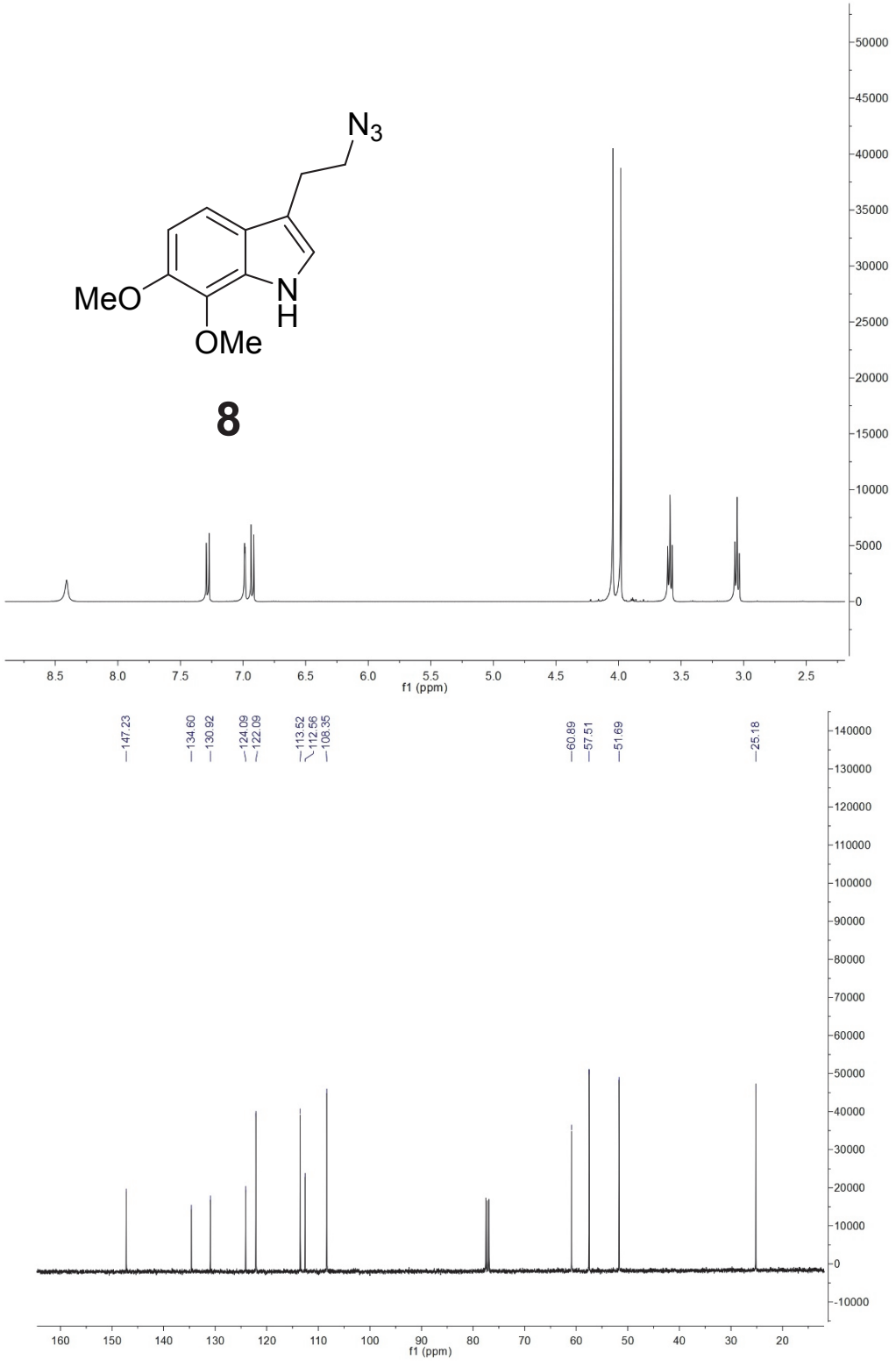

Figure 46. ^{1}H and ^{13}C NMR spectra of **8** ($CDCl_3$)

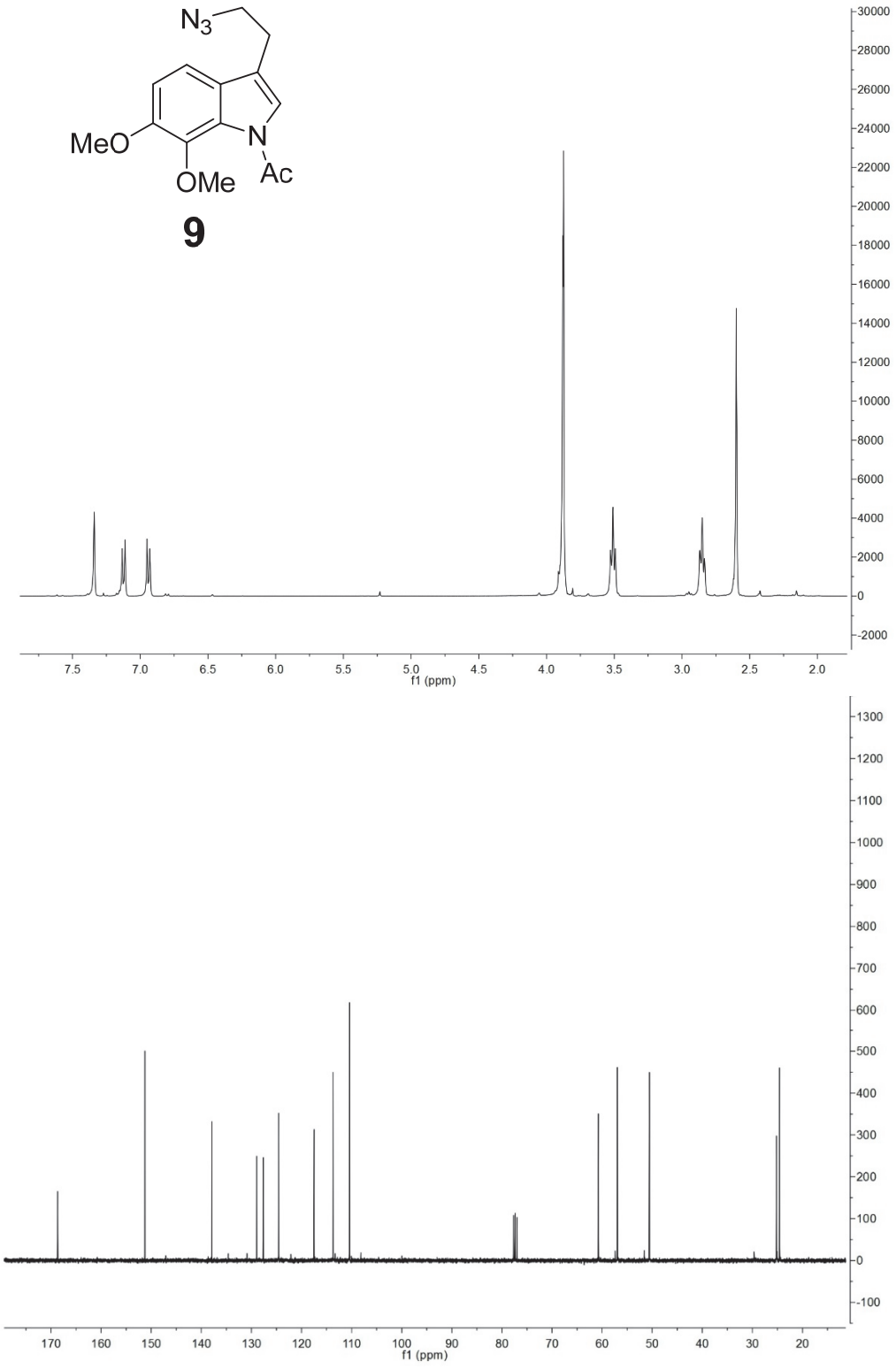

Figure 47. ^{1}H and ^{13}C NMR spectra of **9** ($CDCl_3$)

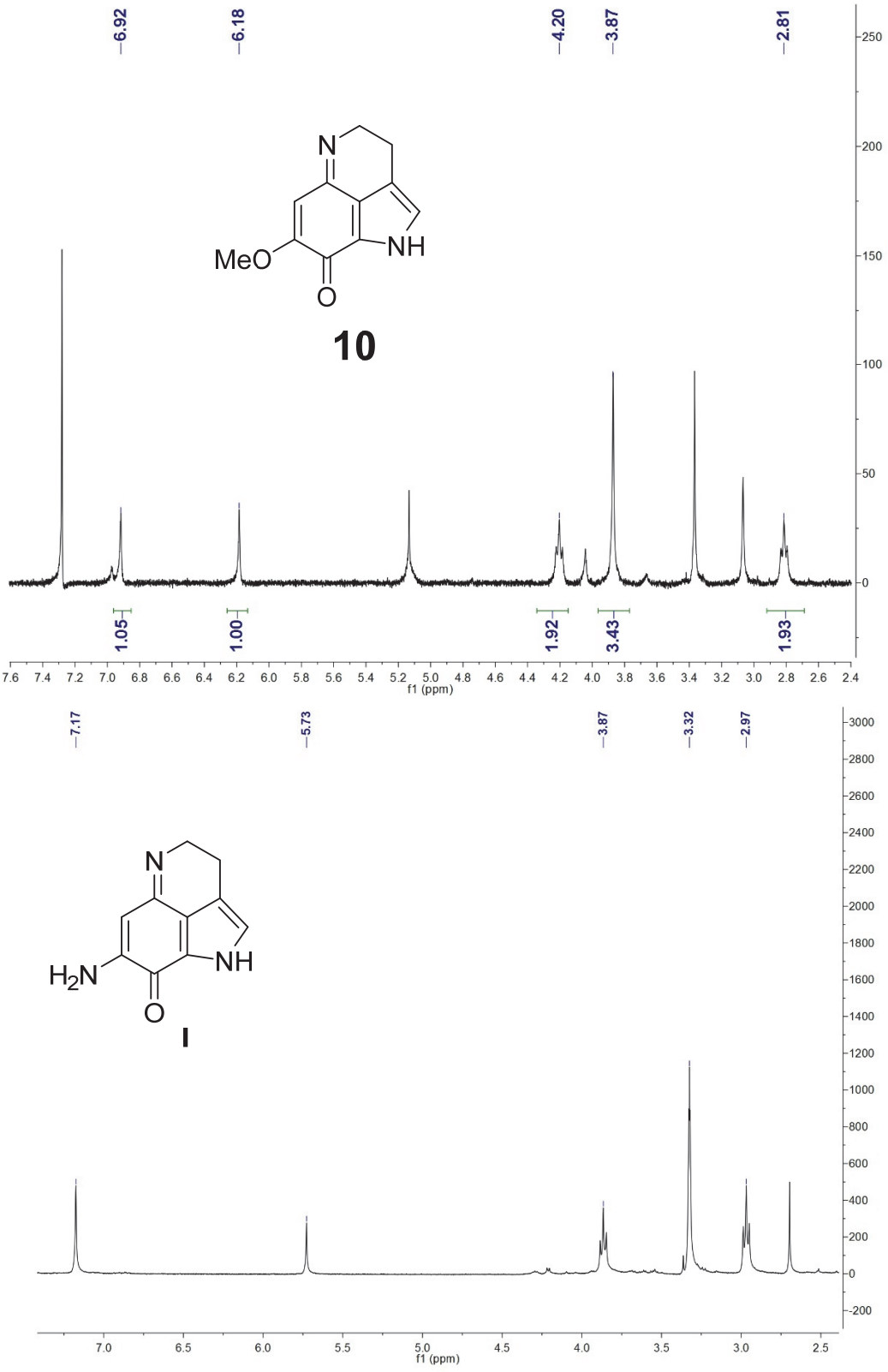

Figure 48. ^{1}H spectra of **10** ($CDCl_3$) and **I** (methanol-d_4)

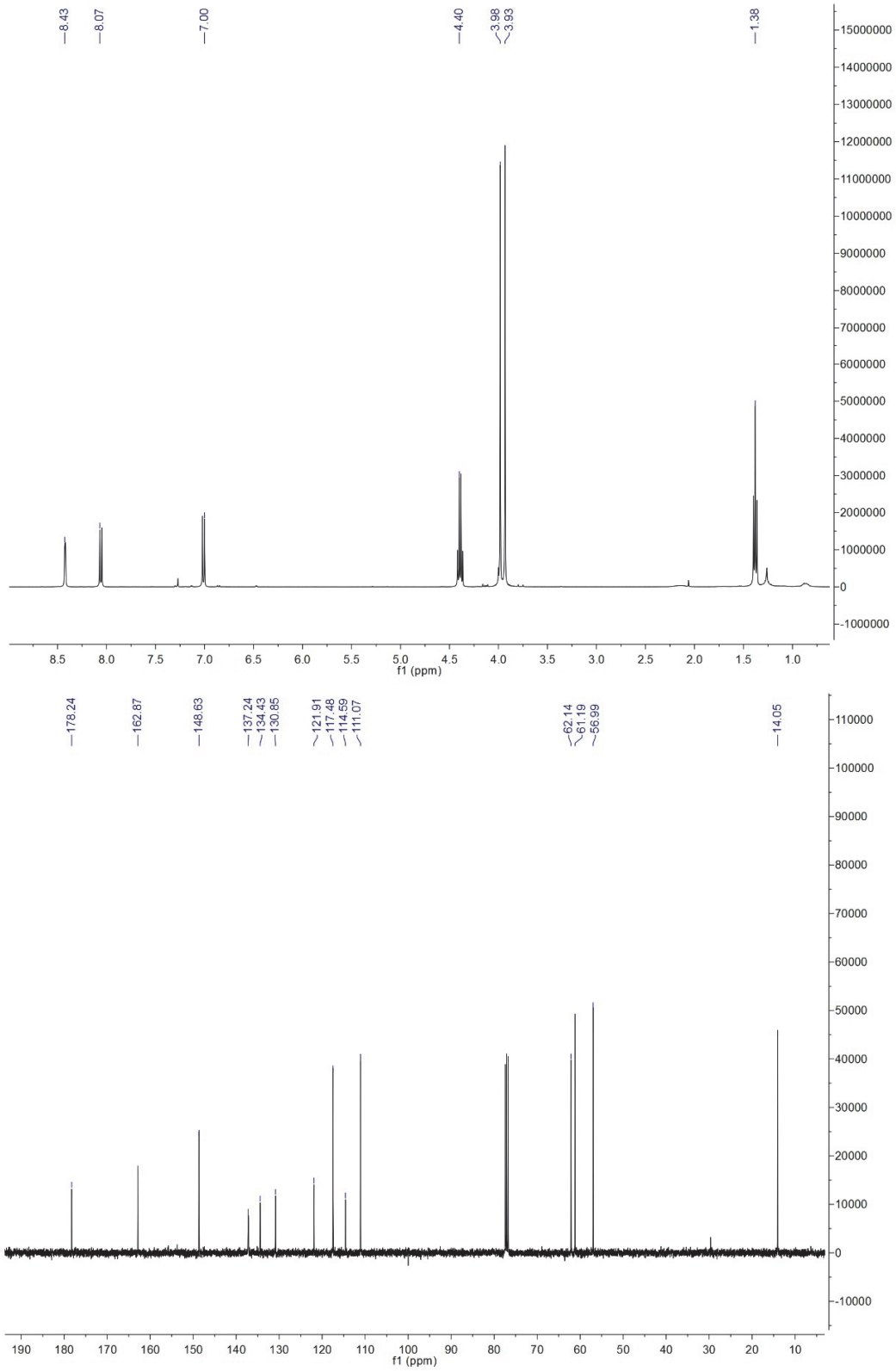

Figure 49. ^{1}H and ^{13}C NMR spectra of **12** ($CDCl_3$)

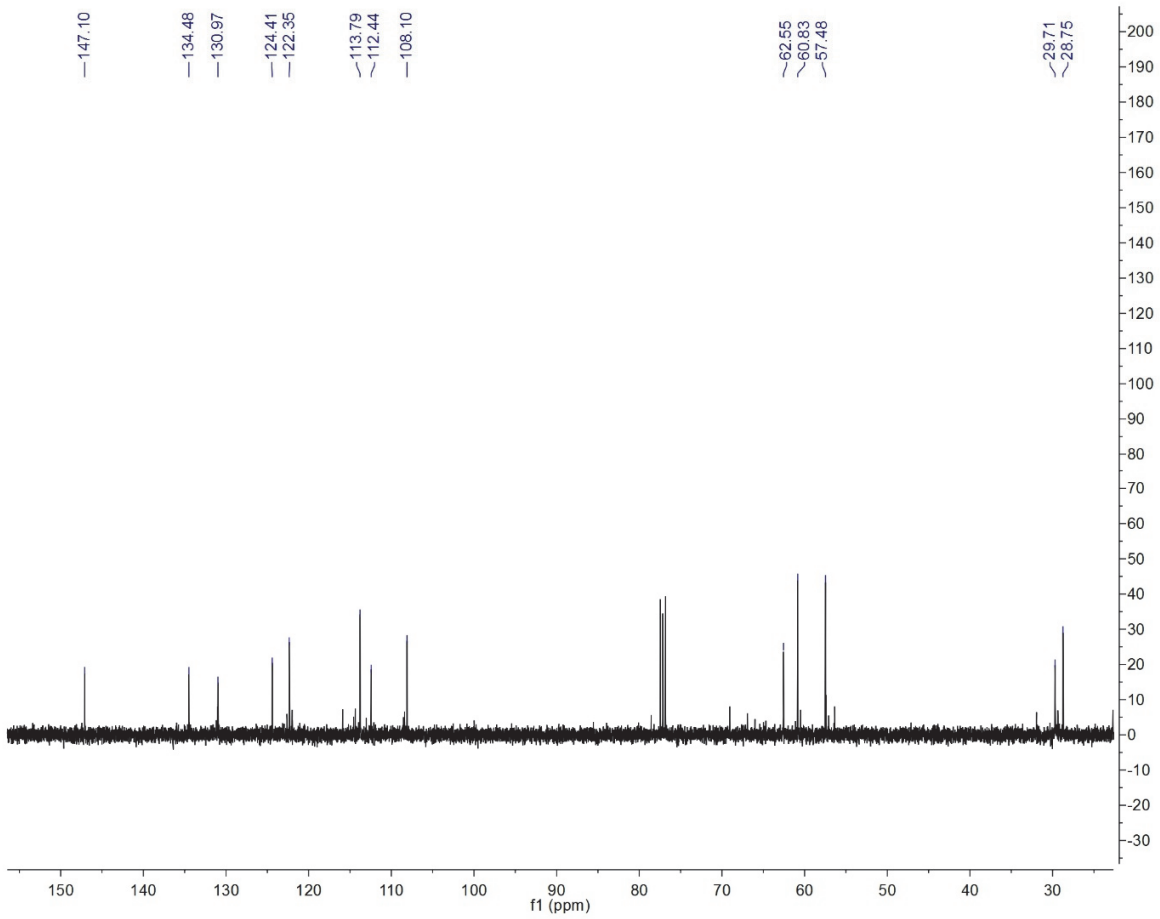

Figure 50. ^{13}C NMR spectra of **13** ($CDCl_3$)

CHAPTER 6: CHARACTERIZATION OF THE 3D STRUCTURE OF BRCA1-IRIS INHIBITORY PEPTIDE EMPLOYING THE ENSEMBLE OF A HIGH-FIELD NMR STUDY AND *IN SILICO* METHODS

INTRODUCTION

Breast cancer is the second most diagnosed cancer in women in the US[146] and the estimated new cases and deaths are 232,670 and 40,000, respectively, for 2014,[147] imposing a serious burden on health care communities and resources. The development of cytotoxic agents targeting breast cancer is challenging because the malignant disease is diverse with various histological and molecular subtypes carrying distinctive biological properties, resistance, and responses to anticancer therapies.[148] The most invasive breast cancer subtype is triple-negative breast cancer (TNBC) characterized by a lack of estrogen and progesterone receptors, and human epidermal growth factor receptor 2 amplification.[149] These malignant features lead to conventional cytotoxic agents, including tamoxifen and herceptin, being ineffective for cancer treatment.[150] The TNBC comprises ~15% of all the cases and shares many common oncogenic features with BRCA1-associated tumors.[149] Despite high susceptibility of TNBC to neo-adjuvant chemotherapy utilizing paclitaxel, invasive breast cancer is prone to recurring upon visceral metastases.[150] To date, there is no comprehensive clinical strategy alleviating TNBC and its associated metastases, raising an urgent need for the establishment of effective antiproliferative strategies for mitigation of this aggressive breast cancer.

BRCA1-IRIS (IRIS) is an oncogenic 1399 amino acid and expressed from the identical locus as the tumor suppressor gene *BRCA1*.[150-152] The up-regulated IRIS expression facilitates the growth of breast tumors and circumvents apoptosis by curbing p53 activity and/or activating the Akt pathway, and ultimately inducing survivin expression.[153] This collectively results in the resistance of the malignant cells to current chemotherapeutic strategies including etoposide, ionizing or UV-radiation, and oxidative stress.[153] The elevated expression of IRIS is typically observed in TNBC cell lines and tumor cells particularly lacking the expression of the tumor suppressor BRCA1.[153] A recent study corroborates that IRIS employs its intron 11 peptide to interact with other unknown proteins (X factors) in the oncogenic functions.[154] Based on this study, a mimetic IRIS-inhibitory peptide (IRIS-IP), composed of the oncogenic intron sequence attached to a nuclear penetrating signal, was formulated to prevent the formation of tumorigenic complex (**Figure 51**).[154]

RESULTS AND DISCUSSION

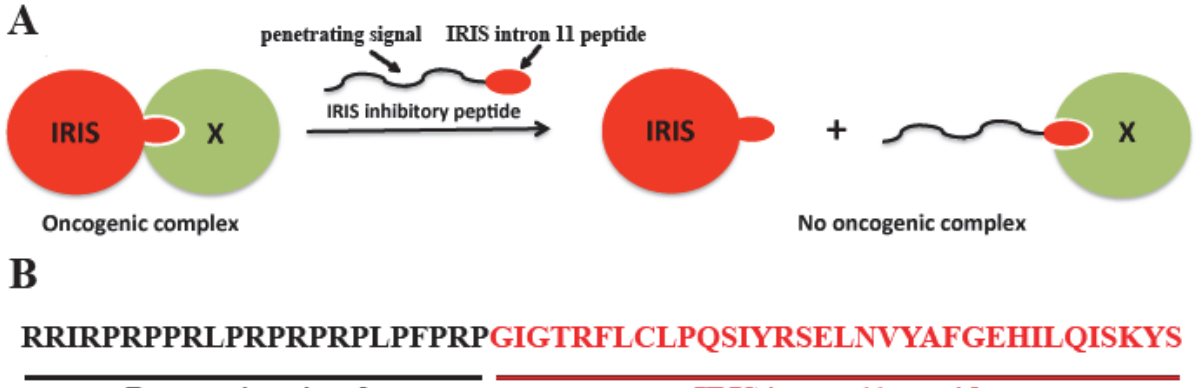

Figure 50. The schematic representation of the anti-oncogenic mechanism of IRIS inhibitory peptide (A) and its sequence (B). X stands for X factors. The figure was obtained from Nature Publishing Group with a permission via Rightslink® (License No. 3584830592805)

The stereostructure of a cytotoxic molecule is crucial in fully examining the underlying antineoplastic mechanism and formulating strategies to enhance the activity. To achieve this goal, it is essential to acquire an NMR solution structure employing a wide array of NMR pulse programs such as TOCSY,[155] COSY,[156] NOESY,[157] ^{1}H-^{13}C and ^{1}H-^{15}N HSQC,[158] and recently developed long range (LR)-HSQMBC.[159] To complement biased and ambiguous structural elucidation processes of macromolecules using NMR spectroscopy,[160] homology modeling of IRIS-IP with its sequence (**Figure 51**) was implemented with reflection of spatial and dihedral information deduced from NMR data. Preliminary homology modeling was conducted using Prime® (Schrodinger LLC.) and successfully built in chain A of rat metallophosphodiesterase Mpped2a (PDB ID: 3RL3, resolution 1.42 Å) (**Figure 52**). The identity score between the two protein structures calculated by the computational software was relatively low (28.1/100), implying a unique folding pattern of IRIS-IP. Spatial distances, vitally important in elucidation of 3D structures of macromolecules, were acquired utilizing NOESY spectra recorded in DMSO-d_6 with 5 or 10 % of trifluoroacetic acid (100 ms mixing time, 800 and 850 MHz cryoprobe). The NMR solution structure of IRIS-IP is being elucidated based on the NOESY and TOCY data and the current progress is shown in **Figure 53**.

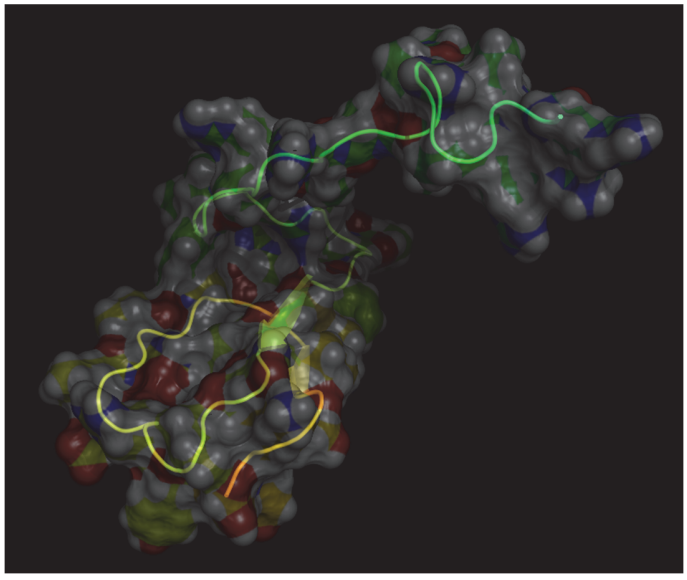

Figure 51. A homology model of the IRIS -IP on rat metallophosphodiesterase (Prime and Pymol, Schrodinger LLC).

These NOE data will be analyzed employing the SPARKY program[161] and categorized into four classes of distance based on signal intensities with reference to an internal standard: 2.5, 3.0, 4.0, and 5.0 Å corresponding to strong, medium, weak, and very weak intensities, respectively.

This interproton distance information will be processed using CYANA 2.1 for an initial solution structure calculation and the crude structure will be refined employing CNS 1.3 with a

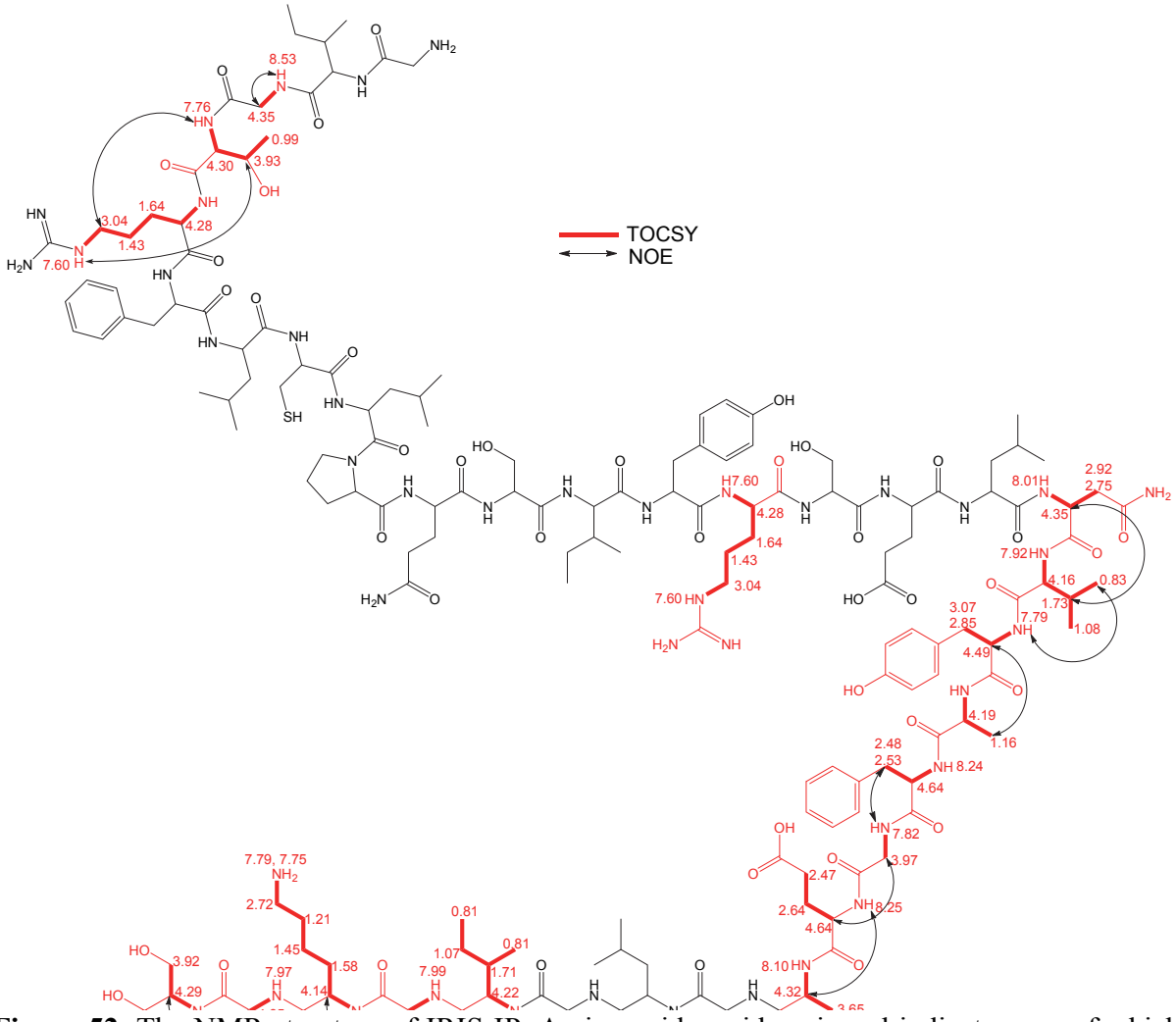

Figure 52. The NMR structure of IRIS-IP. Amino acids residues in red indicate ones of which assignments are tentatively completed. Numbers denote ^{1}H NMR chemical shift values for corresponding protons. Stereodescriptors were omitted for a clearer presentation

simulated annealing process.[162,163] Among the calculated structures, 20 structures with lowest energies without residual restraint violations will be chosen to represent the solution structure of the IRIS-IP and their structure quality will be examined by protein structure validation software.[164]

BIBLIOGRAPHY

(1) Butchart, S. H. M.; Walpole, M.; Collen, B.; van Strien, A.; Scharlemann, J. P. W.; Almond, R. E. A.; Baillie, J. E. M.; Bomhard, B.; Brown, C.; Bruno, J.; Carpenter, K. E.; Carr, G. M.; Chanson, J.; Chenery, A. M.; Csirke, J.; Davidson, N. C.; Dentener, F.; Foster, M.; Galli, A.; Galloway, J. N.; Genovesi, P.; Gregory, R. D.; Hockings, M.; Kapos, V.; Lamarque, J.-F.; Leverington, F.; Loh, J.; McGeoch, M. A.; McRae, L.; Minasyan, A.; Morcillo, M. H.; Oldfield, T. E. E.; Pauly, D.; Quader, S.; Revenga, C.; Sauer, J. R.; Skolnik, B.; Spear, D.; Stanwell-Smith, D.; Stuart, S. N.; Symes, A.; Tierney, M.; Tyrrell, T. D.; Vié, J.-C.; Watson, R. *Science* **2010**, *328*, 1164.

(2) Pitman, N. C. A.; Jørgensen, P. M. *Science* **2002**, *298*, 989.

(3) USDA 2011, http://plants.usda.gov/threat.html accessed 4/10/2011.

(4) Kotiaho, J. S. *Proc. Natl. Acad. Sci. U.S.A.* **2005**, *102*, 1963.

(5) Lee, J. C.; Yang, X.; Schwartz, M.; Strobel, G.; Clardy, J. *Chem. Biol.* **1995**, *2*, 721.

(6) Jensen, N. J. 2007, http://www.cnpsci.org/PlantInfo/RarePlants/VMM_FinalReport_042607minus_sensitive_info.pdf accessed 8/10/2011.

(7) Center for Plant Conservation 2011, http://www.centerforplantconservation.org/Collection/CPC_ViewProfile.asp?CPCNum=630 accessed 5/17/2011.

(8) Joshi, S. C.; Verma, A. R.; Mathela, C. S. *Food Chem. Toxicol.* **2010**, *48*, 37.

(9) Baratta, M. T.; Dorman, H. J. D.; Deans, S. G.; Figueiredo, A. C.; Barroso, J. G.; Ruberto, G. *Flavour Frag. J.* **1998**, *13*, 235.

(10) Semwal, A. D.; Sharma, G. K.; Arya, S. S. *J. Sci. Food. Agric.* **1999**, *79*, 1733.

(11) Schmidt, E.; Jirovetz, L.; Buchbauer, G.; Eller, G. A. S., I.; Krastanov, A.; Stoyanova, A.; Geissler, M. *J. Essent. Oil Bear. Pl.* **2006**, *9*, 170.

(12) Moriarity, D. M.; Bansal, A.; Cole, R. A.; Takaku, S.; Haber, W. A.; Setzer, W. N. *Nat. Prod. Commun.* **2007**, *2*, 1263.

(13) Samarasekera, R. *J. Essent. Oil Res.* **2005**, *17*, 301.

(14) Radford, A. E.; H.E. Ahles; C.R. Bell *Manual of the Vascular Flora of the Carolinas*; University of North Carolina Press: Chapel Hill, 1968.

(15) U. S. Fish and Wildlife Service *Recovery Plan for Pondberry (Lindera melissifolia)*; U. S. Fish and Wildlife Service: Atlanta, GA, 1993.

(16) U. S. Fish and Wildlife Service *Federal Register* **1986**, *51*, 27495.

(17) Centers for Disease Control and Prevention (CDC). 2015, Reported Lyme disease cases and incidence by state, 2004-2013 (http://www.cdc.gov/lyme/stats/), accessed 2/14/2015.

(18) Parola, P.; Raoult, D. *Clin. Infect. Dis.* **2001**, *32*, 897.

(19) Spielman, A.; Wilson, M. L.; Levine, J. F.; Piesman, J. *Annu. Rev. Entomol.* **1985**, *30*, 439.

(20) Sonenshine, D. E. *Biology of Ticks*; Oxford University Press: New York, 1993; Vol. 2.

(21) Goddard, J.; Varela-Stokes, A. S. *Vet. Parasitol.* **2009**, *160*, 1.

(22) Ginsberg, H. S.; Ewing, C. P.; Connell, A. F.; Bosler, E. M.; Daley, J. G.; Sayre, M. W. *J. Parasitol.* **1991**, *77*, 493.

(23) Rozendaal, J. A. *Mosquitoes and Other Biting Diptera*; World Health Organization: Geneva, Switzerland, 1997.

(24) Barnard, D. R.; Xue, R.-D. *J. Med. Entomol.* **2004**, *41*, 726.

(25) Carroll, J. F.; Klun, J. A.; Debboun, M. *Med. Vet. Entomol.* **2005**, *19*, 101.

(26) Evans, S. R.; Korch, G. W.; Lawson, M. A. *J. Med. Entomol.* **1990**, *27*, 829.

(27) Schreck, C. E.; Fish, D.; McGovern, T. P. *J. Am. Mosq. Control Assoc.* **1995**, *11*, 136.

(28) Yap, H. H.; Jahangir, K.; Zairi, J. *J. Am. Mosq. Control Assoc.* **2000**, *16*, 241.

(29) Brown, A. W. *Integrated Mosquito Control Methodologies*; Academic Press: New York, 1983.

(30) Briassoulis, G.; Narlioglou, M.; Hatzis, T. *Hum. Exp. Toxicol.* **2001**, *20*, 8.

(31) Clem; Havemann, D.; Raebel, M. *Ann. Pharmacother.* **1993**, *27*, 289.

(32) Bissinger, B. W.; Roe, R. M. *Pestic. Biochem. Physiol.* **2010**, *96*, 63.

(33) Peterson, C.; Coats, J. *Pestic. Outlook* **2001**, *12*, 154.

(34) Jaenson, T. G. T.; Garboui, S.; Pålsson, K. *J. Med. Entomol.* **2006**, *43*, 731.

(35) Yang, Y. C.; Lee, E. H.; Lee, H. S.; Lee, D. K.; Ahn, Y. J. *J. Am. Mosq. Control. Assoc.* **2004** *20*, 146.

(36) Kubeczka, K. H.; Formácek, V. *Essential Oils Analysis by Capillary Gas Chromatography and Carbon-13 NMR Spectroscopy, 2nd ed.*; Wiley: New York, 2002.

(37) Carroll, J. F.; Solberg, V. B.; Klun, J. A.; Kramer, M.; Debboun, M. *J. Med. Entomol.* **2004**, *41*, 249.

(38) Matthews, J. S.; Coggeshall, N. D. *Anal. Chem.* **1959**, *31*, 1124.

(39) Sköld, R.; Suurkuusk, J.; Wadsö, I. *J. Chem. Thermodyn.* **1976**, *8*, 1075.

(40) Weldon, P.; Carroll, J.; Kramer, M.; Bedoukian, R.; Coleman, R.; Bernier, U. *J. Chem. Ecol.* **2011**, *37*, 348.

(41) Lockhart, B. R.; Gardiner, E. S.; Leininger, T. D.; Connor, K. F.; Hamel, P. B.; Schiff, N. M.; Wilson, A. D.; Devall, M. S. *Ecological Restoration* **2006**, *24*, 151.

(42) Hawkins, T. S.; Schiff, N. M.; Gardiner, E. S.; Leininger, T.; Devall, M. S.; Wilson, D.; Hamel, P.; Mccown, D. D.; Connor, K. *Hortscience* **2007**, *42*, 407.

(43) McLafferty, F. W.; Stauffer, D. B. *The Wiley/NBS Registry of Mass Spectral Data*; J. Wiley and Sons: New York, 1989.

(44) Koenig, W. A.; Joulain, D.; Hochmuth, D. H. *Terpenoids and Related Constituents of Essential Oils*; University of Hamburg, Institute of Organic Chemistry: Hamburg, Germany, 2004.

(45) Joulain, D.; Koenig, W. A. *The Atlas of Spectra Data of Sesquiterpene Hydrocarbons*; EB-Verlag: Hamburg, Germany, 1998.

(46) ESO 2000 *The Complete Database of Essential Oils*; Boelens Aroma Chemical Information Service: The Netherlands, 1999.

(47) Guerrini, A.; Sacchetti, G.; Muzzoli, M.; Moreno Rueda, G.; Medici, A.; Besco, E.; Bruni, R. *J. Agric. Food Chem.* **2006**, *54*, 7778.

(48) Carroll, J. F.; Cantrell, C. L.; Klun, J. A.; Kramer, M. *Exp. Appl. Acarol.* **2007**, *41*, 215.

(49) R Development Core Team *R: A Language and Environment for Statistical Computing. R Foundation for Statistical Computing*; R Foundation for Statistical Computing: Vienna, Austria, 2009.

(50) Venables, W. N.; Ripley, B. D. *Modern Applied Statistics with S. 4th ed.*; Springer: New York, 2002.

(51) Zhu, F.; Qin, C.; Tao, L.; Liu, X.; Shi, Z.; Ma, X.; Jia, J.; Tan, Y.; Cui, C.; Lin, J.; Tan, C.; Jiang, Y.; Chen, Y. *Proc. Nat. Acad. Sci. U.S.A.* **2011**, *108*, 12943.

(52) Oh, J.; Bowling, J. J.; Carroll, J. F.; Demirci, B.; Başer, K. H. C.; Leininger, T. D.; Bernier, U. R.; Hamann, M. T. *Phytochemistry* **2012**, *80*, 28.

(53) Noshita, T.; Kiyota, H.; Kidachi, Y.; Ryoyama, K.; Funayama, S.; Hanada, K.; Murayama, T. *Biosci. Biotechnol. Biochem.* **2009**, *73*, 726.

(54) Plaza, A.; Bifulco, G.; Masullo, M.; Lloyd, J. R.; Keffer, J. L.; Colin, P. L.; Hooper, J. N. A.; Bell, L. J.; Bewley, C. A. *J. Org. Chem.* **2010**, *75*, 4344.

(55) Plaza, A.; Garcia, R.; Bifulco, G.; Martinez, J. P.; Hüttel, S.; Sasse, F.; Meyerhans, A.; Stadler, M.; Müller, R. *Org. Lett.* **2012**, *14*, 2854.

(56) Abbate, S.; Ciogli, A.; Fioravanti, S.; Gasparrini, F.; Longhi, G.; Pellacani, L.; Rizzato, E.; Spinelli, D.; Tardella, P. A. *Eur. J. Org. Chem.* **2010**, *2010*, 6193.

(57) Bringmann, G.; Bruhn, T.; Maksimenka, K.; Hemberger, Y. *Eur. J. Org. Chem.* **2009**, *2009*, 2717.

(58) Woźnica, M.; Butkiewicz, A.; Grzywacz, A.; Kowalska, P.; Masnyk, M.; Michalak, K.; Luboradzki, R.; Furche, F.; Kruse, H.; Grimme, S.; Frelek, J. *J. Org. Chem.* **2011**, *76*, 3306.

(59) Bencivenni, G.; Wu, L.-Y.; Mazzanti, A.; Giannichi, B.; Pesciaioli, F.; Song, M.-P.; Bartoli, G.; Melchiorre, P. *Angew. Chem.* **2009**, *121*, 7336.

(60) Polavarapu, P. L.; Scalmani, G.; Hawkins, E. K.; Rizzo, C.; Jeirath, N.; Ibnusaud, I.; Habel, D.; Nair, D. S.; Haleema, S. *J. Nat. Prod.* **2010**, *74*, 321.

(61) Kwit, M.; Rozwadowska, M. D.; Gawroński, J.; Grajewska, A. *J. Org. Chem.* **2009**, *74*, 8051.

(62) Gao, J.-M.; Qin, J.-C.; Pescitelli, G.; Di Pietro, S.; Ma, Y.-T.; Zhang, A.-L. *Org. Biomol. Chem.* **2010**, *8*, 3543.

(63) Dai, J.; Krohn, K.; Flörke, U.; Pescitelli, G.; Kerti, G.; Papp, T.; Kövér, K. E.; Bényei, A. C.; Draeger, S.; Schulz, B.; Kurtán, T. *Eur. J. Org. Chem.* **2010**, *2010*, 6928.

(64) Stewart, J. *J. Mol. Model.* **2007**, *13*, 1173.

(65) Cossi, M.; Rega, N.; Scalmani, G.; Barone, V. *J. Comput. Chem.* **2003**, *24*, 669.

(66) Wang, J.; Zhai, W.-Z.; Zou, Y.; Zhu, J.-J.; Xiong, J.; Zhao, Y.; Yang, G.-X.; Fan, H.; Hamann, M. T.; Xia, G.; Hu, J.-F. *Tetrahedron Lett.* **2012**, *53*, 2654.

(67) Oh, J.; Bowling, J. J.; Zou, Y.; Chittiboyina, A. G.; Doerksen, R. J.; Ferreira, D.; Leininger, T. D.; Hamann, M. T. *Biochim. Biophys. Acta, Gen. Subj.* **2013**, *1830*, 4229.

(68) Matsumori, N.; Kaneno, D.; Murata, M.; Nakamura, H.; Tachibana, K. *J. Org. Chem.* **1999**, *64*, 866.

(69) Bruhn, T.; Hemberger, Y.; Schaumloffel, A.; Bringmann, G. *SpecDis, Version 1.51*; University of Wuerzburg: Germany, 2011.

(70) Bifulco, G.; Bassarello, C.; Riccio, R.; Gomez-Paloma, L. *Org. Lett.* **2004**, *6*, 1025.

(71) Ibrahim, M. A.; Na, M.; Oh, J.; Schinazi, R. F.; McBrayer, T. R.; Whitaker, T.; Doerksen, R. J.; Newman, D. J.; Zachos, L. G.; Hamann, M. T. *Proc. Nat. Acad. Sci. U.S.A.* **2013**, *110*, 16832.

(72) Choi, Y. H.; Zhou, W.; Oh, J.; Choe, S.; Kim, D. W.; Lee, S. H.; Na, M. *Bioorg. Med. Chem. Lett.* **2012**, *22*, 6116.

(73) Bae, K., H. *The Medicinal Plants of Korea*; Kyo-Hak: Seoul, 2000.

(74) Choi, J.; Young, H.; Park, J.; Choi, J.-H.; Woo, W. *Arch. Pharm. Res.* **1987**, *10*, 169.

(75) Youn, H.; Cho, J. H. *Kor. J. Pharmacogn.* **1991**, *22*, 18.

(76) Riedemann, N. C.; Guo, R. F.; Ward, P. A. *Nat. Med.* **2003**, *9*, 517.

(77) Ranieri, V. M.; Thompson, B. T.; Barie, P. S.; Dhainaut, J.-F.; Douglas, I. S.; Finfer, S.; Gårdlund, B.; Marshall, J. C.; Rhodes, A.; Artigas, A.; Payen, D.; Tenhunen, J.; Al-Khalidi, H. R.; Thompson, V.; Janes, J.; Macias, W. L.; Vangerow, B.; Williams, M. D. *N. Engl. J. Med.* **2012**, *366*, 2055.

(78) Lee, W.; Kim, T. H.; Ku, S.-K.; Min, K.-j.; Lee, H.-S.; Kwon, T. K.; Bae, J.-S. *Toxicol. Appl. Pharmacol.* **2012**, *262*, 91.

(79) Yang, E.-J.; Ku, S.-K.; Lee, W.; Lee, S.; Lee, T.; Song, K.-S.; Bae, J.-S. *J. Cell. Physiol.* **2013**, *228*, 975.

(80) Bae, J.-S. *Arch. Pharm. Res.* **2012**, *35*, 1511.

(81) Zhou, W.; Oh, J.; Li, W.; Kim, D. W.; Lee, S. H.; Na, M. *Bull. Korean Chem. Soc.* **2013**, *34*, 2535.

(82) Miyase, T.; Ueno, A.; Takizawa, N.; Kobayashi, H.; Karasawa, H. *Chem. Pharm. Bull.* **1987**, *35*, 1109.

(83) Smith, S. G.; Goodman, J. M. *J. Org. Chem.* **2009**, *74*, 4597.

(84) Smith, S. G.; Goodman, J. M. *J. Am. Chem. Soc.* **2010**, *132*, 12946.

(85) Lodewyk, M. W.; Tantillo, D. J. *J. Nat. Prod.* **2011**, *74*, 1339.

(86) Uchiyama, T.; Nishimura, K.; Miyase, T.; Ueno, A. *Phytochemistry* **1990**, *29*, 2947.

(87) Zhang, Z.; Zhang, W.; Ji, Y.-P.; Zhao, Y.; Wang, C.-G.; Hu, J.-F. *Phytochemistry* **2010**, *71*, 693.

(88) Yang, H.; Ochani, M.; Li, J.; Qiang, X.; Tanovic, M.; Harris, H. E.; Susarla, S. M.; Ulloa, L.; Wang, H.; DiRaimo, R.; Czura, C. J.; Wang, H.; Roth, J.; Warren, H. S.; Fink, M. P.; Fenton, M. J.; Andersson, U.; Tracey, K. J. *Proc. Nat. Acad. Sci. U. S. A.* **2004**, *101*, 296.

(89) Rittirsch, D.; Huber-Lang, M. S.; Flierl, M. A.; Ward, P. A. *Nat. Protoc.* **2008**, *4*, 31.

(90) Hara, S.; Okabe, H.; Mihashi, K. *Chem. Pharm. Bull.* **1986**, *34*, 1843.

(91) Bittner, M.; Schuster, A.; Jakupovic, J. *Phytochemistry* **1991**, *30*, 1329.

(92) Zdero, C.; Bohlmann, F.; King, R. M. *Phytochemistry* **1992**, *31*, 213.

(93) Urzúa, A.; Andrade, L.; Muñoz, E.; Rodriguez, M. E.; Belmonte, E. *Biochem. Syst. Ecol.* **1997**, *25*, 681.

(94) eFloras *http://www.efloras.org* Missouri Botanical Garden: St. Louis, Missouri & Harvard University Herbaria: Cambridge, Massachusetts, 2008.

(95) Jørgensen, P. M.; Léon-Yánez, S. *Catalogue of the Vascular Plants of Ecuador*; Missouri Botanical Garden: Saint Louis, Missouri, 1999.

(96) Blake, S. F. *Am. J. Bot.* **1928**, *15*, 43.

(97) Popov, D. *Biochem. Biophys. Res. Commun.* **2011**, *410*, 377.

(98) Elchebly, M. *Science* **1999**, *283*, 1544.

(99) Klaman, L. D. *Methods Mol. Cell. Biol.* **2000**, *20*, 5479.

(100) Jia, Z.; Barford, D.; Flint, A.; Tonks, N. *Science* **1995**, *268*, 1754.

(101) Wiesmann, C.; Barr, K. J.; Kung, J.; Zhu, J.; Erlanson, D. A.; Shen, W.; Fahr, B. J.; Zhong, M.; Taylor, L.; Randal, M.; McDowell, R. S.; Hansen, S. K. *Nat. Struct. Mol. Biol.* **2004**, *11*, 730.

(102) Lantz, K. A.; Hart, S. G. E.; Planey, S. L.; Roitman, M. F.; Ruiz-White, I. A.; Wolfe, H. R.; McLane, M. P. *Obesity* **2010**, *18*, 1516.

(103) Berman, H. M.; Westbrook, J.; Feng, Z.; Gilliland, G.; Bhat, T.; Weissig, H.; Shindyalov, I. N.; Bourne, P. E. *Nucleic Acids Res.* **2000**, *28*, 235.

(104) Kamerlin, S. C. L.; Rucker, R.; Boresch, S. *Biochem. Biophys. Res. Commun.* **2007**, *356*, 1011.

(105) Wang, J.-F.; Gong, K.; Wei, D.-Q.; Li, Y.-X.; Chou, K.-C. *Protein Eng. Des. Sel.* **2009**, *22*, 349.

(106) Zhang, X.; Li, X.; Wang, R. *J. Chem. Inf. Model.* **2009**, *49*, 1033.

(107) Andersen, H. S.; Iversen, L. F.; Jeppesen, C. B.; Branner, S.; Norris, K.; Rasmussen, H. B.; Møller, K. B.; Møller, N. P. H. *J. Biol. Chem.* **2000**, *275*, 7101.

(108) Kamerlin, S. C. L.; Rucker, R.; Boresch, S. *Biochem. Biophys. Res. Commun.* **2006**, *345*, 1161.

(109) Bharatham, K.; Bharatham, N.; Kwon, Y.; Lee, K. *J. Comput. Aided Mol. Des.* **2008**, *22*, 925.

(110) Achenbach, H.; Benirschke, M.; Torrenegra, R. *Phytochemistry* **1997**, *45*, 325.

(111) Yahara, S.; Nishiyori, T.; Kohda, A.; Nohara, T.; Nishioka, I. *Chem. Pharm. Bull.* **1991**, *39*, 2024.

(112) Na, M.; Jang, J.; Njamen, D.; Mbafor, J. T.; Fomum, Z. T.; Kim, B. Y.; Oh, W. K.; Ahn, J. S. *J. Nat. Prod.* **2006**, *69*, 1572.

(113) Fu, G.; Liu, H.; Doerksen, R. J. *J. Phys. Chem. B* **2012**, *116*, 9580.

(114) American Cancer Society 2015, http://www.cancer.org/cancer/pancreaticcancer/detailedguide/pancreatic-cancer-key-statistics accessed 03/21/2015.

(115) Cartwright, T.; Richards, D. A.; Boehm, K. A. *Cancer Control* **2008**, *15*, 308.

(116) Molinski, T. F.; Dalisay, D. S.; Lievens, S. L.; Saludes, J. P. *Nat. Rev. Drug Discov.* **2009**, *8*, 69.

(117) Aune, G. J.; Furuta, T.; Pommier, Y. *Anti-Cancer Drugs* **2002**, *13*, 545.

(118) Rinehart, K. L.; Gloer, J. B.; Cook, J. C.; Mizsak, S. A.; Scahill, T. A. *J. Am. Chem. Soc.* **1981**, *103*, 1857.

(119) Hamann, M. T.; Scheuer, P. J. *J. Am. Chem. Soc.* **1993**, *115*, 5825.

(120) Hirata, Y.; Uemura, D. *Pure Appl. Chem.* **1986**, *58*, 701.

(121) Cortes, J.; Vahdat, L.; Blum, J. L.; Twelves, C.; Campone, M.; Roché, H.; Bachelot, T.; Awada, A.; Paridaens, R.; Goncalves, A. *J. Clin. Oncol.* **2010**, *28*, 3922.

(122) Hu, J.-F.; Fan, H.; Xiong, J.; Wu, S.-B. *Chem. Rev.* **2011**, *111*, 5465.

(123) Abbas, S.; Kelly, M.; Bowling, J.; Sims, J.; Waters, A.; Hamann, M. *Mar. Drugs* **2011**, *9*, 2423.

(124) Kita, Y.; Tohma, H.; Inagaki, M.; Hatanaka, K.; Kikuchi, K.; Yakura, T. *Tetrahedron Lett.* **1991**, *32*, 2035.

(125) Kita, Y.; Tohma, H.; Inagaki, M.; Hatanaka, K.; Yakura, T. *J. Am. Chem. Soc.* **1992**, *114*, 2175.

(126) Sadanandan, E. V.; Pillai, S. K.; Lakshmikantham, M.; Billimoria, A. D.; Culpepper, J. S.; Cava, M. P. *J. Org. Chem.* **1995**, *60*, 1800.

(127) Aubart, K. M.; Heathcock, C. H. *J. Org. Chem.* **1999**, *64*, 16.

(128) Nishiyama, S.; Cheng, J.-F.; Tao, X. L.; Yamamura, S. *Tetrahedron Lett.* **1991**, *32*, 4151.

(129) Liang Tao, X.; Cheng, J.-F.; Nishiyama, S.; Yamamura, S. *Tetrahedron* **1994**, *50*, 2017.

(130) Zhao, R.; Lown, J. W. *Synth. Commun.* **1997**, *27*, 2103.

(131) White, J. D.; Yager, K. M.; Yakura, T. *J. Am. Chem. Soc.* **1994**, *116*, 1831.

(132) Iwao, M.; Motoi, O.; Fukuda, T.; Ishibashi, F. *Tetrahedron* **1998**, *54*, 8999.

(133) Kita, Y.; Watanabe, H.; Egi, M.; Saiki, T.; Fukuoka, Y.; Tohma, H. *J. Chem. Soc., Perkin Trans. 1* **1998**, 635.

(134) Kita, Y.; Egi, M.; Tohma, H. *Chem. Comm.* **1999**, 143.

(135) Jia, Y.; Zhu, J. *J. Org. Chem.* **2006**, *71*, 7826.

(136) Mejía-Oneto, J. M.; Padwa, A. *Org. Lett.* **2006**, *8*, 3275.

(137) Ireland, R. E.; Liu, L. *J. Org. Chem.* **1993**, *58*, 2899.

(138) Frigerio, M.; Santagostino, M.; Sputore, S. *J. Org. Chem.* **1999**, *64*, 4537.

(139) Jackson, D. S.; Fraser, S. A.; Ni, L.-M.; Kam, C.-M.; Winkler, U.; Johnson, D. A.; Froelich, C. J.; Hudig, D.; Powers, J. C. *J. Med. Chem.* **1998**, *41*, 2289.

(140) Hu, C.; Qin, H.; Cui, Y.; Jia, Y. *Tetrahedron* **2009**, *65*, 9075.

(141) Alper, P. B.; Hung, S.-C.; Wong, C.-H. *Tetrahedron Lett.* **1996**, *37*, 6029.

(142) Moriarty, R. M.; Sultana, M. *J. Am. Chem. Soc.* **1985**, *107*, 4559.

(143) Kita, Y.; Egi, M.; Takada, T.; Tohma, H. *Synthesis* **1999**, *1999*, 885.

(144) Izawa, T.; Nishiyama, S.; Yamamura, S. *Tetrahedron* **1994**, *50*, 13593.

(145) Rajeswari, S.; Drost, K.; Cava, M. *Heterocycles* **1989**, *29*, 415.

(146) Blanchard, Z.; Mullins, N.; Ellipeddi, P.; Lage, J. M.; McKinney, S.; El-Etriby, R.; Zhang, X.; Isokpehi, R.; Hernandez, B.; ElShamy, W. M. *PLoS ONE* **2014**, *9*, e95663.

(147) Siegel, R.; Ma, J.; Zou, Z.; Jemal, A. *CA Cancer J. Clin.* **2014**, *64*, 9.

(148) Zidan, J.; Dashkovsky, I.; Stayerman, C.; Basher, W.; Cozacov, C.; Hadary, A. *Br. J. Cancer* **2005**, *93*, 552.

(149) Rakha, E.; Chan, S. *Clin. Oncol.* **2011**, *23*, 587.

(150) Shimizu, Y.; Luk, H.; Horio, D.; Miron, P.; Griswold, M.; Iglehart, D.; Hernandez, B.; Killeen, J.; ElShamy, W. M. *PLoS ONE* **2012**, *7*, e34102.

(151) ElShamy, W. M.; Livingston, D. M. *Nature Cell Biol.* **2004**, *6*, 954.

(152) Furuta, S.; Jiang, X.; Gu, B.; Cheng, E.; Chen, P.-L.; Lee, W.-H. *Proc. Nat. Acad. Sci. U.S.A.* **2005**, *102*, 9176.

(153) Chock, K.; Allison, J.; ElShamy, W. *Oncogene* **2010**, *29*, 5274.

(154) Paul, B. T.; Blanchard, Z.; Ridgway, M.; ElShamy, W. M. *Oncogene* **2014**.

(155) Braunschweiler, L.; Ernst, R. R. *J. Magn. Reson. (1969)* **1983**, *53*, 521.

(156) Aue, W.; Bartholdi, E.; Ernst, R. R. *J. Chem. Phys.* **1976**, *64*, 2229.

(157) Jeener, J.; Meier, B.; Bachmann, P.; Ernst, R. *J. Chem. Phys.* **1979**, *71*, 4546.

(158) Bax, A.; Summers, M. F. *J. Am. Chem. Soc.* **1986**, *108*, 2093.

(159) Williamson, R. T.; Buevich, A. V.; Martin, G. E.; Parella, T. *J. Org. Chem.* **2014**, *79*, 3887.

(160) López-Méndez, B.; Güntert, P. *J. Am. Chem. Soc.* **2006**, *128*, 13112.

(161) Goddard, T. D.; Kneller, D. G., *SPARKY 3, University of California, San Francisco*.

(162) Brunger, A. T. *Nat. Protoc.* **2007**, *2*, 2728.

(163) Güntert, P. In *Protein NMR Techniques*; Springer: New York, 2004, p 353.

(164) Protein Structure Validation Software suite (PSVS). http://psvs-1_4-dev.nesg.org/ accessed 2/1/2015.

VITA

Joonseok Oh was born in Jinju, South Korea on December 24, 1980. He attended Yeungnam University where he obtained his Bachelor of Science in Pharmacy and Master of Science in February of 2006 and 2008, respectively. During his tenure there, he implemented multiple projects focused on investigation of natural products capable of whitening human skin. He also completed his military service as a medic during 2002-2004 in the 11th Brigade Republic of Korea Special Forces. In the January of 2010, he joined the research lab of Dr. Mark T. Hamann at the Department of Pharmacognosy in the School of Pharmacy at The University of Mississippi to conduct several projects presented in this dissertation work.